UNIVERSITA' POLITECNICA DELLE MARCHE

Biomolecular Sciences

XXXI Cycle - 2018

DOCTORAL THESIS

Natural and functionalized molecules with antioxidant and scavenging activity as components of innovative lipid-based artificial tears

PhD student:

Minnelli Cristina

Aziendal tutor:
Dott. Dario Rusciano

Academic tutor:
Dott. Giovanna Mobbili

Declaration of Authorship

Abstract

List of Abbreviations

PART I – State of art

CHAPTER I

ROS and Antioxidants: A continuous battle inside the cells

1.1. Properties and generation of Reactive Oxygen Species (ROS)
1.2. Endogenous and exogenous sources of ROS
1.3. Cellular damage induced by ROS
    1.3.1. Nucleic acids
    1.3.2. Lipids
    1.3.3. Proteins
1.4. Essential role of antioxidants in protection against oxidative stress

CHAPTER II

Ocular Diseases Associated with Oxidative Stress

2.1. Introduction
2.2. Age-related Macular Degeneration (AMD)
2.3. Role of ROS and the Oxidative Stress in Cataractogenesis

2.4. Tear Film and its dysfunction in Dry Eye Diseases (DEA)

2.5. Management of ocular diseases – limitation and therapeutics

CHAPTER III

Lipid-based nanocarriers

3.1. Lyotropic Liquid Crystals (LLC)

3.2. Lipid/Water Polymorphysm

3.3. Lipid-based nanocarriers relevant to topical ocular drug delivery

3.3.1. Lamellar phase: liposomes

3.3.2. Reversed bicontinuous Cubic phase and Cubosomes

PART II – Natural and functionalized Epigallocatechin-3-gallate (EGCG) as components of lipid-based eye drops

CHAPTER IV

Epigallocatechin-3-gallate (EGCG)

4.1. Antioxidant Properties

4.2. Stability and strategy to improve the bioavailability of EGCG

CHAPTER V

Liposomal formulations for an efficient delivery of Epigallocatechin-3-Gallate: characterization and protective effect in ARPE19 cells

5.1. Introduction

5.2. Optimization of EGCG encapsulation efficiency inside liposomal formulations

5.2.1. Salts and Lipid Composition effects on EGCG Encapsulation Efficiency inside Multilamellar Vesicles (MLVs)

5.2.2. Interaction of EGCG with lipid bilayer: *in silico* results

5.3. Colloidal stability: optimization of the best liposome formulation

5.3.1. Magnesium chloride effect on the anionic liposome

5.3.2. Effect of Poloxamer-407 addition

5.4. Characterization of bulk and nanodispersed liposomal phase

5.4.1. X-ray diffraction measurements

5.4.2. Dynamic Light Scattering measurements

5.4.3. Encapsulation Efficiency studies in presence of Poloxamer-407

5.4.4. *In vitro* drug release

5.5. Cellular Experiments

5.5.1. Cytotoxicity of EGCG-loaded magnesium-poloxamer liposomes in Retinal Pigment Epithelial Cells

5.5.2. Enhancement of EGCG efficacy by magnesium-poloxamer liposome incorporation

5.6. Conclusion

CHAPTER VI

Epigallocatechin-3-gallate (EGCG)-loaded cubic or hexagonal phase gels and its dispersed forms: pre-formulation studies

6.1. Introduction

6.2. Preparation and Encapsulation Effiency studies of bulk (Nondispersed) phase and its dispersed forms (Cubosomes and Hexasomes)

6.3. Nanostructural Characterization

6.3.1. Small Angle Neutrons Scattering (SANS) studies

6.3.2. Colloidal stability of dispersed phases: Dynamic Light Scattering (DLS)

6.4. Conclusion and future perspective

CHAPTER VII

A new lipophilic derivative of EGCG

7.1. Introduction

7.2. Synthesis and characterization of an ether derivative of EGCG

7.3. Antioxidant properties of new derivative

7.3.1. Scavenging Activity on the DPPH Radical

7.3.2. Protection of liposome oxidation: TBARS assay

7.3.3. Protective effect against oxidative stress induced-cell death

7.4. Conclusion and future perspective

PART III – A new lipophilic derivative of Edaravone: antioxidant properties and liposomal formulations

CHAPTER VIII

Edaravone derivative

8.1. Introduction

8.2. Synthesis and characterization of C18- Edaravone

8.3. Antioxidant activity of C18-Edaravone (C18-EdV)

8.3.1. Scavenging Activity on the DPPH Radical

8.3.2. Protection of liposome oxidation: TBARS assay

8.3.3. Cellular experiments

8.4. C18-EdV loaded liposome: characterization

8.4.1. Fluidity of lipid bilayer: *in silico* studies

8.4.2. Colloidal stability of liposome formulations

8.4.3. Encapsulation efficiency studies

8.5. Cellular Experiments: the effect of liposomal encapsulatin

8.6. Conclusion and perspective

Materials and Method

Bibliography

Declaration of Authorship

I, Cristina Minnelli, declare that this thesis titled "Natural and functionalized molecules with antioxidant and scavenging activity as components of innovative lipid-based artificial tears" and the work presented it are my own and has been generated by me as the result of my own original research. Where I have consulted the work of others, this is always clearly stated.

I confirm that parts of my PhD work have been published in the following papers:

Cristina Minnelli, Paolo Moretti, Gianluca Fulgenzi, Paolo Mariani, Emiliano Laudadio, Tatiana Armeni, Roberta Galeazzi, Giovanna Mobbili**. A Poloxamer-407 modified liposome encapsulating epigallocatechin-3-gallate in the presence of magnesium: Characterization and protective effect against oxidative damage.** International Journal of Pharmaceutics (**2018**), 552:225–234.

Emiliano Laudadio, **Cristina Minnelli**, Adolfo Amici, Luca Massaccesi, Giovanna Mobbili, Roberta Galeazzi. **Design of proper liposomial vector for an efficient encapsulation Epigallocatechin-3-gallate: an in silico/experimental approach.** Molecules (**2018**), 23(2), 441.

Minnelli Cristina, Cianfruglia Laura, Laudadio Emiliano, Galeazzi Roberta, Pisani Michela, Crucianelli Emanuela, Bizzaro Davide, Armeni Tatiana, Mobbili Giovanna. **Selective induction of apoptosis in MCF7 cancer-cell by targeted liposomes functionalised with mannose-6-phosphate.** Journal of Drug Targeting **(2018),** 26(3):242-251.

Andrea Scirè, Laura Cianfrugia, **Minnelli Cristina**, Tatiana Ameni, Francesco Galli. **Glutathione compartmentalization and its role in glutathionylation and other regulatory processes of cellular pathways**. Biofactors (**2018**).

Galeazzi Roberta, Laudadio Emiliano, Falconi Emanuele, Massaccesi Luca, Ercolani Luisa, Mobbili Giovanna, **Minnelli Cristina**, Scirè Andrea, Cianfruglia Laura, Armeni Tatiana. **Protein-protein interactions of human glyoxalase II: findings of a reliable docking protocol.** Organic Biomolecular Chemistry **(2018),** 16(28):5167-5177.

Laudadio Emiliano, Galeazzi Roberta, Mobbili Giovanna, Minnelli Cristina, Barbon Antonio, Bortolus Marco, Stipa Pierluigi. **Depth Distribution of Spin-Labeled Liponitroxides within Lipid Bilayers: A combined EPR and Molecular Dynamics approach**. ACS Omega. Accepted Manuscript. 2019.

Laudadio Emiliano, Mobbili Giovanna, **Minnelli Cristina**, Massaccesi Luca, and Galeazzi Roberta. **Salts Influence Cathechins and Flavonoids Encapsulation in Liposomes: a Molecular Dynamics Investigation**. Molecular Informatics (**2017**), 36 (11).

Gianmarco Mangiaterra, Emiliano Laudadio, Marta Cometti, Giovanna Mobbili, **Cristina Minnelli**, Luca Massaccesi, Barbara Citterio, Francesca Biavasco, Roberta Galeazzi. **Inhibitors of multidrug efflux pumps of Pseudomonas aeruginosa from natural sources: An in silico high-throughput virtual screening and in vitro validation.** Medicinal Chemistry Research (**2017**), 26(2):414–430.

Abstract

This thesis presents an extended work concerning the development of lipid-based drug delivery systems able to prevent and control the ocular diseases associated with oxidative stress.

The eye drops dosage forms account for nearly 90% of currently available marketed formulations thanks of their simplicity, safety and acceptance by patients. However, achievement of adequate bioavailability of topically applied drugs is challenging due to unique anatomical and physiological barriers at the ocular surface that determine a low drug absorption of about 5%.

The lipid-based nanocarriers, which are highly biocompatible, can carry the antioxidant to a specific site, release it in a controlled manner and protect the encapsulated molecule from premature degradation. Among the antioxidants used for ophthalmic applications, the attention was focused on Epigallocatechin-3-gallate and Edaravone molecules, which are well-known for being bioactive in ocular diseases associated with oxidative stress.

Since the final aim was to create a stable and efficient delivery system, the design of lipid-based nanocarriers has been based on three critical targets:
a) High encapsulation efficiency in order to optimize the delivery of the active principle at the target sites.
b) Colloidal stability and characterization of the lipid-based systems
c) Ability to protect the retinal cells from oxidative stress-induced cell death

Briefly, from the obtained results, we concluded that the encapsulation percentage of EGCG inside liposomes showed specific ion effects together with an influence of the lipid matrix composition. More in details, the combination of an anionic lipid matrix with $MgCl_2$ and Poloxamer-407 allowed us to obtain a system highly stable with 100% EGCG encapsulation that was able to protect retinal cells from oxidative stress. Using increasing concentrations of EGCG we optimized the encapsulation efficiency of the catechin into different types of lipidic supramolecular structures, presenting cubic and hexagonal mesophases; these lyotropic liquid crystals are other

interesting systems used in the ophthalmic field. The structures of all systems were characterized by X-Ray and Neutrons experiments. As alternative strategy, the introduction of lipophilic C-18 chain in EGCG and Edaravone molecules also increased their encapsulation efficiency inside a liposomal vector as well as their ability to protect the retinal cells from oxidative stress.

List of Abbreviations

ROS: Reactive **O**xygen **S**pecies

NADPH oxidase: **N**icotinamide **A**denine **D**inucleotide **Ph**osphate oxidase)

5-LOX: **5-L**ip**o**xygenase

DNA: **D**eoxyribo**n**ucleic **A**cid

8-OHdG: **8-h**ydroxy**d**eoxy **g**uanosine

LPO: **L**ipid **P**er**o**xidation

PUFA: **P**olyunsaturated **F**atty **A**cid

GPx: **G**lutathione **P**ero**x**idase

SOD: **S**uper**o**xide **D**ismutase

GR: **G**lutathione **R**eductase

CAT: **Cat**alase

GSH: **G**lutathione

GSSG: **G**lutathione **D**isulfide

MDA: **M**alonyl**di**aldehyde

4-HNE: 4-hydroxy-2-**n**on**e**nal

AMD: **A**ge-**M**acular **D**egeneration

RPE: **R**etinal **P**igment **E**pithelium

DEA: **D**ry **E**ye **D**isease

DES: **D**ry **E**ye **S**yndrome

EGCG: **E**pi**g**allo**c**atechin- 3-**g**allate

TF: **T**ear **F**ilm

TFLL: **T**ear **F**luid **L**ipid **L**ayer

LLC: Lyotropic **L**iquid **C**rystals

CPP: **C**ritical **P**acking **P**arameter

EE: Encapsulation **E**fficiency

DLC: **D**rug **L**oading **C**apacity

X-RD: **X-R**ay **D**iffraction

DLS: **D**ynamic **L**ight **S**cattering

MLV: Multilamellar Vesicles

TEM: **T**ransmission **E**lectron **M**icroscopy

TBARS: **T**hiobarbituric **R**eactive **S**pecies

ARPE-19: **A**dult **R**etinal **P**igment **E**pithelial cell line**-19**

PART I - State of Art

"Success is the ability to go from one failure to another with no loss of enthusiasm"
-Winston Churchill-

CHAPTER I

ROS and Antioxidants: A continuous battle inside the cell

1.1. Properties and generation of Reactive Oxygen Species (ROS)

A free radical can be defined as any species capable of independent existence that contains one or more unpaired electrons (Halliwell, 2007). Additionally, the term is also used to describe certain non-radicals that contain their full complement of electrons, but in an unstable or reactive state, like ozone (O_3), hypochlorous acid (HClO), singlet oxygen ($^1O_2$), and hydrogen peroxide (H_2O_2) and that can be converted easily to radicals (Halliwell, 2007). All these entities are usually reactive, although the chemical reactivity of free radicals varies over a wide spectrum.

Radicals can be formed via homolytic cleavage of a covalent bond in a non-radical species, by breakage of a radical to give another one, and via redox reactions (Halliwell, 2007; Bahorun et al 2006). In order to achieve a stable state, they react with other molecules, which become unstable by this interaction, thereby causing an oxidative chain reaction.

Radicals derived from oxygen represent the most important class of radical species generated in living systems. They are collectively referred to as "Radical Oxygen Species" (ROS). The molecular oxygen (dioxygen; O_2) has in its ground state two unpaired electrons and therefore it is qualified as radical. Since the most stable organic molecules are in singlet state (electron spin quantum number equal to one), the molecular oxygen, in triplet state, is less reactive to cellular component respect to others ROS (Halliwell and Gutteridge, 1989). However, triplet oxygen may be converted to the much more reactive ROS forms either by energy transfer or by electron transfer reactions. The first mechanism leads to the formation of singlet oxygen, whereas the latter process results in the sequential reduction to superoxide, hydrogen peroxide, and others (**Figure 1**).

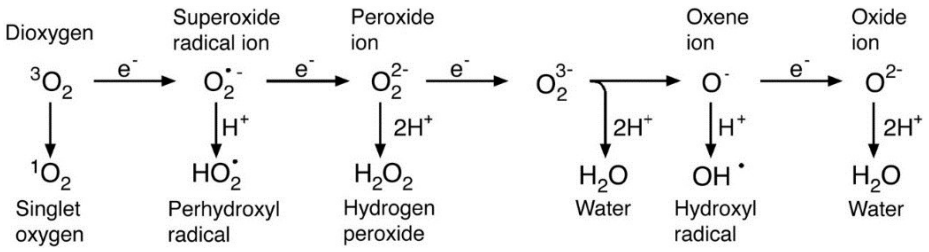

Figure 1. Generation of different ROS by energy transfer or sequential univalent reduction of ground state triplet oxygen.

Some of them, such as superoxide anion ($O_2\bullet^-$), hydroxyl radical (•OH) and hydrogen peroxide (H_2O_2) are the most relevant ROS in physiological or pathophysiological conditions (see below). They are generated from both endogenous and exogenous sources by reactions that can be mediated or not by enzymes.

The generation of $O_2\bullet^-$ occurs by iron-based oxidation reactions (Eq. 1) and by enzymatic and non-enzymatic reactions in which an electron is transferred to molecular oxygen (Eq. 2) (Michelson et al, 1977). The non-enzymatic reaction represents the major source of $O_2\bullet^-$ and occurs within the mitochondria. The enzymes involved in superoxide anion formation comprise several cellular oxidase systems such as NADPH oxidase (nicotinamide adenine dinucleotide phosphate oxidase), xanthine oxidase, lipooxygenase and peroxidases (Babior, 1999; Vignais, 2002). Superoxide anion is a relatively unreactive intermediate with poor ability to cross biological membranes but can inactivate specific enzymes or initiate lipid peroxidation, also in its protonated form, hydroperoxyl $HO_2\bullet$. Under physiological pH the most occurring form is superoxide. It can act as reducing agent and transform iron Fe^{+3} to Fe^{+2} thus stimulating the Fenton reaction (Eq. 6).

$$O_2 + Fe^{2+} \rightarrow Fe^{3+} + \mathbf{O_2\bullet^-} \quad (1)$$

$$O_2 + e^- \rightarrow \mathbf{O_2\bullet^-} \quad (2)$$

H_2O_2 is mainly formed in a dismutation reaction catalyzed by a scavenging enzyme, the superoxide dismutase (SOD) (Eq. 3) (Halliwell and Gutteridge, 1999). The production of H_2O_2 can occur also by the non-enzymatic dismutation of $O_2\bullet^-$ (Eq. 4). It is a non-radical potent oxidizing agent, which can diffuse across cell membrane because it is electronically not charged.

$$2O_2\bullet^- + 2H^+ \xrightarrow{\text{Cu, Zn, Mn-SOD}} O_2 + \mathbf{H_2O_2} \quad (3)$$

$$O_2\bullet^- + e- \rightarrow (O_2^{2-} - + 2H^+) \rightarrow \mathbf{H_2O_2} \quad (4)$$

OH• is the most reactive free radical *in vivo* (Bedwell et al, 1989). It is formed by the reaction between superoxide radical and H_2O_2 in a reaction called Haber–Weiss reaction (Eq. 5). It is

also produced by the Fenton reaction (Fenton, 1893), in which H_2O_2 reacts with metal ions (Fe^{+2} or Cu^{+}), often bound in complex with different proteins such as ferritin (an intracellular protein that stores iron) and ceruloplasmin (plasma copper carrying protein) or other molecules (Haber and Weiss, 1934). This reaction represents the major non-enzimatically sources of OH• inside the cells. The Fe^{3+} ions react more slowly (if at all) with H_2O_2 than Fe^{2+} complexes so that reducing agents stimulate Fenton reactions. This can occur with ascorbate ($AscH_2$) (Walling, 1982) and even with superoxide radical (Fenton, 1893) (Eq. 6). The •OH radical could be also generated by photolytic decomposition of alkyl hydroperoxides (Valko et al, 2004). Finally, the exogenous sources, such as ionizing radiations, can produce two •OH radicals by radiolysis of water (homolytic scission) (Riley, 1994). The hydroxyl radical is a diffusible molecule resulting in a very reactive entity, within and out of the cells (Al-Guborya et al, 2010), and it is the oxidant primarily responsible for oxidative damage of DNA bases.

$$H_2O_2 + O_2\bullet^- \longrightarrow \bullet\mathbf{OH} + OH^- + O_2 \qquad (5)$$

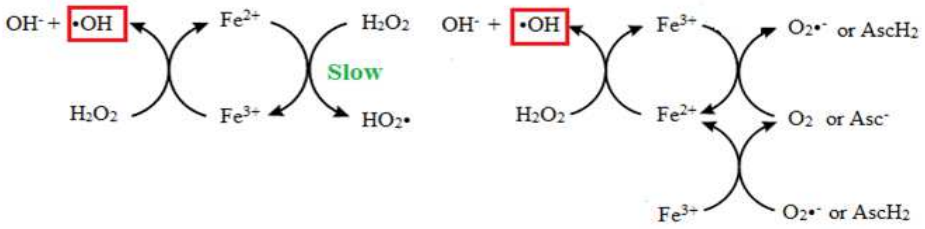

(6)

1.2. Endogenous and exogenous sources of ROS

Mitochondria, NADPH oxidase (NOX) complexes and 5-Lipoxygenase represent the major endogenous sources of ROS in living non-photosynthetic cells in addition to photosensitizers that are present mainly at retina level (**Figure 2**).

Mitochondria provides energy from aerobic metabolism mainly with an oxidative phosphorylation process, which involves the transport of protons (hydrogen ions) across the inner mitochondrial membrane by the electron transport chain. The electrons are transferred through a series of proteins via oxidation-reduction reactions. The last destination is oxygen molecule, which accepts four electrons, thus forming two water molecules. Approximately 1-5% of electrons 'flowing' through the mitochondrial electron transport chain, in particular at complex I and complex II levels and $O_2\bullet^-$ is formed (**Fig. 2A**). Then, the SOD enzyme converts it into H_2O_2 that can easily cross the mitochondrial membrane (Cadenas and Davies, 2000).

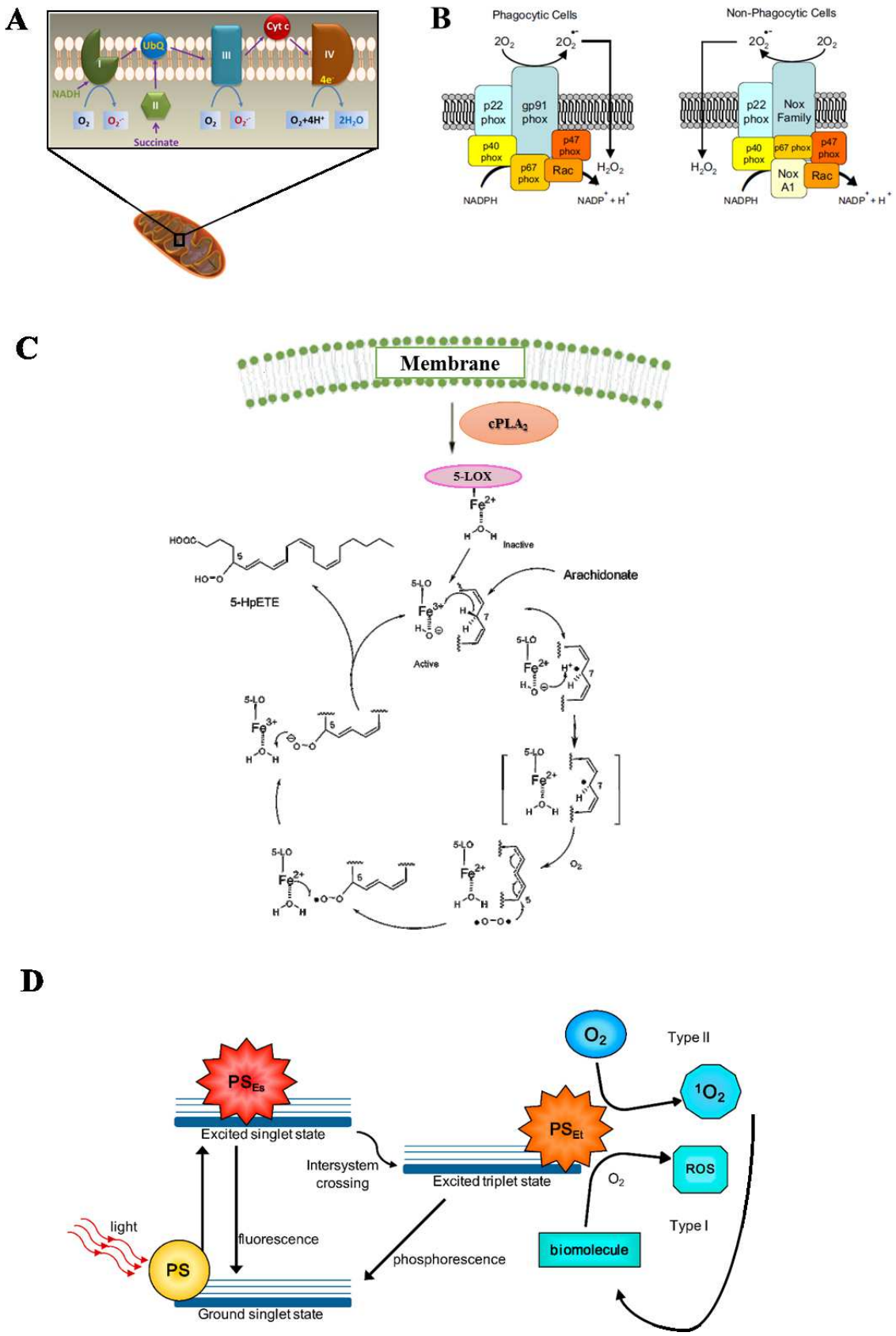

Figure 2. The most relevant source of ROS in living cells: **(A)** mitochondria, (**B)** NADPH oxidase, **(C)** 5-lipooxigenase and **(D)** photosensitizer.

The NADPH oxidases enzyme of the NOX family are the major cellular sources of ROS (Reviewed in Bedard and Krause, 2007) (**Fig. 2B**). They catalyze the production of superoxide by the one-electron reduction of oxygen using NADPH as electron donor; then, the $O_2•^-$ radical generated is the starting material for the production of a large variety of reactive oxidants, including oxidized halogens and singlet oxygen. It is presents in both professional phagocytic cells (macrophages, neutrophils and eosinophils) and nonphagocytic cells. They have a similar structure composed by six subunits (Schalk et al. 1996). The enzyme is normally dormant in phagocytic cells but is rapidly activated upon several stimulation such as hormones, growth factors, cytokines, lipopolysaccharide and mechanical stress. Activation of NADPH oxidase occurs by relocation of the cytosolic components to the cell membrane with consequential $O_2•^-$ generation that plays a vital role in killing intracellular pathogens (Babior et al, 2002). This can be illustrated by examining patients with chronic granulomatous disease caused by mutations in the genes encoding subunits of the NADPH oxidase system leading to poor formation of $O_2•$. Thus, the patient suffer severe and persistent multiple infections (Deffert et al, 2014). In the nonphagocytic cells the NOX is instead constitutively active, producing low level of $O_2•^-$ that may influence the redox signaling in numerous cellular processes such as cell growth, apoptosis, migration, and extracellular matrix remodeling (Nowicki et al, 2001).

5-Lipoxygenase (5-LOX) is a regulator of chronic inflammation and oxidative stress generation (Gubitosi et al, 2008). 5-LOX, a nonheme iron enzyme, catalyzes the dioxygenation of arachidonic acid (AA) in response to several stimuli, particularly growth factors and cytokines (**Fig. 2C**). The reaction cascade starts from activation of phospholipase A2 (PLA_2) that induces the release of AA from phospholipids. Then, 5-LOX catalyzes the stereoselective hydrogen abstraction (L•); the resulting radical migrates over the neighboring double bond and can react with molecular oxygen to form a peroxyl radical (LOO•). Oxidation by Fe^{2+}, present in the active site, delivers to LOO• one electron; the formation of a peroxyl anion (LOO^-) followed by protonation gives a 5-hydroper-oxyeicosatetraenoic acids (5-HPETEs), which is a lipid hydroperoxide (LOOH). Finally, the 5-LOX catalyzes the dehydration reaction to form the epoxide moiety of leukotrienes-A4 (LT4, R-epoxide moiety) that is rapidly metabolized to leukotriene B4. This latter is linked to the ROS generation, cytokine activation, and apoptosis. Generally, the expression of 5-LOX is limited to leukocytes, such as granulocytes, mast cells, and monocytes; however, the detection of its expression in foam cells within atherosclerotic lesions, illustrates the potential importance of this enzyme in the initiation and/or development

of atherosclerosis (Mehrabian et al, 2002). In the same way, Gubitosi-Klug et colleagues have shown the involvement of 5-LOX in degeneration of retinal capillaries and therefore in the pathogenesis of diabetic retinopathies (Gubitosi-Klug et al, 2008).

A photosensitizer is a light absorbing substance involved in the initiation of photochemical reactions that are responsible of light damage, particularly in the retina (Mellerio, 1994). After initial photon absorption, a change in distribution of electrons in the photosensitizer molecules occurs, generating an excited triplet state. In the type I photosensitization, the ROS are produced via electron transfer from excited photosensitizer to biomolecules forming a radical which reacts with molecular oxygen to generate ROS; while, in the type II photosensitization, the excited sensitizer transfers its excess energy to ground-state molecular oxygen ($^3O_2$), producing excited state singlet oxygen ($^1O_2$). This latter reacts with the biomolecules to generate oxidized products (Kruft and Greer, 2011) (**Fig. 2D**). The photosensitizers included the lipofuscin, melanin, bilirubin, hemoglobin and other iron containing proteins (e.g. cytochrome C), flavins, flavoproteins, visual pigments in photoreceptor cells such as rhodopsin, and others (Boulton et al, 2001). An important photosensitizer is lipofuscin, a lipid-protein aggregate that has an autofluorescens activity when excited with short wavelength light. It is formed in the lysosomal compartment and found in active postmitotic cells such as cardiac myocytes, select neurons, and in RPE. Because it accumulates with age, lipofuscin is usually defined an “age pigment,” and it is considered a marker of cellular senescence. The pathological accumulation of lipofuscin can compromise the normal function of cells through distortion of cellular architecture (Young, 1988). Moreover, the lipofuscin acts as photosensitizers, inducing the generation of ROS and therefore the oxidative damage of surrounding tissue (Gaillard et al, 1995). For these reasons, its presence is correlated to a variety of age-related diseases such as ADM, Alzheimer's disease, certain lysosomal disorders, and myopathy (Jeffrey and Keller, 2006; Futerman and Van Meer, 2004).

Others endogenous sources comprise the peroxisomes, that are known to produce H_2O_2 (Valko et al, 2004), and enzymes such as nitric oxide synthase (Vazquez-Vivar and Kalyanaramam, 2000), xanthine oxidase (Halliwell and Gutteridge, 1999), and lysyl oxidase (Rojkind et al, 2002), the enzyme catalyzing the formation of the aldehyde precursors of cross-links in collagen and elastin, can give rise to H_2O_2.

Exogenous ROS result from air and water pollution, cigarette smoke, alcohol, heavy or transition metals, certain drugs (cyclosporine and tacrolimus), industrial solvents, cooking

(smoked meat, used oil, fat), ultraviolet-A light (UVA) and radiation (Kielbassa et al, 1997; Riley, 1994; Halliwell and Cross, 1994). After penetration into the body by different routes, these exogenous compounds are decomposed or metabolized into free radicals. For example, the ionizing radiation, such as x-rays and neutrons, can produce OH• by radiolysis of water or ROS via secondary reactions (Riley, 1994); the cigarette smoke contains more than 7,000 chemical compounds and oxidative agents (Halliwell and Cross, 1994) that are responsible of ROS generation in the human body.

1.3. Cellular damage induced by ROS

Membrane lipids, protein and nucleic acids are the mainly molecular target of oxidative damage caused by ROS. This damage contributes to the pathogenesis of many diseases including ocular disorder.

1.3.1. Nucleic acids

Oxidative damage of deoxyribonucleic acid (DNA) leads to the formation of different oxidative DNA lesions including single and double stranded breaks in DNA. In particular, the OH• radical directly reacts with all components of DNA such as bases (purine and pyrimidine) and deoxyribose sugar backbone (Halliwell and Gutteridge, 1999) thus modifying their structures. One of the resultant purine adducts, 8-hydroxydeoxy guanosine (8-OHdG), is the major oxidative DNA-damage product that can produce mutations because of its base pairing with adenine as well as cytosine. The body has several mechanisms to defend itself against these attacks, for example by using DNA-repair enzymes (base excision repair or mismatch repair) but only the 86% of 8-Oxo-dG is restored to G (Yasui et al, 2014). The levels of 8-OHdG are higher in mitochondrial DNA than in nuclear DNA because it is located in close proximity to the electron transport chain (Barja, 2000). It is not a surprise that increased levels of 8-oxo-dG are frequently associated with several diseases including cancer, Alzheimer's and systemic lupus erythematosus (Valavanidis et al, 2013; Cooke et al, 2003).

The ribonucleic acid (RNA) is more vulnerable to oxidative attack than DNA, in humans, due to its single stranded nature and due to the lack of an active repair mechanism for oxidized RNA (Hofer et al, 2005). Even here, the oxidized guanosine

nucleotide is the main damage product and its levels increase in various pathological conditions like Alzheimer's disease (Abe et al, 2002), Parkinson's disease (Kikuchi et al, 2002), atherosclerosis (Martinet et al, 2004) and myopathies (Tateyama et al, 2003).

1.3.2. Lipid

Lipid peroxidation is a complex and dynamic process that produces numerous peroxidation compounds over time. The membrane lipids, especially the polyunsaturated fatty acid residues (PUFA) of phospholipids are particularly susceptible to oxidation induced by free radicals. In response to membrane lipid peroxidation (LPO), and according to specific cellular repair capacities, the cells may promote cell survival or induce cell death. The cellular response is dependent on the lipid peroxidation amount. At low peroxidation levels, antioxidant defense systems or signaling pathways are activated, resulting in an adaptive stress response. At high level, instead, the lipid peroxidation results in the loss of membrane functioning, for example, alteration of fluidity, permeability, inactivation of membrane bound enzymes and receptors. Moreover, LPO products have been shown to be mutagenic and carcinogenic and are implicated in numerous pathologic conditions such as cardiovascular diseases, cancer, neurological disorders, and aging.

The autoxidation mechanism is a radical-chain process involving three sequences: initiation, propagation, and termination. The **Figure 3** shows a schematic process of the lipid peroxidation.

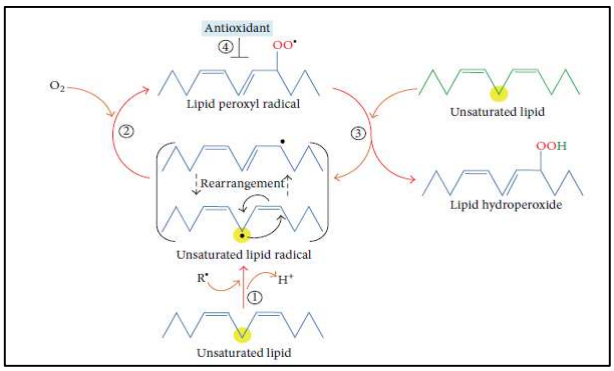

Figure 3. Lipid peroxidation process. In the initiation process, prooxidants abstract an allylic hydrogen from a polyunsaturated fatty acid and form the carbon-centered lipid radical; the carbon radical tends to stabilize by a molecular rearrangement to form a conjugated diene (***step 1***). In the propagation phase, lipid radical rapidly reacts with oxygen to form a lipid peroxyl radical (***step 2***) which abstracts a hydrogen from another lipid molecule generating a new lipid radical and lipid hydroperoxide (***step 3***). In the termination

In the initiation step, the key event is the formation of a lipid radical (L•): the free radical (R•) subtracts an allylic hydrogen atom from a reactive methylene group of polyunsaturated fatty acid side chains (Eq. 7).

$$LH + R\bullet \rightarrow \mathbf{L\bullet} + HR \qquad \text{(Eq. 7)}$$

The free radical initiator can be a superoxide anion, a hydroxyl radical or a hydrogen peroxide. Metal ions contribute to these radical formations by Fenton reaction (Eq. 6) and therefore it is a detrimental participant in lipid peroxidation. Alternatively, thermal or photochemical homolytic cleavage of LH bound may occur. In all cases, the resulting carbon-centered lipid radical can have several fates but the most likely one in aerobic cells is to undergo bond rearrangement that results in stabilization by diene-conjugate formation.

In the propagation step, the oxygen reacts with a carbon centered radical to give a peroxyl lipid (LOO•) (Eq. 8). The addition of molecular oxygen to a lipid radical is the faster than other radical reactions: therefore, the peroxyl species is the principal chain-carrying species. LOO• propagates a free radical chain by hydrogen atom abstraction to give a conjugated diene lipid hydroperoxide (LOOH) and a new lipid radical, which continues another chain reaction (Eq. 9). The hydrogen atom transfer represents the rate limiting reaction. Furthermore, the peroxyl free radical undergoes addition reactions to carbon-carbon double bonds but this process has not been studied extensively in the context of lipid peroxidation.

$$L\bullet + O_2 \rightarrow \mathbf{LOO\bullet} \qquad \text{(Eq. 8)}$$

$$LOO\bullet + LH \rightarrow \mathbf{LOOH} + L\bullet \qquad \text{(Eq. 9)}$$

Lipid hydroperoxides, also called lipid peroxide, is the first stable product of the lipid peroxidation reactions. However, in the presence of transition metal ions, LOOH gives raise to the generation of alkoxyl radicals, LO• (Eq. 10) and peroxyl radicals (Eq. 11), thus perpetuating the chain reaction of lipid peroxidation (Eq. 12, 9) (Halliwell and Gutteridge, 1984).

$$LOOH + Fe^{2+} \rightarrow \mathbf{LO\bullet} + Fe^{3+} + {}^{-}OH \qquad \text{(Eq.10)}$$

$Fe^{3+} + LOOH \rightarrow \mathbf{LOO\bullet} + H^{+} + Fe^{2+}$ (Eq. 11)

$LO\bullet + LOOH \rightarrow LOH + \mathbf{LOO\bullet}$ (Eq.12)

The termination stage is mainly characterized by the formation of non-radical secondary oxidation products through the radical–radical combination (radical quenching) (Eq.13-15). The reaction can also terminate in the presence of a chain-breaking antioxidant like vitamin E (α-tocopherol, α-TOH) (Halliwell and Gutteridge, 1984), which donates a hydrogen atom to the LOO•, LO• and L• species, thus forming the corresponding protonated forms (Eq. 16-18) and vitamin E radical (α-TO•). Glutathione (GSH) and ascorbic acid (Vitamin C) may complement the antioxidant function of α-tocopherol by providing reducing equivalents necessary for its recycling/regeneration. Moreover GSH is also able to reduce the tocopherol radical of Vitamin E indirectly, via reduction of semidehydroascorbate ($AscH^{-}$) to ascorbate ($AscH\bullet^{-}$), reaction catalyzed by dehydroascorbate reductase (DHAR). In the **Figure 4**, I want to give a summary of these linked reactions. Another important chain-branching antioxidant is an isoform of Glutathione peroxidase (GPx4) that converts glutathione (GSH) into oxidized glutathione (also called glutathione disulfide, GSSG) and, during this process, reduces lipid hydroperoxides (LOOH) to corresponding stable alcohols (Liang et al, 2009) (Eq. 19). More in details, the GPx4-mediated reduction of lipid peroxides may depend on vitamin E, another key redox player. This fat-soluble vitamin can be defined as a pre-conditioning cofactor that prepares the substrates for the reaction. Vitamin E is in fact responsible for the 1-e^{-} step (proton-donation reaction) that reduces a peroxyl radical to the peroxide substrate of the GPx reaction (Eq. 18, **Fig. 4**) (Galli et al., 2017).

$\mathbf{LOO\bullet + LOO\bullet \rightarrow LOO\text{-}OOL}$ (Eq. 13)

$\mathbf{LOO\bullet + LOO\bullet \rightarrow LOH + LO + {}^{1}O_2}$ (Eq. 14)

$\mathbf{L\bullet + L\bullet \rightarrow L\text{-}L}$ (Eq. 15)

$\mathbf{L\bullet + \alpha\text{-}TOH \rightarrow LH + \alpha\text{-}TO\bullet}$ (Eq. 16)

$\mathbf{LO\bullet + \alpha\text{-}TOH \rightarrow LOH + \alpha\text{-}TO\bullet}$ (Eq. 17)

$\mathbf{LOO\bullet + \alpha\text{-}TOH \rightarrow LOOH + \alpha\text{-}TO\bullet}$ (Eq. 18)

$2\ GSH + \mathbf{LOOH} \xrightarrow{GPx4} GSSG + \mathbf{LOH} + H_2O$ (Eq. 19)

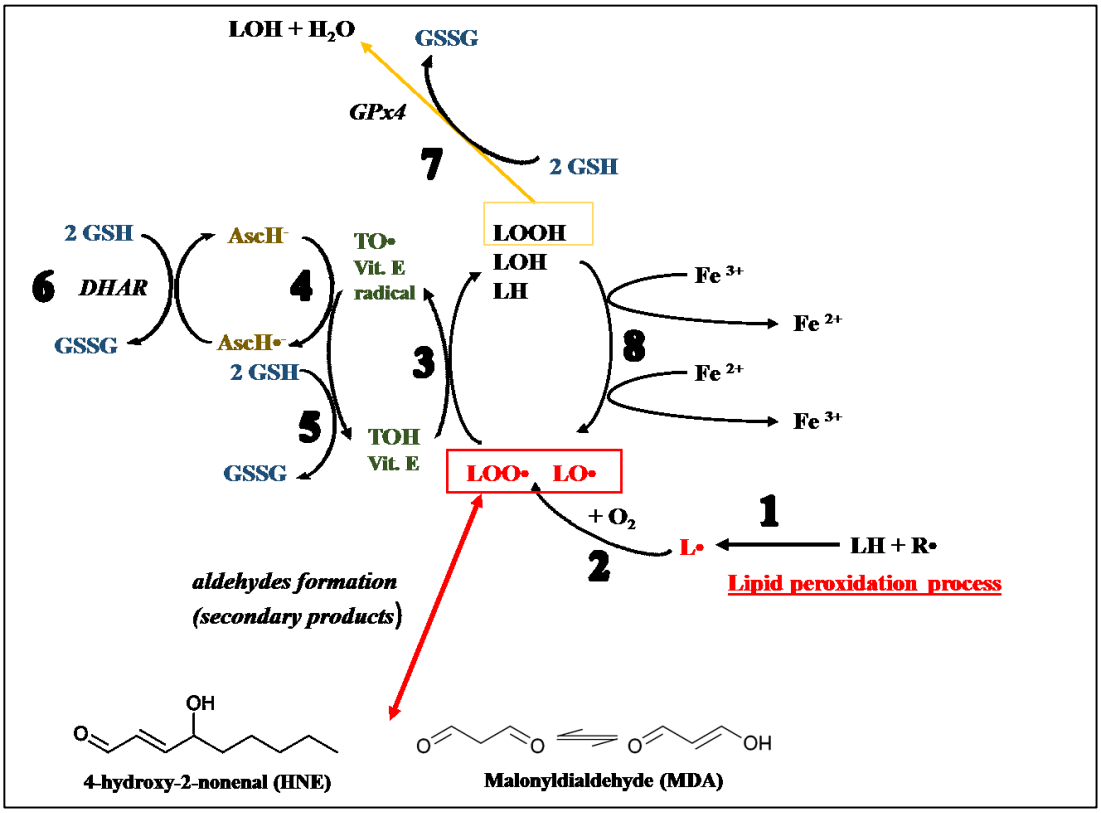

Figure 4. **Role of antioxidants in the management of lipid peroxidation process**. ***Reaction 1***: The generic radical (R•) can abstract an electron from a polyunsaturated fatty acid (LH) and give rise to a carbon-centered lipid radical (L•). ***Reaction 2:*** The lipid radical (L•) can further interact with O_2 to give a peroxyl radical (LOO•). ***Reaction 3***: The LOO• is reduced within the membrane by the reduced form of Vitamin E (TOH) resulting in the formation of a lipid hydroperoxide (LOOH) and a radical of Vitamin E (TO•). ***Reaction 4***: The regeneration of Vitamin E by Vitamin C: the Vitamin E radical (TO•) is reduced back to Vitamin E (TOH) by ascorbic acid (ascorbate monoanion, AscH−) leaving behind the ascorbyl radical (Asc•−). ***Reaction 5***: The regeneration of Vitamin E by GSH: the oxidised Vitamin E radical (TO•) is reduced by GSH and GSSG is formed. ***Reaction 6:*** The ascorbyl radical (Asc•−) is reduced back to ascorbate monoanion, AscH−, by GSH. ***Reaction 7***: Lipid hydroperoxides are reduced to alcohols and water by GPx4 using GSH as the electron donor. ***Reaction 8***: Lipid hydroperoxides can react with Fe^{2+} to form lipid alkoxyl radicals (LO•), or with Fe^{3+} to form lipid peroxyl radicals (LOO•). ***Reaction 9:*** The peroxidation reactions leads to the production of several aldehydes such as malonyldialdehyde (MDA) and 4-hydroxy-2-nonenal (HNE).

The LPO alters the functions of the cells and their survival, since membranes form the basis of many cellular organelles like mitochondria, plasma membranes, lysosomes,

peroxisomes, reticulum endoplasmic, etc. Moreover, the damage associated to LPO may also impair the efficiency of liposomial dispersion containing PUFAs as drug delivery systems. Thus, prevention of LPO represents an interesting therapy in many diseases and pathologies involving free radicals and is an important aspect in the preparation and preservation of liposomes used as carriers for several agents in medicinal, pharmaceutical, cosmetic and food industry applications.

In addition to the changed characteristics of cellular membranes, the peroxidation reactions lead to the production of several aldehydes that, as well as ROS, exhibit high reactivity with biomolecules, such as proteins, nucleic acids and phospholipids. Compared with free radicals, aldehydes are highly stable and spread out from the cell attacking targets far from the site of their production. About 32 saturated and unsaturated aldehydes are identified as products of lipid peroxidation. Among them, unsaturated 4-hydroxy-2-nonenal (HNE) is the most important aldehydes causing cellular damage (**Fig. 4**) (Uchida, 2003; Uchida, 1992). The hydroxyl-group close to a carbonyl group present in HNE chemical structure is related to its high reactivity. In particular, this lipidic product reacts with proteins and phospholipids thus modifying their structure and therefore their functions (Uchida, 2003; Uchida, 1992). Instead, the malonyldialdehyde (MDA) (**Fig. 4**), considered for a long time the most important lipid peroxidation metabolite, is practically no toxic (Uchida, 2003; Uchida, 1992).

1.3.3. Proteins

The ROS attack on proteins, results in specific amino acid modifications, fragmentation of the peptide chain, aggregation of cross-linked reaction product, alteration of electrical charge and increased susceptibility to proteolysis (Butterfield et al, 1998). The mainly amino acids susceptible to oxidation by ROS is the sulphur containing amino acids such as methionine and cysteine that are converted to disulphides and methionine sulphoxide (Pryor et al, 1994; Brodie and Reed, 1990) respectively. The ROS oxidize also others amino acid residues such as lysine, proline, threonine and arginine and yields carbonyl derivatives that have been considered as the marker of ROS mediated protein oxidation

(Chevion et al, 2000). Oxidative degradation of proteins is enhanced by the presence of metal cofactors that are capable of redox cycling.

1.4. Essential role of antioxidants in protection against oxidative stress

The cellular antioxidant defense system comprises both enzymatic and non-enzymatic mechanisms that are usually distributed within the cytoplasm and various cell organelles. Moreover, the protection against ROS is also supplied by non-enzymatic exogenous antioxidants, which cannot be synthetizes endogenously by humans.

The major endogenous antioxidant enzymes directly involved in the neutralization of ROS and other free radicals are superoxide dismutase (SOD), catalase (CAT), glutathione peroxidase (GPx) and glutathione reductase (GR) **(Figure 5)**.

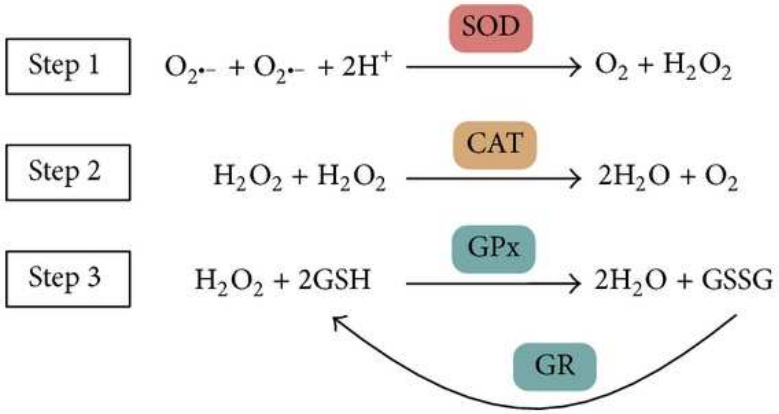

Figure 5. Main enzymatic antioxidant defense system in vivo and their reactions on scavenging free radicals and hydrogen oxide. SOD, superoxide dismutase; CAT, catalase; GPx, glutathione peroxidase; and GR, glutathione reductase.

These enzymes are the main defense system against ROS *in vivo*. The Superoxide dismutase (SOD) is the most powerful antioxidant in the cell. It acts as a component of first line defense system against reactive oxygen species (ROS) catalyzing the dismutation of two molecules of superoxide anion radical ($O_2^{\bullet-}$), a precursor of several other ROS, to hydrogen peroxide (H_2O_2) and molecular oxygen (O_2) (**Fig. 5**, Step 1). The SOD category comprises metalloenzymes and although they differ in respect to their metal cofactor, all isoenzymes catalyze the same reaction. The three isoforms of SOD present in humans are CuZnSOD (SOD1), which mainly exist in

the cytoplasm, MnSOD (SOD2), located in the mitochondrial matrix, with manganese being present in the active site, and an extracellular Cu-Zn containing SOD (EC-SOD or SOD3) (Nozik-Grayck et al, 2005). Compartmentalization of different forms of SOD provides an important mechanism for fine spatial control of ROS homeostasis. The importance of SOD isoforms is manifested by severe pathologies associated with the lack of this enzyme in mouse models (Lee et al, 2013; Kliment et al, 2009). In addition, the levels of all SOD isoforms decline with age, whereas free radical formation increases. It has been suggested that proper daily SOD supplementation could protect the immune system, thus reducing the development of age-related diseases, and ultimately slows down aging process (Krishnamurthy and Wadhwani, 2012). The human catalase (CAT) is a heme enzyme using iron as cofactor. It catalyzes the degradation or reduction of two molecules of hydrogen peroxide (H_2O_2) to two water molecules and molecular oxygen, consequently completing the detoxification process started by SOD (**Fig. 5**, Step 2). It is found mainly in peroxisomes but it is absent in mitochondria of mammalian cells (Schrader and Fahimi, 2006). This implies that another enzyme known as glutathione peroxidase carries out the scavenging of hydrogen peroxide. The deficiency or mutation of CAT enzyme have been linked with various disease conditions and abnormalities (Góth et al, 2004) such as colorectal cancer, type 2 diabetes mellitus and retinal disorders. The glutathione peroxidase (GPx) enzyme converts GSH into GSSG and, during this process, reduces H_2O_2 to H_2O (**Fig. 5,** Step 3) and lipid hydroperoxides (LOOH) to the corresponding alcohols (**Fig. 4**; Eq. 18). Generally, its activity depends on a micronutrient cofactor known as selenium. For this reason, GPx is often referred to as a selenocysteine peroxidase. The GPx reaction couples to glutathione reductase (GR), which maintains reduced GSH levels (**Fig. 5**). There are eight GPx enzymes in humans and the GPx4 is the only isoform of GPx that breaks down phospholipid hydroperoxides (Ighodaro and Akinloye, 2017). Therefore, GPx4 enzyme is essential in inhibition of lipid peroxidation process (Gill and Tuteja, 2010), lipid signaling functions, such as that of the 12/15-lipoxygenase-induced apoptosis and regulation of inflammatory responses (Conrad and Friedmann, 2015; Toppo et al, 2009).

The non-enzymatic antioxidants involved in the protection against ROS and oxidants comprise endogenous and exogenous antioxidants, also called metabolic antioxidants and nutrient antioxidants respectively. Examples are GSH, metal-chelating proteins, antioxidants vitamin such as vitamin E and C, flavonoids, trace metals (selenium, manganese, zinc), etc.

The GSH is a tripeptide constituted from glutamic acid, cysteine and glycine. The sulfhydryl group (SH) of cysteine is the functional group of the molecule, responsible for its biological activity. The thiol group of GSH is a potent reducing agent, rendering GSH able to scavenge many dangerous endobiotic and xenobiotic electrophiles, both through direct or indirect enzymatic reactions (Birben et al, 2012; Galano and Alvarez-Idaboy, 2011). This ubiquitous molecule is the main low-molecular-weight thiol found in living cells, also considered one of the major non-protein defenders against oxidative stress and the most important thiol-disulfide redox buffer of the cell. As described above, the GSH acts as a substrate for H_2O_2-removing enzymes and it is a cofactor of other enzymes such as glutathione transferase. The glutathione is also able to regenerate the most important antioxidants, Vitamins C and E, back to their active forms; glutathione can reduce the tocopherol radical of Vitamin E directly, or indirectly, via reduction of semidehydroascorbate to ascorbate (**Fig. 4**).

The metal-chelating proteins as ceruloplasmin, ferritin, transferrin and albumin, inhibit the formation of new reactive species by binding transition metal ions (e.g. iron and copper).

Vitamin E (the most biologically active form is -tocopherol) is a key essential fat-soluble vitamin with high antioxidant potency. Because of its fat-solubility, α-tocopherol safeguards cell membranes from damage by free radicals. *In vivo* and *in vitro* studies have shown that vitamin E acts as a chain-breaking antioxidant protecting unsaturated lipids from peroxidation by scavenging peroxyl radicals (**Fig. 4**). Animals and humans with a low vitamin E status present several problems at muscles and at neurological level that have been related to the protective effects of vitamin E against damage to PUFA in cell membranes and confirm its role as an essential nutrient. Vitamin E has shown to prevent several diseases development such as colon and breast cancer, arthritis and certain neurological disorders (Traber and Stevens, 2011; Traber, 2014). Moreover, the high dietary intake of vitamin E appears to decrease the risk of cataracts (Tavani et al, 1996; Theodoropoulou et al, 2014) and age-macular degeneration (AMD) (van Leeuwen et al, 2005; Bibiloni et al, 2014). However, despite its reputation of being healthy, vitamin E has a dark side: Mitchel et al. (Mitchel and McCann, 1993) have shown that vitamin E owns tumor-promoting activity in the skin of mice; in one *in vitro* model, in the presence of Cu^{2+}, α-tocopherol shows an oxidative DNA-damaging effect (Yamashita et al, 1998). Finally, the α-Tocopherol can also reduce iron or copper, as a pro-oxidant (Yamamoto and Niki, 1988). Therefore, the benefit or the dangerous effect of vitamin E appears to be associated with its concentration.

Zinc (Zn), copper (Cu), manganese (Mn), and selenium (Se) ions are the key components of enzymes with antioxidant function, and are designated as antioxidant micronutrients. For examples, Zn, Mn, and Cu ions are cofactors of superoxide dismutase (Cu/Zn-SOD) while the selenium is essential for GPx activity. Vitamin C or ascorbic acid, which is the primary antioxidant in plasma and cells, must be provided from fresh fruits and vegetables since the humans are not able to synthesize it.

CHAPTER II
Ocular Diseases Associated with Oxidative Stress

2.1. Introduction

The eye is one of the highest oxygen-consuming tissue in the human body and the mainly part of the body normally exposed to light. Thus, oxidative and particularly photo-oxidative damage occurs in the eye causing from ocular to retinal diseases. Most of them are linked with aging that has been defined as "the progressive accumulation of changes with time that are associated with or responsible for the ever-increasing susceptibility to disease and death which accompanies advancing age" (Harman, 1981). The eye is one of the organs subjected to the processes of aging in which antioxidant level declines and ROS level increases, ensuring oxidative stress. By aging, glutathione S-transferase-1 expression level (Hammond et al, 1997), and vitamin E level (Hammond et al, 1998) decrease while lipofuscin (Hammond et al, 1997), mitochondrial DNA damage, and lipid peroxidation (Hammond et al, 1997) increase. These processes can lead to functional and morphological impairments in retinal pigment epithelium (RPE), endothelial cells, lens epithelium cells (LECs) and retinal ganglion cells (RGCs).

There are mainly ocular disorder linked with oxidative stress including the age-related macular degeneration (AMD), cataracts and dry eye disease (DEA). I will briefly discuss the pathologies in which the oxidative stress play pivotal roles in their development and in which the uses of antioxidants may be an effective therapeutic strategy.

2.2. Age-related Macular Degeneration (AMD)

Age-related macular degeneration (AMD) is the leading cause of permanent and irreversible blindness in elderly individuals throughout the world, and approximately 50 million people suffers of AMD (Gordois et al, 2012). The disease affects the macula at the center of the eye, which may lead to a partial or complete vision loss in one or both eyes in older people (age > 55 years). The rise in life expectancy has determined the increase in the absolute number of affected people globally (Williams et al, 1998; Gordois et al, 2012).

AMD is classified into two types: “dry” and “wet” that account for about 85% and 15% of cases respectively (Bhutto and Lutty, 2012; De Jong, 2006). However, dry-type AMD pathology may progress to the wet-type AMD, which contributes to rapid loss of vision (Fine et al 2000). The wet-type AMD also called “exudative-AMD” is the most severe form of AMD and is generally associated with subretinal (i.e. between the retina and choroid) neovascularization because of pathological angiogenesis: the use of antiangiogenic agents (e.g. Lucentis and Avastin) can ameliorate the patients conditions (e.g. Lucentis and Avastin) (Andreoli and Miller, 2007). In the dry-type AMD the visual loss is caused mainly by the “geographic atrophic” death of photoreceptors and retinal pigment epithelial (RPE) cells. It is typifies over that by cell loss, also by oxidative stress, drusen (yellow deposits located under the retina), and the lipofuscin accumulation. All these characteristic represent the diagnostic features of dry-type AMD (Bhutto and Lutty, 2012). Apart from positive correlation of the disease with age, other risk factors are cigarette smoking, white race, female sex, blue iris colour, obesity, nutritional factors and insufficient antioxidants in the diet (Kaarniranta et al. 2011).

Retinal cells are in fact highly metabolically active and are constantly exposed to light thus representing an ideal environment for the generation of reactive oxygen species, especially with increasing of age. As mentioned above, the retina is one of the highest oxygen consuming tissues in the human body and consequently a large oxygen gradient is created from the choroid and its associated vasculature towards the inner retina and residing photoreceptors. Instead, the continuous exposition to light generates the photon flux across the retina in which photosensitizer are most abundant, leading to light-induced reactive oxygen species. More in details, radiation reaching the eye is partially absorbed by the cornea and the lens, but the rest of it (400–760 nm) penetrates the eye reaching the retina. The sensitivity of the retina to light damage is dependent both to wavelength light, which is greater with shorter wavelength light, and duration of exposure (Wiegand et al, 1983). At a retinal level, the visible light stimulates RPE cells to phagocytosis (ingestion) of rod outer segments thus inducing the formation of superoxide anion (**Figure 6**).

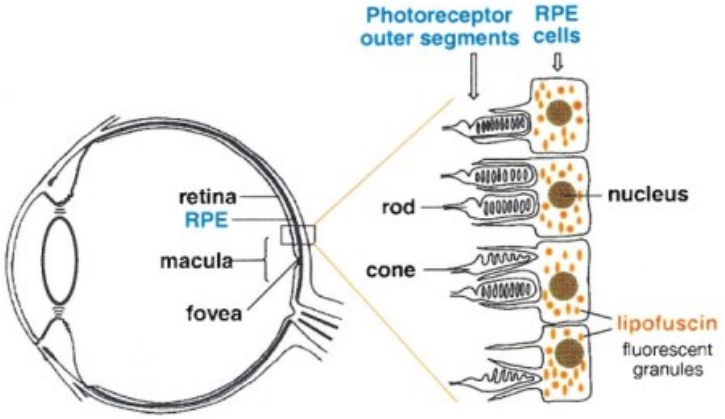

Figure 6. Diagram of the eye. The macula is the central portion of the retina, which contains photoreceptor cells (rods and cones) adjacent to a monolayer of RPE. In this cartoon, the outer segment to RPE ratio is simplified for clarity. RPE, retinal pigment epithelium. From Ben-Shabat et al, 2001.

Epidemiological evidences suggest a direct relationship between phototoxicity (cumulative light exposure) and the development of AMD (Hunter et al, 2012). Since the photoreceptors and retinal synapses are rich in polyunsaturated fatty acids, the retina is also particularly vulnerable to auto-oxidation. In fact, the polyunsaturated fatty acid docosahexanoic acid (DHA) (22:6ώ-3) represents the 30-50% of the lipid bilayer of rod outer segment membranes, and proteins make up the remaining percentage (Stone et al, 1979). This very high proportion of long-chain PUFAs is a feature unique of the retinal lipids. Their oxidation leads to the development of high levels of peroxides and organic radicals, as well as other secondary products such as 4-HNE, which form adducts with proteins thus accumulating in the retina. The results of lipid peroxidation is the functional and structural impairment of cell membranes and finally leads to the degeneration of photoreceptors. Furthermore, oxidized PUFAs are not efficiently digested in the lysosomes of aged RPE cells and become deposited in the form of lipofuscin that represents the main component of drusen (**Figure 6**). As described above, the lipofuscin is a RPE photosensitizer that, after having absorbed a high-energy photon especially that of blue light, undergoes a variety of photochemical reactions. One of the formed reactive photoproducts is the N-retinylidene-N-retinylethanolamine A2E that represents the main fluorophore of RPE lipofuscin and it is responsible of singlet oxygen and superoxide generation (Sparrow et al. 2000). Indeed, the elevated level of lipofuscin may induce apoptosis. Since RPE cells are postmitotic, their death result in the reduction of RPE cell density in the RPE layer (Del Priore et al. 2002). Thus, the oxidative stress increases and the antioxidant molecules level declines, resulting in pathogenic process. Therefore, effective ROS scavenging may be essential for preventing and/or treatment AMD.

Natural and synthetic antioxidants as ascorbic acid (Organisciak et al, 1985) and ginkgo biloba extract (Ranchon et al., 1999) prevent retinal light damage and photoreceptor cell loss; they probably act as antioxidants during light exposure. The same effect has epigallocatechin- 3-gallate (EGCG), a major polyphenol in green tea, which is able to protect human retinal pigment epithelium (ARPE-19) cells from viable blue light-induced disorders (Li et al, 2014). Others, including saffron (Maccarone et al., 2008) and sulforaphane (Tanito et al, 2005), induce the synthesis of antioxidant enzymes. Synthetic antioxidants that have also protective and curative effect on ADM are free radical spin trap such as phenyl-N-tert-butylnitrone (PBN) that catalyzes the degradation of superoxide (Ranchon et al, 2001). The synthetic Edaravone (3-methyl-1-phenyl-2-pyrazolin-5-one), a free radical scavenger which will be widely described in the followed chapter, has shown to be effective against retinal degeneration both *in vivo* and *in vitro* (Imai et al, 2010; Masuda et al, 2016).

2.3. The Role of ROS and the Oxidative Stress in Cataractogenesis

Cataract, as well as AMD, is one of the leading causes of blindness in the world affecting about 25 million people (World Health Organization, 2009). The pathology is characterized by progressive loss of transparency of the eye lens that results in visual impairment. The transparency of the eye lens depends on maintaining the native tertiary structures and solubility of the lens crystallin proteins over a lifetime.

The cataract formation is caused by several factors (genetic factors, diabetes, aging, smoking, drugs, malnutrition, and radiation) but the free radical induced oxidative stress is considered as one of the major underlying mechanism of cataract disorder (Beebe et al, 2010). The UV radiation represents the mainly contributory factor to oxidative damage of the lens tissue. As widely discussed, the UV light induces the photochemical generation of ROS resulting in oxidation of proteins, nucleic acid and lipid. However, the opacity of lens is mainly caused by protein oxidation and altered redox balance. Over 90% of crystalline protein sulfhydryl (protein-SH) groups are lost and as a consequence the cross link by non-disulfide bonds may occur (Berthoud and Beyer, 2009). The result is the insolubilization of the lens crystallins and this is the major cause of the yellow color residing in the lens. The toxic product such as HNE, produced during lipid peroxidation processes, induces the fragmentation of lens proteins contributing towards the opacity of the lens. The light absorbed by cornea may activate the

tryptophan amino acids, forming several photoproducts (Boettner and Walter, 1962). These photoproducts gradually accumulate in the center of the lens and successively bind to the crystalline proteins thus altering their electrical and solubility properties. Such a process may be involved in human lens browning and brunescent cataracts (Zigman et al, 1973). The loss of glutathione is a crucial feature that precedes cataract formation (Giblin, 2000). GSH is the essential and primary lenticular antioxidant (Reddy, 1990) and provides the maintenance of the lens transparency by scavenging ROS and protecting protein thiols.

Several *in vitro* and *in vivo* studies have shown how the antioxidant molecules can prevent or delay the light-induced protein oxidation as well as photoperoxidation of lens lipids. The key player in the protection of the lens from oxidation is the vitamin C, which plays an important part in lens biology, both as an antioxidant and as a UV filter when present in aqueous (Hegde and Varma, 2004). The supplemental of Vitamin E decreases the lens opacity in human (Seth and Kharb, 1999). Even here, the EGCG molecules are able to prevent the tryptophan oxidation thus protecting the γB-crystallin and lens epithelial cells in humans from UV-induced damage (Chaudhury et al, 2015). The lycopene carotenoid as well as the curcumin, the active principle of turmeric, protect against oxidative stress-induced experimental cataract (Gupta et al, 2003; Padmaja and Raju, 2004).

2.4. Tear Film and its dysfunction in Dry Eye Disease (DEA)

The International Dry Eye Workshop (DEWS) defines dry eye as a multifactorial disease of the tears and ocular surface that results in symptoms of discomfort, visual disturbance and tear film instability with potential damage to the ocular surface. It is accompanied by increased osmolality of the tear film and inflammation of the ocular surface (Lemp, 2007).

The tear film (TF) is a liquid layer covering the cornea and acting as a barrier between the eye and environment. Acting as a shield of our ocular surfaces, its damage results in several symptoms, most of which have been associated with Dry Eye Syndrome (DES).

The tear film serves to remove foreign materials from the cornea and conjunctiva; to supply the cornea with nutrients by transporting oxygen and a limited number of other nutrients; to maintain a smooth surface for light refraction. Moreover, it has a lubricating power and contains immunoglobulins, lysozymes, lactoferrin which are involved in infections protection (Lakshmi, 2014).

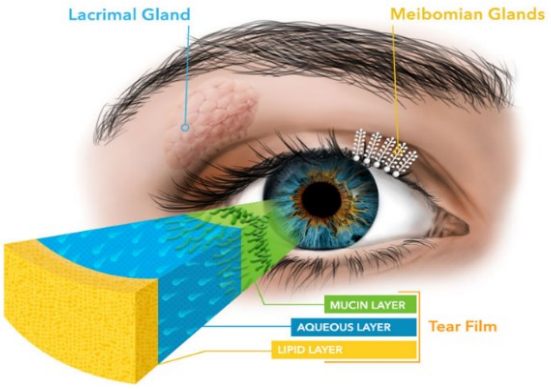

Figure 7. Tear film layers.

The tear film is divided into three layers: the innermost mucin-rich layer, an aqueous layer in the middle, and the outermost tear fluid lipid layer (TFLL) (**Figure 7**). The mucin (mucous) layer at the bottom of the tear film provides a "sticky" foundation and acts as a barrier in the eye surface. The mucus helps the overlying watery layer to spread evenly over the eye. The aqueous layer is the "juicy" center and contains essentially a very dilute saltwater solution (Lakshmi, 2014). It is comprised of tears produced by the lacrimal glands. This layer keeps the eye moist and helps in the removal of any dust, debris, or foreign particles. Defects of this layer cause DES in most cases (Lemp, 1995). Finally, the top "oily" lipid layer of the tear film is made up of lipids or oils produced from the meibomian glands. This layer helps to decrease evaporation of the watery layer and it is very important for stability of tear film.

Causes for DES include decreased tear production, excessive tear evaporation, and abnormality in the production of mucus or lipids of tear layer by meibomian gland. As a consequence, the concentration of solutes in the aqueous layer increases leading to hyperosmolarity of the tear film. This condition causes dryness and irritation and is associated with symptoms of discomfort (Lemp, 2007).

Epidemiological studies have shown that the incidence of dry eyes increases with age (Viso et al. 2009) and therefore with increased oxidative stress. Transgenic animal's model with compromised antioxidant defenses have shown decreased production of tears, increased meibomian gland dysfunction (Ibrahim et al. 2014) and increasing ROS formation resulting in dry eye. Moreover, the hyperosmolarity of tears contributes to increase oxidative stress (Deng et al, 2015).

Many clinical trials have in fact suggested that oxidative stress can be a potential therapeutic strategy in dry eyes (Seen and Tong, 2018). Supplementation with oral antioxidants may

improve both tear stability and quantity (Drouault-Holowacz et al, 2009). Topical application of herbal extracts also improved clinical signs, decreased inflammation, and ameliorated oxidative stress marker as well as the ROS production on the ocular surface of the DES in model mice (Choi et al, 2016). In addition, lipids are helpful in attempting to supplement abnormal lipid production. In fact, the oily component can merges with the natural lipid layer reducing evaporative fluid loss.

2.5. Management of ocular diseases – limitation and therapeutic interventions

Oxidative stress can be reduced with systemic interventions in the form of dietary supplements, vitamins, omega-3 fatty acids, exercise, etc. However, these have antioxidant effects elsewhere in the body apart from the lacrimal glands and the ocular surface. Therefore, the ocular drug delivery requires different routes of administration including intravitreal and topical administrations. Although the intravitreal route has high therapeutically efficacy, it is associated with potential risks of complications (Gaudana et al, 2010): as a consequence, the topical application of drugs, typically in the form of eye drop formulations, represents the most common method of drug delivery for the treatment of ophthalmic ailments. This conventional dosage forms account for nearly 90% of currently available marketed formulations thanks of their simplicity, safety and acceptance by patients. However, achievement of adequate bioavailability of topically applied drugs is challenging due to unique anatomical and physiological barriers at the ocular surface that determines a low drug adsorption of about 5% (Urtti and Salminen, 1993).

Two major barriers to topical ocular drug delivery are present **(Figure 8)**.

- ***Precorneal tear film***. As described above, an intact tear film is essential for a healthy ocular surface and its alteration has been associated with DES. However, for the penetration of drugs applied topically to ocular surface, tear film is a significant barrier. First, the tear film is subjected to a high turnover rate: reflex tearing, which may occur after drug instillation, results in an accelerated washout of the drug after application. Moreover, blinking creates a pumping mechanism to facilitate the flow of tears into the nasal cavity thus resulting in drug loss (Peters and Colby, 2006). The presence of gel-like mucus layer, which has a protective role for the ocular surface, also acts as a barrier to drug delivery systems.

- C*orneal epithelium*. The epithelium of the cornea is in continuation with the conjunctiva and consists of 5–6 layers of cells packed closely and connected by tight junctions. These layers form a lipophilic barrier against water-soluble drugs. In particular, in order to penetrate these layers the optimal drug lipophilicity corresponds to log D values of 2–3 (Mannermaa et al, 2006). The presence of conjunctival blood capillaries and lymphatics can also cause significant drug loss into the systemic circulation, thereby lowering ocular bioavailability (Peters and Colby, 2006).

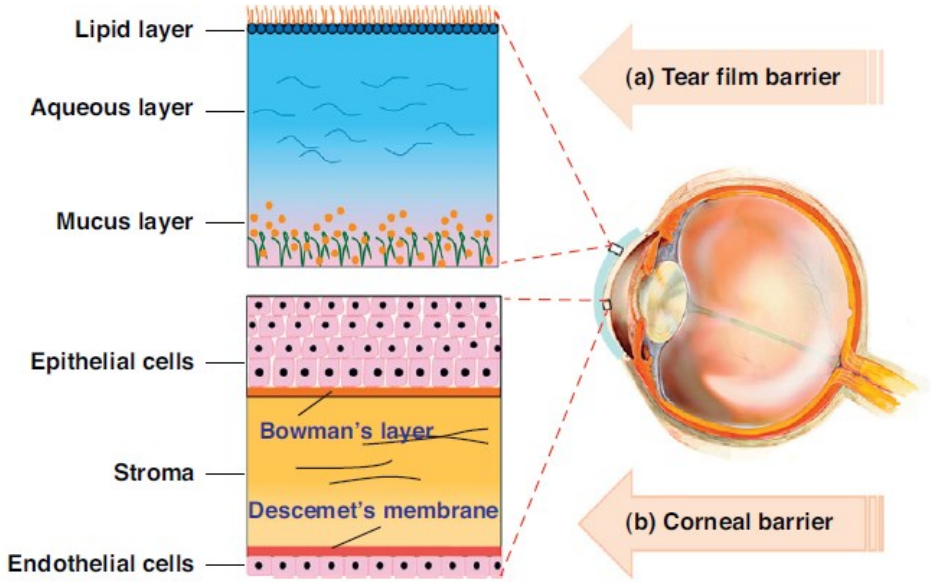

Figure 8. Two major barriers to topical ocular drug delivery. **(a)** Tear film barrier: a high turnover rate and the gel-like mucus layer make tear film a barrier in topical ocular drug delivery. **(b)** Corneal barrier: tight junctions exist in the corneal epithelial cells. Moreover, five layers of alternating polarity make the cornea an important barrier to most lipophilic and hydrophilic drugs. From Gan et al, 2013.

Finally, the enzymatic degradation in tears and cornea reduces the ocular bioavailability of drugs (Lee et al, 1982). Therefore, eye drops are normally administered multiple times daily in order to achieve therapeutic efficacy.

In order to circumvent the permeation barriers for topically applied drugs, several ophthalmic drug delivery strategies have been emerged. These include hydrogels, polymeric micelles, nanosuspensions and lipid based-nanocarriers. Among them, the lipid-based nanocarriers are the most biocompatible and offer potential advantages as delivery systems for ocular

administration (Gan et al, 2013). As illustrated in **Figure 9**, the interactions between oil-in-water (o/w) emulsions and the tear film increase the bioavailability of the drug since:

- The lipids that make up these transport systems interact more effectively with the lipid layer of the tear film, facilitating the transport of the drug through the tear film barrier;
- Furthermore, the lipids released in aqueous solution contribute to the thickening of the superficial lipid layer, reducing the aqueous losses by evaporation resulting in enhanced tear film stability.

This intrinsic bionic tear film property of lipid-based nanocarriers makes them particularly suitable for the treatment of dry eye syndrome. Moreover, the lipid-based nanocarriers can be modified with mucoadhesive materials such as polymers, thus improving pre-corneal retention time and permeation (Mishra et al, 2011).

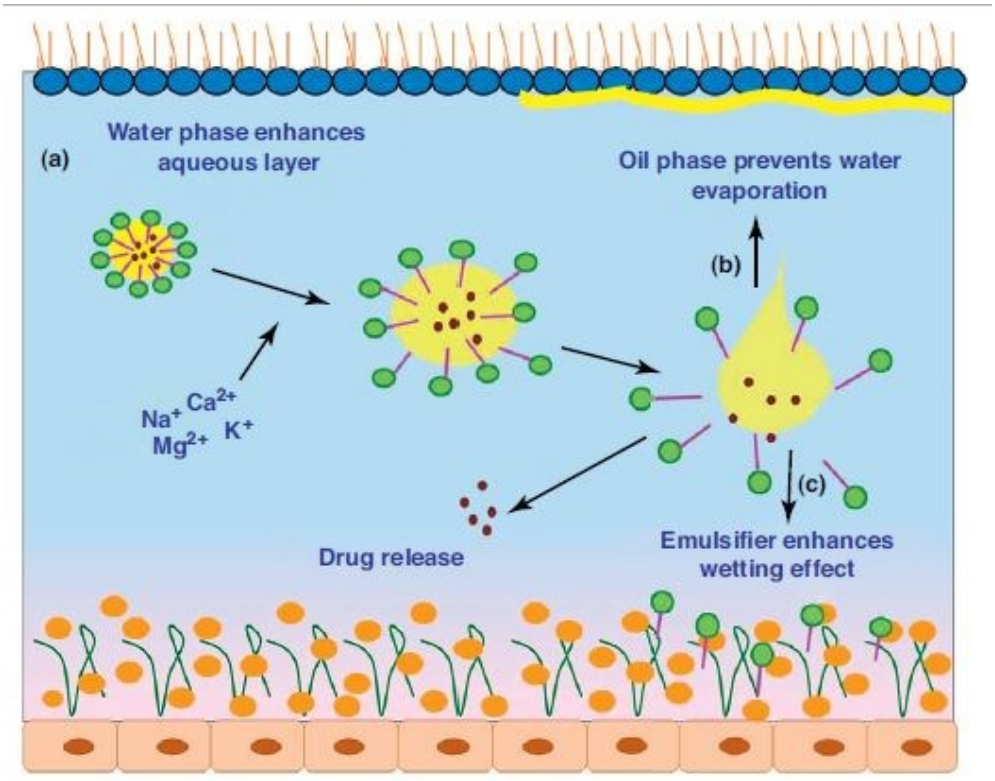

Figure 9. **Interactions between o/w emulsions and the tear film**. **(a)** After instillation, the water phase of the emulsion can enhance the aqueous layer of tear film and moisten the cornea. **(b)** As the oil droplets break down, they release encapsulated emulsion components. The oil phase then merges with the natural lipid layer and enhances it, reducing fluid loss caused by evaporation. **(c)** Emulsifiers have been found to increase the depth of the mucus layer and improve the 'wettability' of tear film.

CHAPTER III
Lipid-based nanocarriers

3.1. Lyotropic Liquid Crystals (LLC)

Lyotropic Liquid Crystals (LLC) are interesting systems to be explored in the development of lipid-based nanocarriers; they can target the anterior and the posterior ocular structure and most of them have been clinically approved (Gan et al, 2013). They are often termed "mesophases," representing intermediate states of matter between an isotropic liquid and a solid crystal (Friberg, 1977). The characteristic of the molecular structures that commonly generate LLC phases is the amphiphilicity. Molecules with a hydrophilic head and a lipophilic tail form aggregates through a self-assembly process that is driven by the "hydrophobic effect" when they are mixed with water. Simply varying composition (concentration of amphiphiles, water or additives) and temperature, a wide range of mesophases can be obtained. In the next section, I want to give a brief description of different structures observable in lipid-water systems, focusing the attention on the lipid carriers used in my PhD work.

3.2. Lipid/Water Polymorphism

Amphiphilic molecule such as polar lipids, through a self-assembly process, can form different ordered structures in an aqueous environment which can be classified into lamellar (Lα), hexagonal and cubic phases. The architecture is mainly influenced by the water concentration as well as the molecular structure of the amphiphiles. It is possible to predict the phase structure by using the critical packing parameter (CPP) (Eq. 20),

$$\mathbf{CPP} = \boldsymbol{v} / \boldsymbol{a}\,\boldsymbol{l} \qquad \text{(Eq. 20)}$$

where (*v)* is the volume of hydrophobic liquid tail, (*a)* is the cross-sectional area of the head group, and (*l)* is the length of the lipid chain (Israelachvili, 1992). This critical packing parameter (CPP) enables the determination of the preferred structures formed because it estimates the lipid layer curvature. Lipids with CPP = 1 usually self-assemble into planar or

bilayer structures with zero mean curvature and bilayer lamellar structures are formed. When CPP < 1 the polar heads of the lipids form a convex interface and "normal oil in water" morphologies (Type 1) with positive curvature are formed including spherical micelles. On the contrary, if the CPP > 1, the curvature is towards the aqueous environment, resulting in negative curvature with "inverse water in oil" (Type 1) structures such as reversed bicontinuous cubic (QII) phase and the reversed hexagonal (HII) phase (**Figure 10**). By dispersion of these bulk structures in aqueous media, the main typically obtained nanostructures are liposomes, as result of the dispersion of a lamellar phase; cubosomes, formed by reversed bicontinuous cubic phase; and hexosomes, from the reversed hexagonal phase (Chang et al, 2015).

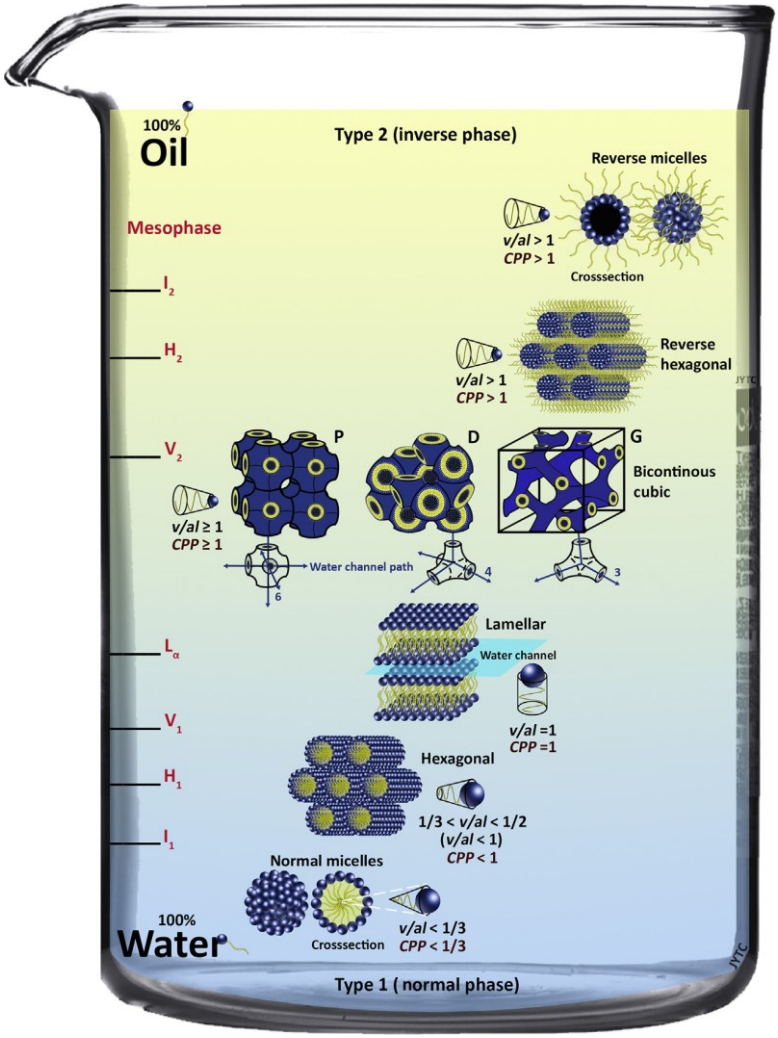

Figure 10. An illustration of the main types of lyotropic liquid crystal phases depending on the interface curvature (molecular shape or concentration in water). The mesophases are denoted as I1, I2 (discrete micellar cubic phase), H1, H2 (hexagonal phase), V1, V2 (bicontinuous cubic phase), and Lα (lamellar phase). From Chong et al, 2015.

In addition to lipid molecular geometry, many factors including temperature, pressure, light, ions, water content and additives can alter the architecture of lipid system (Venugopal et al, 2011).

3.3. Lipid-based nanocarriers relevant to topical ocular drug delivery

3.3.1. Lamellar phase: liposomes

In nanoparticle technology, liposomes are the most widely studied lamellar phases, which are formed when the CPP is equal to one (**Figure 10**). They are defined as nanosized vesicular structures consisting of an aqueous core surrounded by one or more phospholipid layers; therefore, their structure is very similar to cell membrane (**Figure 11**). Liposomes can be classified into Multilamellar Vesicle (MLV), Large Unilamellar Vesicle (LUV) and Small Unilamellar Vesicle (SUV) according to their particle size and number of lamellae. MLVs are formed by more lamellae with size ranging from 400 to 3500 nm in diameter. LUVs generally range from 200 to 1000 nm with the largest entrapment volume and the highest encapsulation efficiency. SUVs are in the range of 25 to 100 nm with the most uniform size distribution, which can be obtained from MLVs and LUVs by size reduction process (such as sonication and size extrusion).

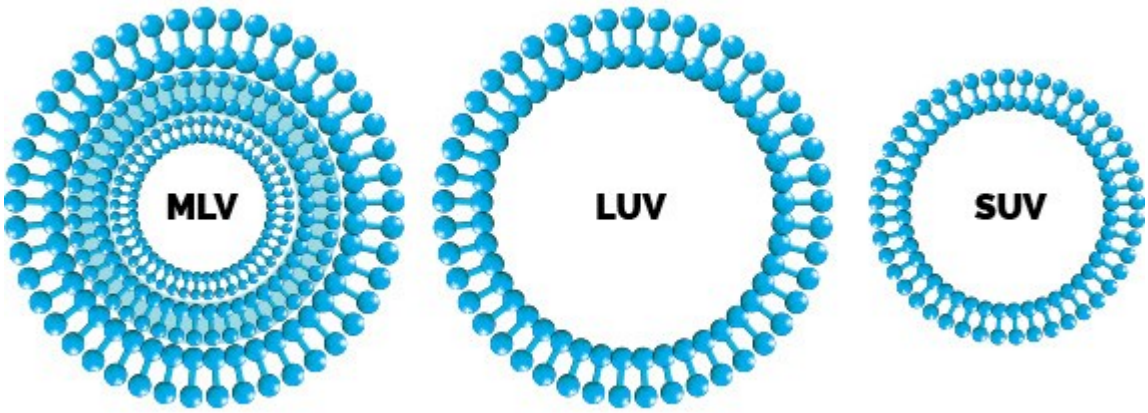

Figure 11. Schematic representation of basic structures and different types of liposome**.**

These supramolecular aggregates can encapsulate enzymatic antioxidants but also hydrophilic and lipophilic chemical antioxidants, shielding and protecting them from

inactivation or rapid clearance from cells. The use of natural phospholipid for their preparation make them highly biocompatible because the lipids can be re-utilized by the body as fuel; they represent therefore promising vector for the delivery of drugs.

The liposomal formulations were first proposed as drug delivery vehicles in ophthalmology to enhance ocular drug penetration. Several drug-loaded liposomal eye drops have been used to treat various ocular disorders of both the anterior and posterior segments, including infections, DED, corneal transplant rejection and AMD (Honda et al, 2013). When applied topically, liposomes can interact with the hydrophobic corneal epithelium and release the bound drug content thus decreasing the bioavailability of drugs. However, the major drawback of liposomes is related to their physical and chemical instability: the hydrolysis of ester bonds or oxidation of unsaturated acyl chains as well as the aggregation or fusion phenomena can change the structure of the lipid system, the load and/or release capacity. In order to overcome these problems surface modification and polymerization can be carried out: if repulsion forces are present, due to electrical charges on the particle surfaces or to the polymers adsorbed on their surface, the aggregation can be avoided. For example, the use of polymer chitosan (8 kDa) as coating agent can significantly improve the physicochemical stability of liposomes (Li et al, 2009) as well as the Poloxamer-407, which has demonstrated to prevent liposome aggregation phenomena (Minnelli et al, 2018). Moreover, the polymer can also improve the pre-corneal retention time and permeation (Mishra et al, 2011). Finally, the use of lipophilic antioxidant molecules can protect liposomes from lipid peroxidation thus improving their chemical stability.

3.3.2. Reversed bicontinuous Cubic phase and Cubosomes

Cubic phase are liquid crystalline particles formed by particular amphiphilic lipids, which can arrange in an interesting structure consisting of curved bicontinuous lipid bilayer in three dimensions, separating two congruent networks of water channels (**Figure 12**).

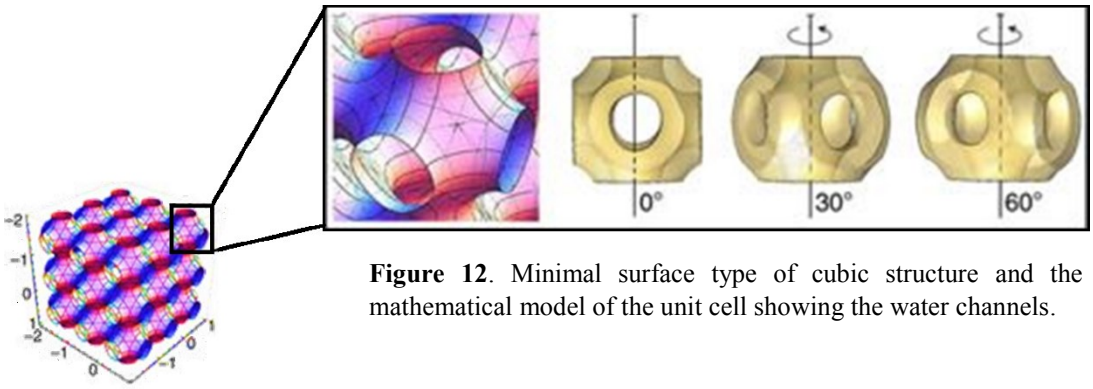

Figure 12. Minimal surface type of cubic structure and the mathematical model of the unit cell showing the water channels.

The three structures of the cubic phase, defined by crystallographic space, are: (i) diamond surface (Pn3m, Q224, D-surface); (ii) primitive surface (Im3m, Q229, P-surface); (iii) gyroid surface (Ia3d, Q230, G-surface). The corresponding aqueous channels are indicated in **Figure 13** as arrows: 3 for G, 4 for D and finally 6 for P. Cubic phases can be formed by different type of lipids such as sphingolipids, monoacylglycerides, glycolipids and also galactolipids (Fontell, 1990).

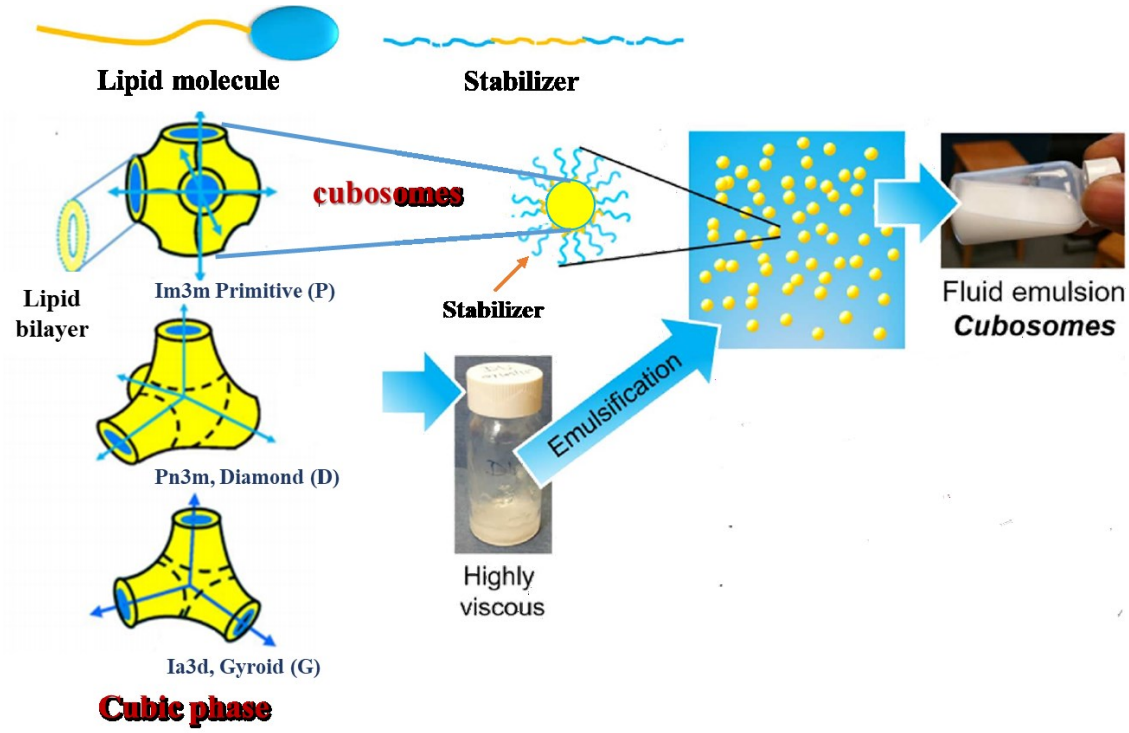

Figure 13. Schematic diagram of Cubic phases and Cubosomes. Blue and yellow indicates hydrophilic and hydrophobic parts/regions, respectively. Bicontinuous cubic phases of Im3m, Pn3m, and Ia3d types with 6, 4, and 3 corresponding aqueous channels, respectively, as represented by arrows. Highly viscous cubic phase shown at the bottom of a glass bottle. Cubosomes (left) displaying the cubic phase as an internal self-assembly (yellow circle) with surfactant molecules stabilizing the interface (blue tails), and a dispersion of such Cubosomes in the glass bottle (right). Readapted from Kulkarni et al, 2017.

They are interesting for several applications such as membrane protein crystallization, biosensor preparation, and drug delivery (Karami and Hamidi, 2016). In particular, they have been evaluated for mucosal, periodontal, transdermal and local drug delivery mainly owing to their bioadhesion properties and high loading capacity. Despite these amazing properties, the application of cubic phases in ocular drug delivery is limited because of their high viscosity. The emulsification of cubic lipid phases in water results in the production of cubosomes that can be defined as submicrometer disperse systems termed cubosomes that retain the internal structure of the nondispersed cubic phase (**Figure 13**) but unlike them, much lower viscosity. The particles are not colloidally stable and are typically dispersed with the addition of a stabilizer, such as the polymer Poloxamer-407 (Chong et al, 2015).

Since cubosomes are characterized by high biocompatibility and bioadhesivity (Larsson, 2000), these versatile delivery systems can be administered by different routes (such as orally, parenterally, or topically) and therefore they are used in several fields. Compared to liposomes, the cubosomes possess higher physiochemical stability due to the strong steric repulsion (Salonen et al, 2010; Gordon et al, 2012). Moreover, the microstructure of cubosomes is similar to that of biological membranes leading the lipid carrier to fuse with the lipid bilayer of the tear film (Zhang and Wang, 2009; Gan et al, 2013). Thanks to their unique bicontinuous structure, they are also employed as controlled release delivery systems (Larsson, 2000; Boyd, 2003) making the cubosomes a drug reservoir that releases the drug in the aqueous layer of tear film. In addition, they are low-irritant vehicles for ocular surface (Han et al, 2010) and, thanks to their bioadhesion properties; cubosomes can improve the pre-corneal retention time representing therefore an interesting drug delivery system for ophthalmic applications.

PART II – Natural and functionalized Epigallocatechin-3-gallate (EGCG) as components of lipid-based eye drops

"Success is the ability to go from one failure to another with no loss of enthusiasm"
-Winston Churchill-

CHAPTER IV

Epigallocatechin -3-gallate (EGCG)

4.1. Antioxidant Properties

Among the pool of antioxidant molecules used for ophthalmic formulations, I focused my attention on epigallocatechin-3-gallate (EGCG), which is well known for being bioactive in age-associated pathologies where oxidative stress plays a preeminent role (Mandel et al, 2011; Frei et al, 2003) including AMD, cataract and DEA.

EGCG is the most abundant catechin in green tea and accounts for 55 up to 79 % of the total catechin content. The EGCG structure presents a benzenediol ring (label A) joined to a tetrahydropyran moiety (C), a pyrogalloyl ring (B) and a galloyl ring (D) (**Figure 14**).

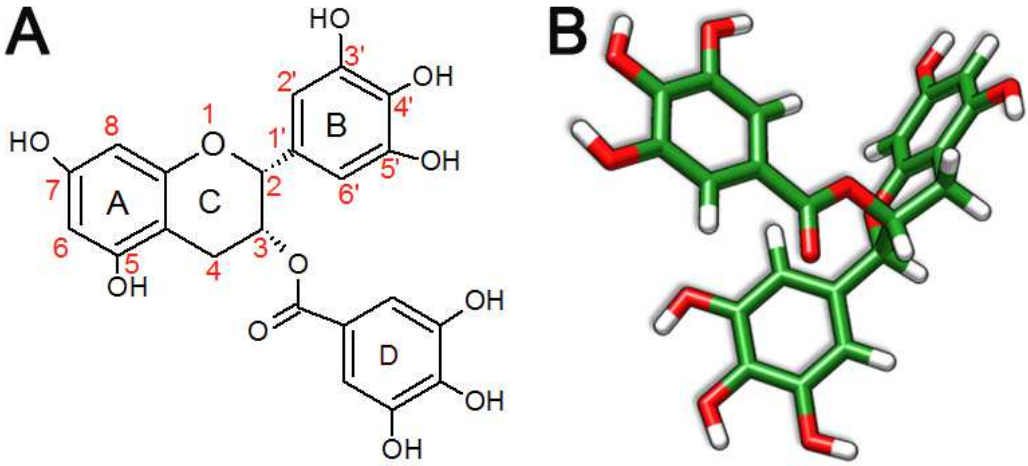

Figure 14. Epigallocatechin 3-Gallate structure. (A) shows 2D structure, (B) shows 3 D structure.

The antioxidant power of this molecule is mainly due to three mechanisms: (i) radical scavenging activity, (ii) chelating activity and (iii) ability to induce the expression of antioxidant enzymes (**Figure 15**).

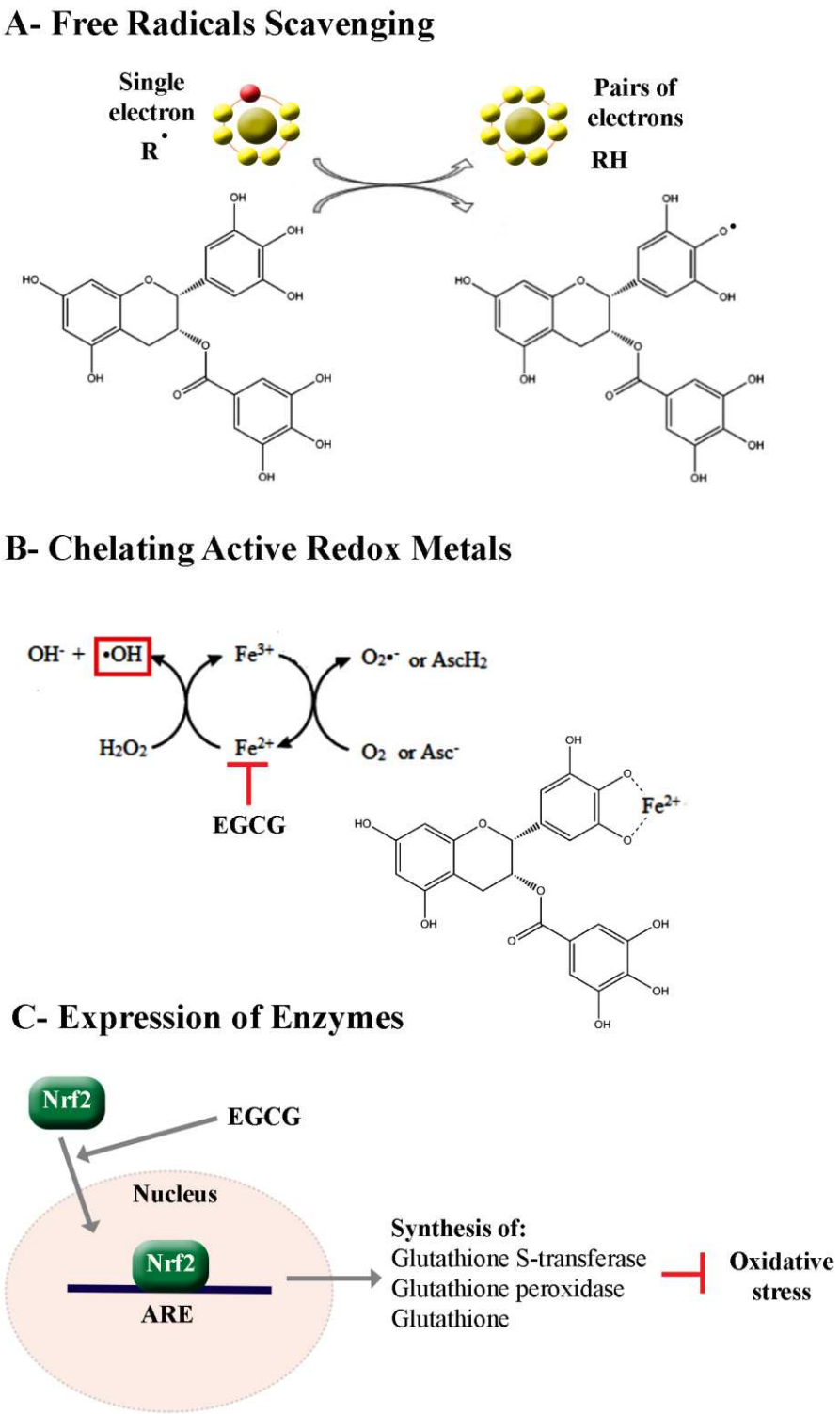

Figure 15. EGCG can exert direct antioxidant effects by **(A)** free radicals scavenging activity, **(B)** chelating redox-active metals and **(C)** induction of the expression of antioxidant enzymes.

One hypothesis to explain EGCG powerful antioxidant activity is the low reduction potential due to its high capacity for giving an electron (Higdon and Frei, 2003). For green tea catechins, the antioxidant potential mainly comes from the strong presence of hydroxyl groups in their

molecular structure; EGCG, with 8 hydroxyl groups notably in 3', 4' and 5' positions and with a gallate moiety in C-3 is a better electron donor than the others catechins and thus the best scavenger of free radicals species (Higdon and Frei, 2003).

As free radical scavengers, EGCG can react towards both superoxide and hydroxyl radicals as well as nitric oxide and others Reactive Nitrogen Species (RNS). It can act as chain-breaking antioxidant by trapping the peroxyl radicals and thus suppressing radical chain autoxidation in the lipid peroxidation processes (Salah et al, 1995). The EGCG antioxidant efficacy is due to its particular structure (**Figure 15A**) (Nanjo et al, 1999):

(i) catechin can donate one-electron of phenolic OH groups to reduce free radicals;

(ii) the aromatic group stabilizes by resonance the resultant aroxyl radical (Rice-Evans, 1999). For example, the peroxyl radical will get the electron of the catechins, resulting in breaking the free radical chain reaction (Eq. 21).

$$LOO^{\bullet} + EGCG\text{-}OH \rightarrow LOOH + EGCG\text{-}O^{\bullet} \qquad \text{(Eq. 21)}$$

The high potency of EGCG as chain-breaking is dependent on the high stability of the produced EGCG-O$^{\bullet}$. Electron paramagnetic resonance (EPR) spectroscopy and density functional theory calculations have been used to examine the rings involved in these reactions: it is reported that the scavenge of ROS induces oxidation of the D and B ring (Severino et al, 2009).

In addition, the ability of EGCG to chelate several metal ions contribute to its antioxidant activity (**Figure 15B**). Chelating groups in EGCG are the 3,4-dihydroxyl groups on the B ring as well the gallate hydroxyl group; they are able to bind several metals bearing strong positive charges (Fe^{3+}, Al^{3+} and Cu^{2+}) (Zhang et al, 2007). In particular, the inactivation of iron and copper ions may terminate the superoxide-driven Fenton reaction, inhibiting H_2O_2 formation and lipid peroxidation, which is believed to be a further source of harmful ROS in degenerative diseases (Mandel et al., 2007).

Various *in vitro* and *in vivo* studies provide evidence of the ability of EGCG to regulate the expression of the enzymatic antioxidant activity hence providing yet another mechanism to inhibit ROS formation (Simos et al, 2012). For example, the EGCG facilitates the cytosolic release of transcription factor Nrf2 (Nuclear Factor Erythroid 2-Related Factor 2); therefore, it moves to the nucleus, binds to antioxidant response element (ARE) genes, and finally induces

the expression of antioxidant enzymes (GST, Gpx and SOD), and antioxidant molecules such as Glutathione (**Figure 15C**) (Zhou et al, 2003; Li et al, 2011). Finally, the EGCG also has the ability to counteract the formation of ROS by inhibiting the ROS-generating enzymes (e.g., xanthine oxidase, cyclooxygenase, NADPH-oxidase and lipoxygenase) (Lin et al., 2000).

It is important to emphasize that the antioxidant activity of EGCG is intimately related to its concentration. The nontoxic concentration of EGCG in vitro lies between 1 and 150 μM in relation to the cell type (Luo et al, 2018; Singh and Shankar, 2011), but over these concentration values, certain toxic effects may occur and EGCG exerts pro-oxidant actions (Wu et al, 2009). This is mainly due to its chemical instability that determines an auto-oxidation of molecule in the physiological environment. The result is the production of hydrogen peroxide, semiquinone radicals and superoxide that can damage the cells (Hou et al, 2005; Elbling et al, 2005). However, the exact EGCG dose that has a pro-oxidative effect *in vivo* is controversial because the plasma proteins and antioxidants can enhance its stability (Zinellu et al, 2015). Cases of hepatotoxicity and nephrotoxicity upon consumption of high doses (10–29 mg/kg/day) of green tea in both animals and humans are reported (Lambert et al, 2010; Isbrucker et al, 2006) as well as the mice death after one injection of EGCG (150 mg/kg EGCG) (Galati et al, 2006). However, the safe dose cannot be extrapolated from animal studies because the differences in pharmacokinetics and bioavailability of EGCG between species (rats, human and mice).

Extensive researches have shown that this antioxidant-oxidant dual effect is responsible of some of the therapeutic effects observed for EGCG against various human diseases other than pathologies associated with oxidative stress. For example, EGCG can inhibit carcinogen activity, tumorigenesis, proliferation, and angiogenesis by modulation of ROS production. It is reported that EGCG is able to prevent the invasion of hepatoma cells by its scavenging activity (Zhang et al, 2000), while the ROS produced by auto-oxidation of EGCG induces cell death in many cancer cells such as the pancreatic carcinoma cells (Qanungo et al, 2005) and the myeloid leukemia (Nakazato et al, 2005). In the same way, the accumulation of ROS induced by EGCG can trigger the cell death in several bacterial cells such as E. Coli and P. aeuroginosa (Cuia et al, 2012).

Obviously, although the therapeutic effects of EGCG is also due to its interaction with specific targets, its ability to scavenge and produce ROS represents the most important mechanism to counteract and prevent several human disorders.

4.2. Stability and strategy to improve the bioavailability of EGCG

A possible setback in the employment of EGCG as antioxidant is its chemical and metabolic instability, which can determine a low concentration of the antioxidant within the biological system after administration (Lambert and Yang, 2003; Chen et al, 2001). It has been shown that orally ingested EGCG undergoes rapid metabolic changes in the gastrointestinal (GI) tract and in liver including methylation reactions, glucuronidation and sulfation (Chow and Hakim, 2011). Although these conjugates, which still contain intact catechol and gallate moiety, can have a biological activity as their parent compound, their intestinal adsorption can be very low (Dvorakova et al, 1999; Cai et al, 2002). Then, the conjugated EGCG's are excreted in the bile, reaching the large intestine where they may be metabolized by colonic bacteria and absorbed. More in detail, at the colon level, bacterial enzymes may deconjugate or break down catechin into simple compounds leading to the loss of EGCG health-promoting effects (Chow and Hakim, 2011). Moreover, the enzymatic transformation reactions by esterase, which start already in the saliva (Higdon et al, 2003) and in corneal epithelium (Lee et al, 1982), results in a rapid hydrolysis of EGCG.

In addition to metabolic instability, the chemical structure of EGCG makes it susceptible to degradation, which complicates EGCG's clinical application. The instability of EGCG is caused by two major reactions, auto-oxidation and epimerization (Sang et al, 2005) (**Figure 16)** and their kinetics are affected by several factors like pH, presence of oxygen, metal ions, antioxidants, temperature, and EGCG concentration (Sanga et al, 2007). In the auto-oxidation reaction (**Figure 16A)**, probably catalyzed by metal ions, the EGCG is oxidized by molecular oxygen to form EGCG radical (EGCG$^{\bullet}$) and superoxide radical. The $^{\bullet}O_2^-$ can further react with another EGCG molecule to produce H_2O_2 and EGCG$^{\bullet}$. Subsequently, the collision of two EGCG$^{\bullet}$ leads to dimers formation: theasinensin A and compound P2. These are the major products of B-ring autooxidation formed in alkaline fluids, in which the proton-donating potential of EGCG is higher, and in presence of micromolar EGCG concentrations (Sanga et al, 2007). The dimers can be further transformed into other compounds, presumably polymers, in a similar manner of oxidation. The epimerization reaction (**Figure 16B**) is more favorable at high temperature (>50°C) and in acidic environment (pH >5.5). The *trans*-epimer (−)-gallocatechin gallate (GCG) shows similar antioxidant activity to their *cis* counterparts but can have different biological activities (Sanga et al, 2007).

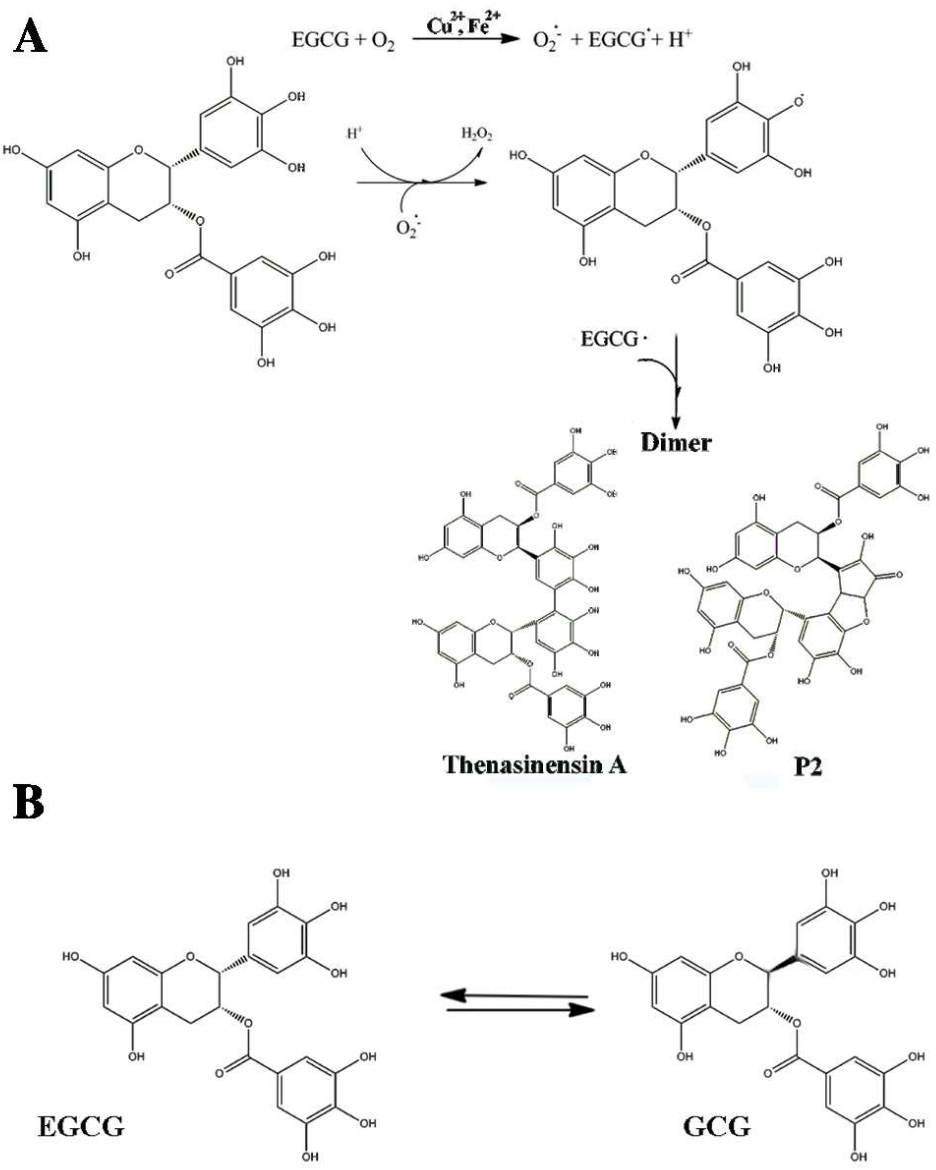

Figure 16. Autoxidation **(A)** and epimerization **(B)** reactions of EGCG.

The stabilization of EGCG can be achieved by different approaches including the use of reducing agent, structural modification and/or drug delivery systems (Dvorakova et al, 1999; Chen et al, 2001; Lemarie, et al 2013). Among several such strategies, DDS are novel and promising and have shown to be an appropriate approach to increase EGCG bioavailability (Wang et al, 2014). The most successful results have been obtained with the use of lipid-based drug delivery systems, thanks to the ability of EGCG to interact with lipid layer (Laudadio et al, 2018); however, the classical encapsulation strategies generally used show relatively low encapsulation efficiency. In the following chapters will be presented my results in the research

of the optimal condition to obtain a high encapsulation efficiency of EGCG into lipid-nanocarriers such as liposomes, cubic phase, hexagonal phase and cubosomes.

CHAPTER V

Liposomal Formulations for an Efficient Delivery of Epigallocatechin-3-Gallate: characterization and protective effect in ARPE19 cells

---

5.1. Introduction

The epigallocatechin-3-gallate (EGCG), a polyphenolic catechin from green tea, is characterized by a high chemical and metabolic instability that determines a poor concentration of the antioxidant within the biological systems after administration (Granja et al, 2016).

For this reason, a primary goal of my project was to create a stable and efficient EGCG delivery system, able to improve the bioavailability of the antioxidant molecule. As described above (Chapter III), liposomes offer several advantages because of their biocompatibility, their low toxicity and non-immunogenicity ([a]Minnelli et al, 2018; [b]Minnelli et al, 2018). These supramolecular aggregates were first proposed as drug delivery vehicles in ophthalmology to enhance ocular drug penetration. Several drug-loaded liposomal eye drops have been used to treat various ocular disorders of both the anterior and posterior segments, including infections, DED, corneal transplant rejection and AMD (Honda et al, 2013). In addition, the ability of polyphenols to interact with the lipid bilayer (Laudadio et al, 2018; [b]Minnelli et al, 2018) promotes the encapsulation of these compounds inside lipidic nanoparticles making liposomes potential delivery systems for EGCG. In addition, as described in the previous chapter (Chapter III, section 3.3.1.), the lipid nanoparticles can notably improve the bioavailability of drug at the ocular level.

Since my aim was to maximize the amount of drug entrapped in lipid vehicle, I have combined an *in silico-in vitro* approach to study the influence of salts and lipid matrix composition on the interaction of EGCG with bilayer leaflets. In particular, after having studied the effect of divalent salts $CaCl_2$ and $MgCl_2$ on the affinity of EGCG for anionic and neutral vesicles, I chose the formulation able to maximize the EGCG encapsulation efficiency, anionic multilamellar liposomes prepared from POPC, DOPE and CHEMS in the presence of Mg^{2+} ions. However, these liposomes resulted very unstable and nanodispersions suitable for drug delivery were obtained only after treatment with Poloxamer-407, a polyethylene–propylene glycol copolymer. X-ray diffraction and Dynamic Light Scattering experiments were carried out in order to study the structural properties and colloidal stability of the produced dispersion. The characterization was completed by evaluating both encapsulation efficiency (100%, in the final

formulation) and *in vitro* EGCG release. Since oxidative stress is involved in numerous retinal degenerative diseases, such as age-related macular degeneration, the ability of these liposomes to contrast H_2O_2-induced cell death was assessed in human retinal cells by evaluating cell viability and morphological changes at the subcellular level.

5.2. Optimization of EGCG encapsulation efficiency inside liposomal formulations

5.2.1. Salts and Lipid Composition effects on EGCG Encapsulation Efficiency inside Multilamellar Vesicles (MLVs)

The efficacy of liposomes as drug delivery vehicles depends, among other things, on the percentage of the entrapped species. The high polarity of EGCG determines a diffusion process into the aqueous phase during the emulsion process; in order to improve the EGCG encapsulation efficiency it is consequently important to employ liposome formulations able to enhance the interaction of the molecule with the lipid matrix.

We found out that EGCGs naturally bind to polar headgroup of liposomal systems made up of 1-palmitoyl-2-oleoylphosphatidyl-choline (POPC). However, the presence of salts clearly influences the EGCG molecules' absorption and the total effect depends strongly on the salt nature and concentration. Starting on these *in silico* results, we proceeded to investigate also the effects of mixed membrane composition systems on the EGCG encapsulation; therefore, we compared the encapsulation efficiency of EGCG inside neutral and anionic vesicles in presence of divalent salts.

We mixed the POPC lipid, the most common unsaturated phosphatidylcholine (PC) in eukaryotic membranes whit DOPE (1,2-Dioleoyl-sn-glycero-3-phosphoethanolamine) chosen for its fusogenic properties in prevision of an EGCG delivery application. In order to obtain negative self-assembling lipid systems, we use the CHEMS (Cholesteryl hemisuccinate), a cholesteryl derivative in which a cholesterol molecule is functionalized with a succinate moiety at the headgroup. (**Figure 17**). The CHEMS molecule has been replaced by cholesterol (Chol) in the preparation of neutral MLVs. The presence of the cholesterol skeleton increases the packing density of liposomes thus contributing to the bilayer stability (Briuglia et al, 2015). Moreover, it is able to enhance the encapsulation efficiency of polar drugs by reducing the bilayer permeability to solutes (Cagdas et al, 2011).

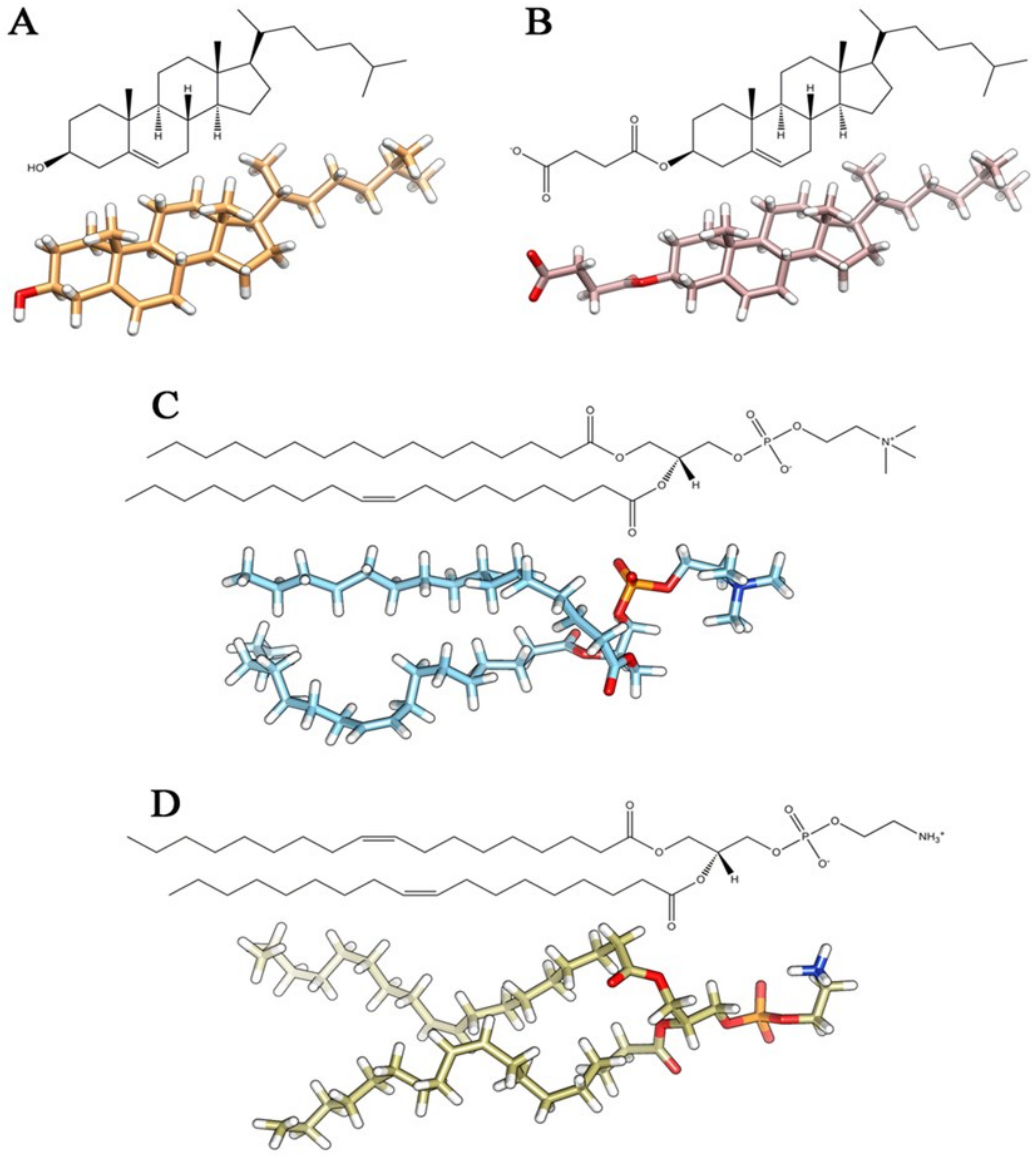

Figure 17. 2D and 3D structures of cholesterol (Chol) (**A**), cholesteryl hemisuccinate (CHEMS) (**B**), 1-palmitoyl-2-oleoylphosphatidyl-choline (POPC) (**C**) and 1,2-Dioleoyl-sn-glycero-3-phosphoethanolamine (DOPE) (**D**).

The magnesium and calcium chloride are salts widely used as additives in topical ophthalmic formulations. The divalent salts can interact not only with neutral and charged phospholipids by Coulombic forces but also with the phenolic and aromatic groups of EGCG; this binding can mediate the efficacy of the lipid bilayer interaction with encapsulated molecules. Moreover, the interaction between metal cations (particularly Mg^{2+} and Ca^{2+}) and lipids are also able to induce aggregation and fusion of liposomes with the cellular membrane, thus improving the penetration of the drugs

carried by the liposomes inside the cells (Martın-Molina et al, 2012; Binder and Zschörnig, 2002).

Based on these considerations, neutral and anionic MLVs, containing 1 mM EGCG, were prepared with an equimolar lipid ratio of POPC/DOPE/Chol and POPC/DOPE/CHEMS, respectively, and a final lipid concentration of 3 mg mL^{-1}. The choice of EGCG amount is crucial, in fact too high concentration of EGCG can alter and finally disrupt the membrane structure (Nakayama et al, 2000). The hydration of the systems was carried out with increasing concentrations of $MgCl_2$ and $CaCl_2$ (1:1, 3:1, 5:1 and 6:1 salt and EGCG molar ratio). With the aim to investigate the effect of salt amount on the EGCG affinity for the lipid systems, we separated by centrifugation the aqueous phase from liposomes loaded with EGCG. The unentrapped EGCG concentration was determined by UV spectroscopy at 280 nm to calculate the encapsulation efficiency (EE) of EGCG liposomes (see Material and Methods). The Stewart test has been used to verify the absence of phospholipids in every supernatant after centrifugation and showed that speed and centrifugation conditions are suitable for a complete sedimentation of liposomes (**Table 1**)

Formulation	Ratio $MgCl_2$: EGCG	mg mL^{-1} ± SD	Ratio $CaCl_2$: EGCG	mg mL^{-1} ± SD
Neutral System	0	0.005 ± 0.001	0	0.005 ± 0.001
	1:1	0.002 ± 0.005	1:1	0.010 ± 0.005
	3:1	0.006 ± 0.003	3:1	0.009 ± 0.003
	5:1	0.008 ± 0.003	5:1	0.011 ± 0.003
	6:1	0.007 ± 0.006	6:1	0.009 ± 0.006
Anionic System	0	0.006 ± 0.006	0	0.006 ± 0.006
	1:1	0.008 ± 0.001	1:1	0.008 ± 0.003
	3:1	0.001 ± 0.002	3:1	0.001 ± 0.001
	5:1	0.005 ± 0.002	5:1	0.005 ± 0.001
	6:1	0.006 ± 0.001	6:1	0.006 ± 0.002

Table 1. Results of the Stewart assay applied to the eluates of every formulation after centrifugation to determine if phospholipids are present.

In order to exclude EGCG precipitation due to the salt presence, we prepared as control also aqueous solutions containing free EGCG and calcium or magnesium chloride at the same concentrations used for the liposomal formulation. These controls did not show any sign of EGCG precipitation after centrifugation; in fact the solutions did not show

significative decrease OD (λ = 280 nm) with respect to the corresponding reference solutions also using the same speed and conditions selected for sedimentation of liposomes (**Table 2).**

	OD (ʎ = 280 nm)	
Molar ratio $MgCl_2$ / EGCG	**Before centrifugation**	**After centrifugation**
-	0.464 ± 0.025	0.464 ± 0.025
1 : 1	0.481 ± 0.025	0.481 ± 0.052
3 : 1	0.510 ± 0.025	0.530 ± 0.042
5 : 1	0.525 ± 0.025	0.519 ± 0.066
6 : 1	0.682 ± 0.025	0.672 ± 0.035
Molar ratio $CaCl_2$ / EGCG	**Before centrifugation**	**After centrifugation**
-	0.464 ± 0.025	0.464 ± 0.025
1 : 1	0.498 ± 0.025	0.502 ± 0.031
3 : 1	0.560 ± 0.025	0.582 ± 0.044
5 : 1	0.700 ± 0.025	0.761 ± 0.059
6 : 1	0.861 ± 0.025	0.845 ± 0.030

Table 2. EGCG OD (ʎ =280 nm) before and after centrifugation in control solutions containing the polyphenol alone in aqueous suspension mixed with calcium or magnesium chloride at the same concentrations used for the liposomal formulations.

The percentage of EGCG encapsulated inside the different liposomal formulation are reported in **Table 3**; the results show a certain encapsulation degree of EGCG also in the absence of salts of about 53.5 and 65% for neutral and anionic systems, respectively. These data confirmed the EGCG ability to interact with lipid bilayer. Moreover, the amount of encapsulated molecule was strongly influenced by Ca^{2+} and Mg^{2+} presence (**Table 3**).

Table 3. Formulations and encapsulation efficiency (%) of multilamellar liposomes loaded with Epigallocatechin-3-gallate (EGCG); standard deviation (SD) is also reported.

Liposomes Formulation	Molar Ratio Mg^{2+} /EGCG	Encapsulation efficiency (%) ± SD	Molar Ratio Ca^{2+} /EGCG	Encapsulation efficiency (%) ± SD
Neutral system	0	53.5 ± 6.2	0	53.5 ± 6.2
	1:1	71.7 ± 7.8	1:1	32.7 ± 4.3
	3:1	79.1 ± 5.3	3:1	23.9 ± 2.4
	5:1	82.3 ± 3.2	5:1	12.6 ± 6.4
	6:1	79.2 ± 3.5	6:1	4.1 ± 1.9
Anionic system	0	65.5 ± 3.8	0	65.5 ± 3.8
	1:1	76.7 ± 5.5	1:1	9.3 ± 2.5
	3:1	82.6 ± 2.3	3:1	5.9 ± 3.6
	5:1	98.9 ± 2.6	5:1	14.7 ± 1.7
	6:1	76.8 ± 4.2	6:1	9.9 ± 5.3

In particular, we observed that magnesium chloride improves the EGCG encapsulation efficiency inside both neutral and anionic liposomes. However, we obtained the best result with the anionic system (POPC/DOPE CHEMS) and a magnesium/EGCG molar ratio of 5:1; in this condition, we reached a practically complete encapsulation. Magnesium chloride improves the encapsulation efficiency inside neutral liposomes too, but without reaching the very high value of the anionic system. Also, with neutral MLV the optimal ratio EGCG: Mg^{2+} is 5:1. For any further increase of the Mg^{2+} concentration (6:1, magnesium/EGCG molar ratio), the percentage of antioxidant molecules inside the anionic liposomes decreases by about 20%. Besides, the calcium salt is not able to optimize the efficiency of encapsulation neither in anionic nor in neutral systems. On the contrary, the calcium presence seems to prevent the insertion of EGCG in the liposome bilayer and we obtained the worst results with anionic liposomes where the encapsulation efficiency is drastically reduced respect to the system without a bivalent salt (**Table 3**). In conclusion, we can achieve a high EE by using anionic liposomes in presence of a favorable concentration of magnesium salt.

With the aim to better understand and rationalize the EGCGs interactions with lipid bilayer in presence of Ca^{2+} and Mg^{2+} divalent salts and therefore the encapsulation efficiency results, MD simulations were carried out in collaboration with Molecular Modeling Laboratory of our Department.

5.2.2. Interaction of EGCG with lipid bilayer: *in silico* results

Neutral Lipid Models. In the absence of divalent salts, at the end of MD simulations (*see Material and Methods*), we observed part of the EGCG molecules involved in intramolecular aggregates (Laudadio et al, 2017); the other molecules interact with the neutral lipid bilayer's phosphates (**Figure 18**) thus confirming the experimental data.

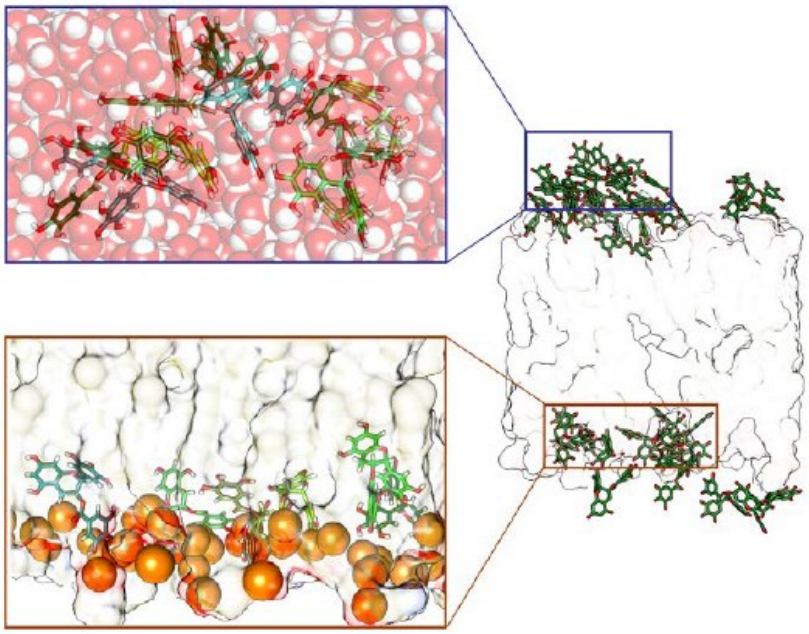

Figure 18. Neutral lipid system in absence of divalent salts: Epigallocatechin-3-gallate (EGCG) molecules (as green tube models), and the lipid leaflets (as transparent surface) are shown. The permanence of the EGCGs aggregate during the interactions with the bilayer can be observed.

In $CaCl_2$ neutral bilayer models (**Figure 19**), we observed that the increasing concentrations of calcium chloride promotes the interaction of Ca^{2+} ions with DOPE and POPC' phosphates, thus preventing the catechins' insertion at the bilayer surface. Therefore, the Ca^{2+} ions compete with EGCG molecules in the interactions with the lipids' phosphate groups. This behavior leads to an overall decrease of EGCG encapsulation degree.

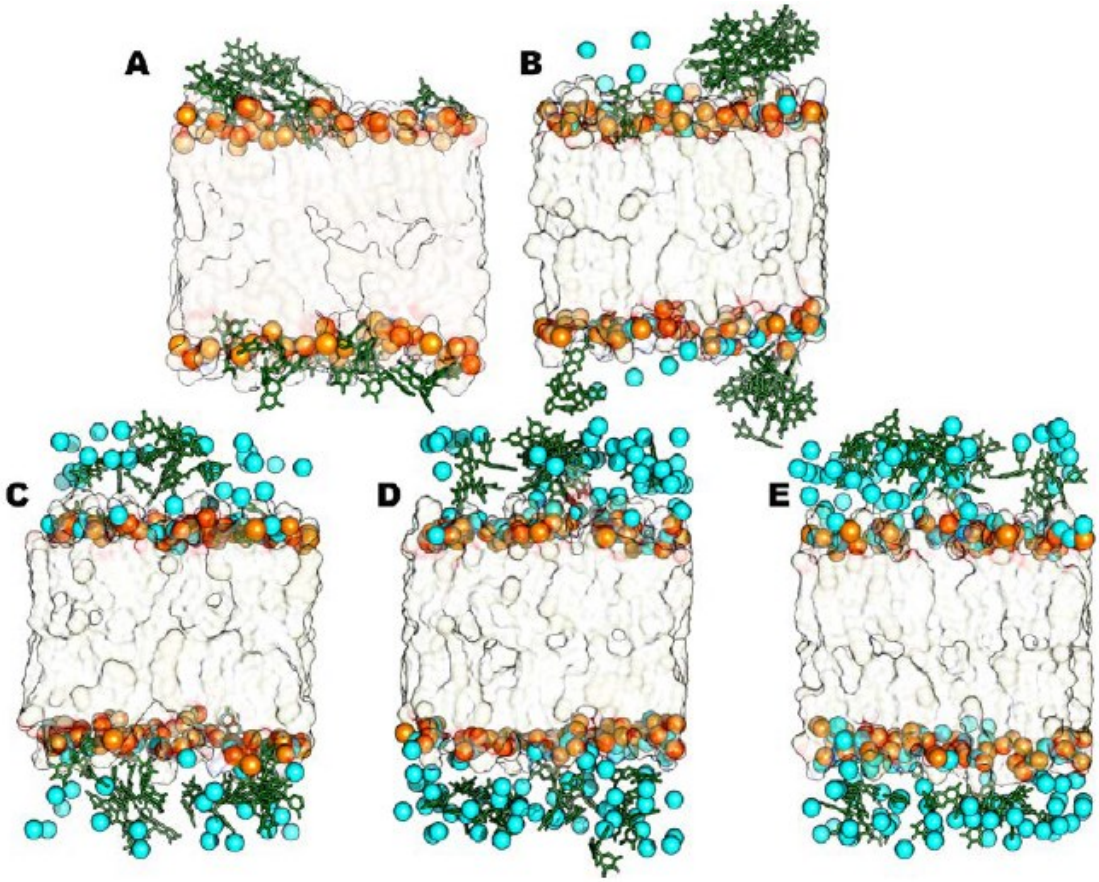

Figure 19. Representative structures for the steady states of neutral models with $CaCl_2$. The models without salts **(A)**, 1:1 **(B)**, 3:1 **(C)**, 5:1 **(D)** and 6:1 **(E)** are shown. Ca^{2+} ions (cyan VdW spheres), Epigallocatechin-3-gallate (EGCG) molecules (green sticks), phosphorous atoms (orange VdW spheres) and lipid leaflets (as transparent surface) are highlighted.

Therefore, EGCGs stay more in the aqueous phase respect to the system where divalent ions are absent and the encapsulation efficiency is consequently very low thus confirm the experimental results.

Switching to $MgCl_2$, we observe that Mg^{2+} lies in solution more than Ca^{2+} and thus it does not compete with EGCG in interacting with the lipids' phosphates. As shown by the representative structures of the steady state (**Figure 20**), the Mg^{2+} ions interact electrostatically with POPC lipids' phosphate groups but lie in the water phase due to their high hydration enthalpy.

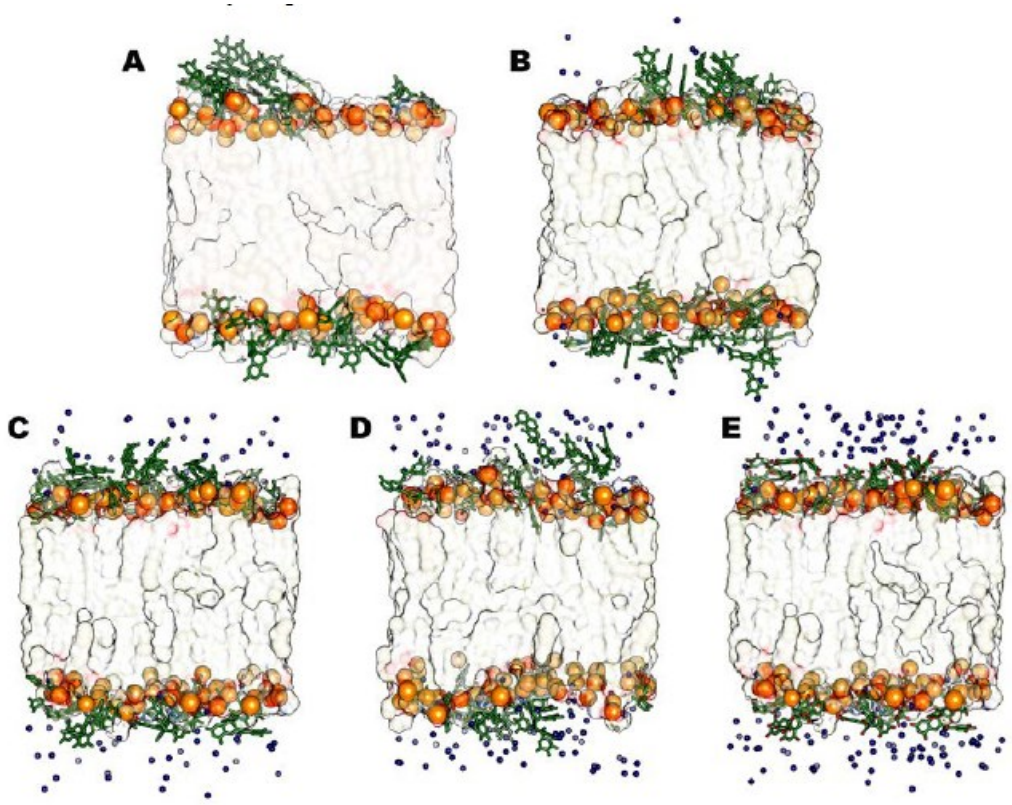

Figure 20. Representative structures for the steady states of neutral models with $MgCl_2$. The models without salts (**A**), 1:1 **(B)**, 3:1 **(C)**, 5:1 **(D)** and 6:1 **(E)** are shown. Mg^{2+} ions (blue VdW spheres), Epigallocatechin-3-gallate (EGCG) molecules (green sticks), phosphorous atoms (orange VdW spheres) and lipid leaflets (as transparent surface) are highlighted.

Respect to the systems with calcium chloride, the membrane slightly stretches along the bilayer long axis (Z) and EGCGs are then able to go further inside the bilayer thus increasing their absorption (**Figure 21**).

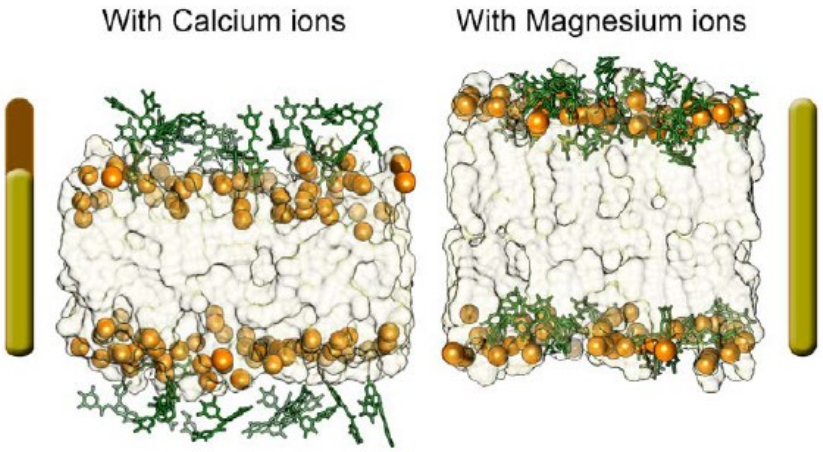

Figure 21. Comparison of bilayer dimension along Z-axis between (5:1) salt: Epigallocatechin-3-gallate (EGCG) neutral models ($CaCl_2$ model left, $MagCl_2$ model right).

Anionic Lipid Models. We applied the same computational protocol to build the corresponding anionic lipid bilayers, substituting Chol with CHEMS molecules. Once again, we considered the corresponding model without the divalent salt and besides we simulated the bilayer anionic models containing $CaCl_2$ and $MgCl_2$ in the same molar ratios reported for the neutral lipid ones.

At the end of the MD simulations, we observed an increase of the catechins' insertion within the leaflets with respect to the corresponding neutral system analyzed in the absence of divalent salt thus confirming the encapsulation efficiency results (**Table 3**). In this case, the aggregation effect between catechins that we observed in the neutral control system (**Figure 18**) is not so evident, and a majority of the EGCG molecules interacts efficiently with the anionic lipids' phosphates (**Figure 22A**).
As for the neutral models, the presence of calcium chloride determines the localization of catechin in the water phase (**Figure 22B-D)**. This phenomenon is due to the strong interaction of Ca^{2+} ions with the anionic CHEMS molecules, and the negatively charged phosphate groups of DOPE and POPC. The strong interactions between divalent cations and CHEMS molecules did not allow the EGCG molecules to interact with bilayer, even in the model with a 1:1 molar ratio.

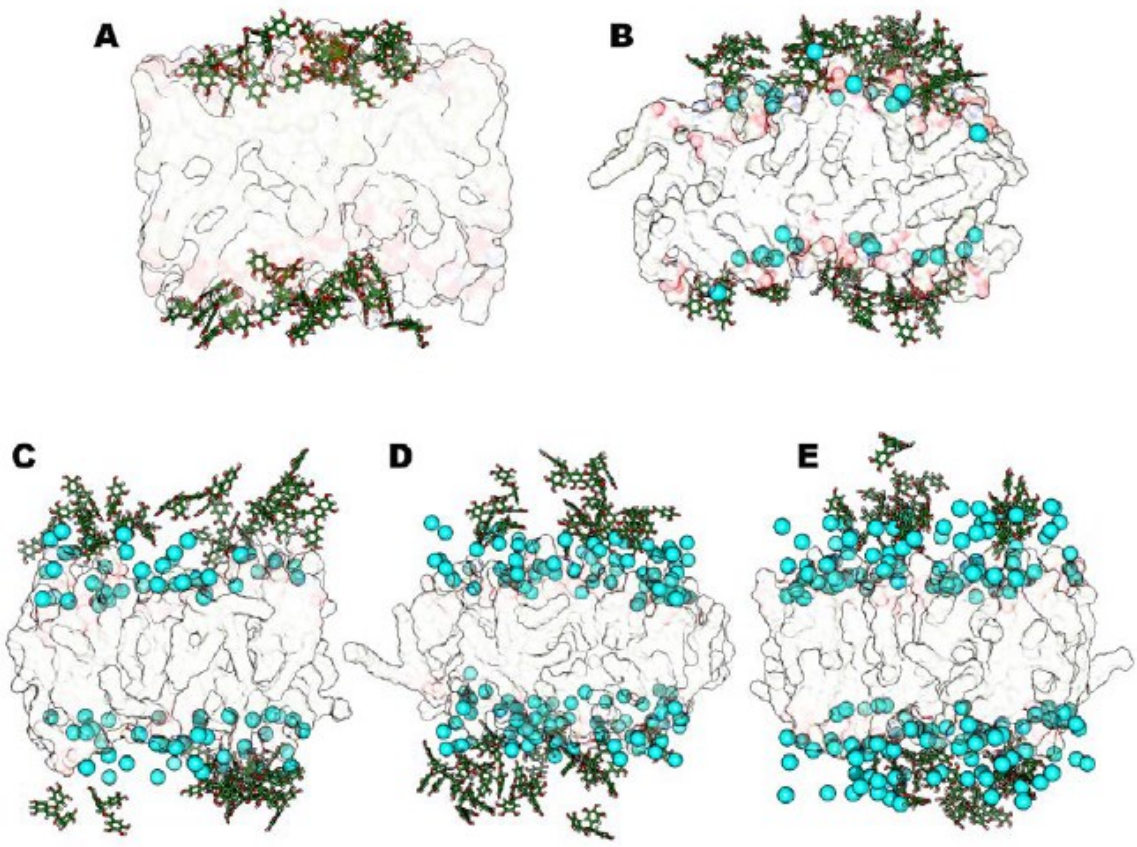

Figure 22. Representative structures for the steady states of anionic systems with $CaCl_2$. The models without salts **(A)**, 1:1 **(B)**, 3:1 **(C)**, 5:1 **(D)** and 6:1 **(E)** are shown. Ca^{2+} ions (cyan VdW spheres), Epigallocatechin-3-gallate (EGCG) molecules (green sticks), and lipid leaflets (as transparent surface) are highlighted.

Finally, we considered bilayers containing $MgCl_2$ salt in the described negative charged lipid environment. The results confirmed the experimental data: $MgCl_2$ can extensively improve the EGCG interactions with the anionic bilayer lipids where $CaCl_2$ cannot **(Figure 23**). In fact, also in these anionic systems, magnesium ions interact with phospholipids but lie in the solvent medium and do not compete with catechin molecules for phosphate lipids' interaction. Therefore, in the presence of $MgCl_2$ we always observe an evident increase of EGCG penetration. The analysis of some representative structures of all simulated models points out that the 5:1 $MgCl_2$-EGCG model appears very different from the others.

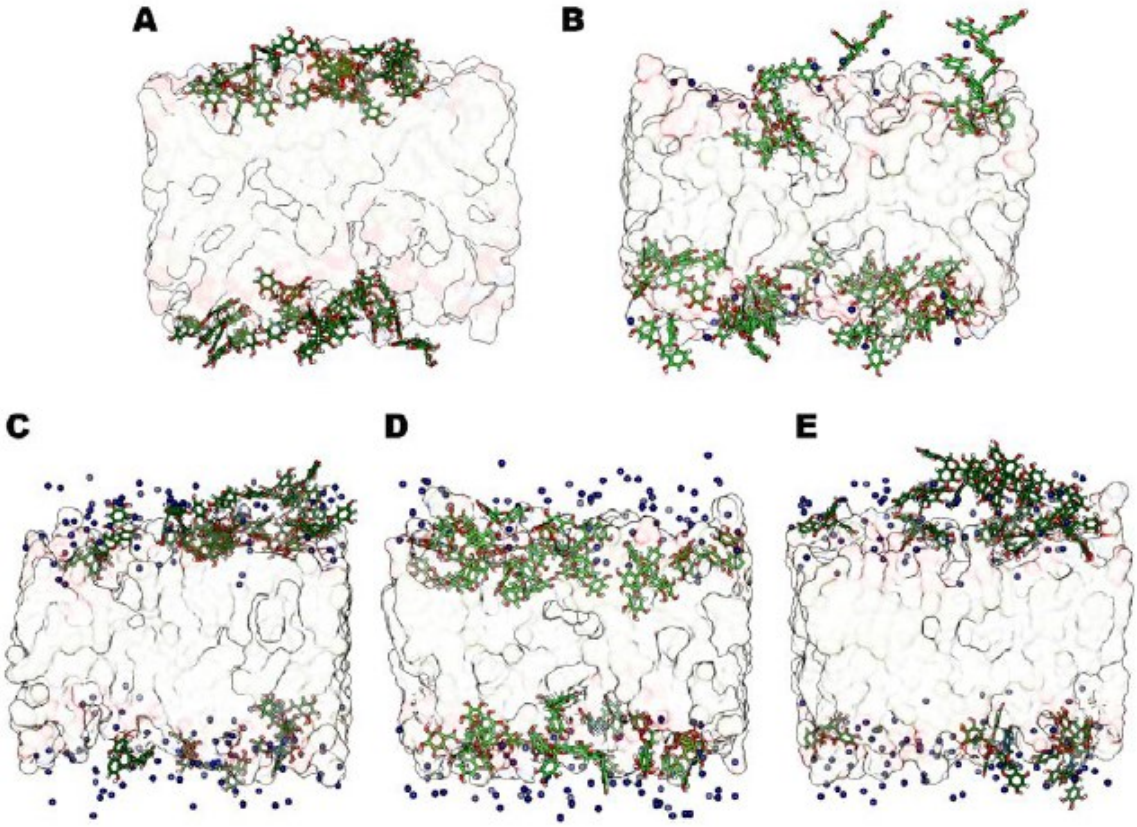

Figure 23. Representative structures for the steady states of anionic systems with $MgCl_2$. The models without salts **(A)**, 1:1 **(B)**, 3:1 **(C)**, 5:1 **(D)** and 6:1 **(E)** are shown. Mg^{2+} ions (blue VdW spheres), Epigallocatechin-3-gallate (EGCG) molecules (green sticks), and lipid leaflets (as transparent surface) are highlighted. The model D shows that all EGCG molecules are inserted inside the membrane.

In fact, this model (5:1) shows all catechin molecules inserted in the anionic bilayer leaflets (**Figure 23D).** This behavior is once again mediated by Mg^{2+} ions lying in the water phase promoting the membrane stretching, thus increasing membrane thickness anionic system without salt (**Figure 24**).

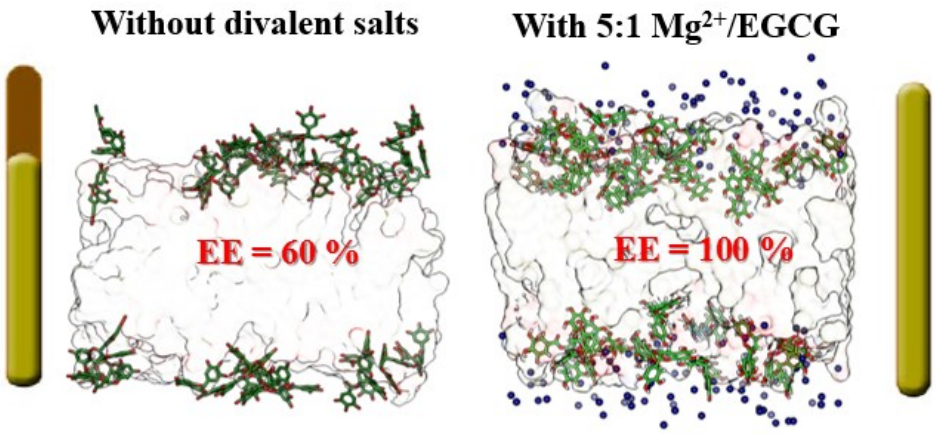

Figure 24. Comparison of bilayer dimension along Z-axis between anionic model without salt and anionic model with (5:1) salt: Epigallocatechin-3-gallate (EGCG).

In the 6:1 model, the catechin's insertion degree is in line with 1:1 and 3:1 systems. Since the Mg^{2+} ions concentration is very high, part of magnesium ions directly interacts with CHEMS compounds and POPC and DOPE polar headgroups, competing with catechin compounds and thus decreasing the degree of EGCG insertion within the bilayer surface compared to the 5:1 model. All these experimental findings are in line with the reported experimental results and can explain the different trend of encapsulation in different vectors (**Table 3**). Our approach shows that by combining *in silico*/experimental methods liposomal structure can be modulated with the insertion of modified lipid or salts and lipid vectors designed to efficiently entrap guests.

We demonstrated that the anionic vector POPC/DOPE/CHEMS with a specific concentration of $MgCl_2$ maximize EGCG encapsulation, thus potentially increasing the bioavailability of antioxidant in biological target. The following step of my research work has been the optimization of the best liposomal formulation, in which we reached 100% of EGCG encapsulation.

5.3. Colloidal stability: optimization of the best liposome formulation

5.3.1. Magnesium chloride effect on the anionic liposome

Although the presence of magnesium salts had maximized the EGCG encapsulation inside anionic POPC/DOPE/CHEMS liposomes, it induced an increase in particle size and cluster aggregate's formation (**Figure 25A).** It is well known (Martin-Molina et

al, 2012) that Ca^{2+} and Mg^{2+} can induce fusion of the lipid bilayer by forming dehydrated intermembrane complexes and the liposomes composition as well as the nature of encapsulated molecule can strongly influence the fusion properties (Silvius et al, 1984; Name et al, 2009).

A

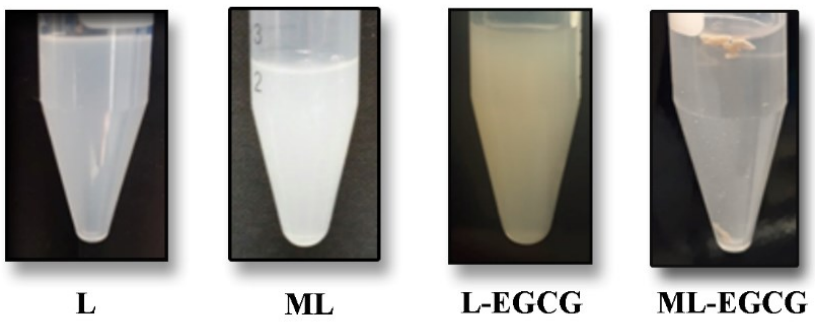

B

	L	*ML*	*L-EGCG*	*ML-EGCG*
OD (λ, 500 nm)	0.700 ± 0.167	1.215 ± 0.098	0.558 ± 0.098	0.069 ± 0.025

Figure 25. Aggregation induced by EGCG and magnesium salt. **(A)** Photography of MLV liposomes in the presence of only magnesium salt and EGCG alone or their combination. **(B)** Optical density (OD) at 500 nm of all MLV suspensions studied.

With the aim to better study the influence of magnesium ions and EGCG on the colloidal behavior of the liposomal formulations, turbidimetric measurements were performed by measuring optical density at 500 nm where light absorption is negligible for vesicles containing lipids without conjugated double bonds. The change in absorbance indicates a change in turbidity of the liposomal solution, corresponding to increased particle size (aggregation).

The turbidimetric measurement (**Figure 25B**) of magnesium-containing liposomes (ML systems) demonstrated that magnesium promotes the formation of large particles but not of precipitates, whereas L-EGCG (liposomes loaded with EGCG) suspension, containing only the polyphenol, showed a turbidimetric value slightly lower than empty liposomes (L).

Every attempt to obtain a stable suspension of ML-EGCG (magnesium-containing liposomes loaded with EGCG) nanosized particles failed; DLS measurements carried

out after sonication showed the presence of a polydispersed system (size 345 ± 43.97 nm, PDI 0.503 ± 0.041) that tends to aggregate in the following 24 h and gives particles larger than 1 μm (**Figure 26**). The high encapsulation of EGCG achieved and the presence of magnesium seem to be responsible for the physical instability of the liposome suspension in terms of aggregation/flocculation, probably due to the presence of numerous hydrogen bond donors in the EGCG structure and to its metal chelating properties.

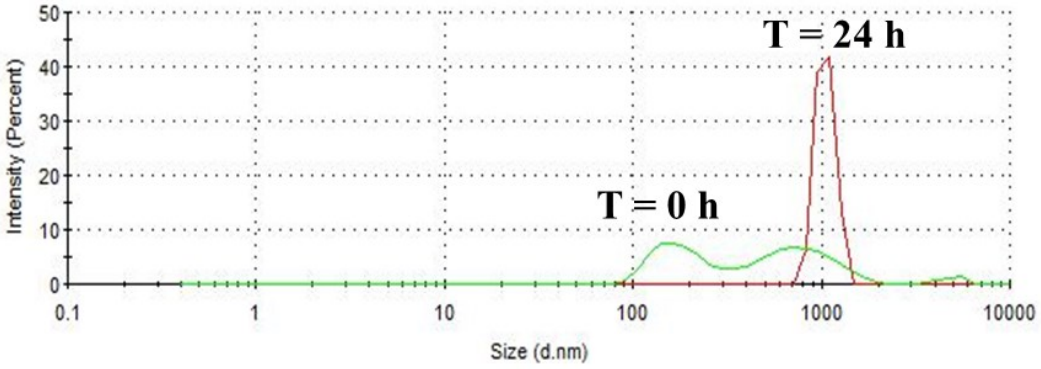

Figure 26. Dynamic Light Scattering measurement at t=0 and after 24 hours of treatment

Therefore, this formulation could not be used in this form for drug delivery applications and the need of optimize the long-term stability of liposomal formulation emerged.

5.3.2. Effect of Poloxamer-407 addition

Considering the well-known properties of several surfactants that drastically increase the stability of lipid dispersions and prevent their aggregation (Hsu and Nacu, 2003) we used Poloxamer-407 as stabilizing agent. It is a non-ionic triblock copolymer composed by a central hydrophobic poly(propylene oxide) chain (PPO) capped by two hydrophilic chains of poly(ethylene oxide) (PEO), which functions as emulsifier and stabilizer (Gustafsson et al, 1996; Gustafsson et al, 1997) (**Figure 27A**). Poloxamer-407 is approved as an inactive ingredient by the FDA for various types of pharmaceutical formulations and is accepted as GRAS (Generally Recognized as Safe) excipient (Dumortier et al., 2006), making it an excellent candidate for the preparation of drug

delivery systems. Moreover, the polymers can increase the bioadhesion properties of liposomes thus increase their potential as ocular drug delivery system (Mishra et al, 2011).

Therefore, we added the polymer to the non-homogeneous suspension of liposomes until the agglomerates were efficiently resuspended as shown in **Figure 27B.** The presence of the polymer seems to influence the interaction between liposomes and gives rise to an opalescent homogeneous suspension demonstrating that the Poloxamer-407 can hinder liposomes aggregation. As pointed by the sketch (**Fig. 27B**) probably the polymer shields the colloidal surface of liposomes with its two hydrophilic portions of the polymer; consequently, steric repulsion between bilayer could occur thus avoiding the aggregation phenomena. The final concentration of Poloxamer-407 necessary to obtain a homogeneous suspension was 0.8 mg mL^{-1}, which is less than its critical micelle concentration values (Katakam and Banga, 1997).

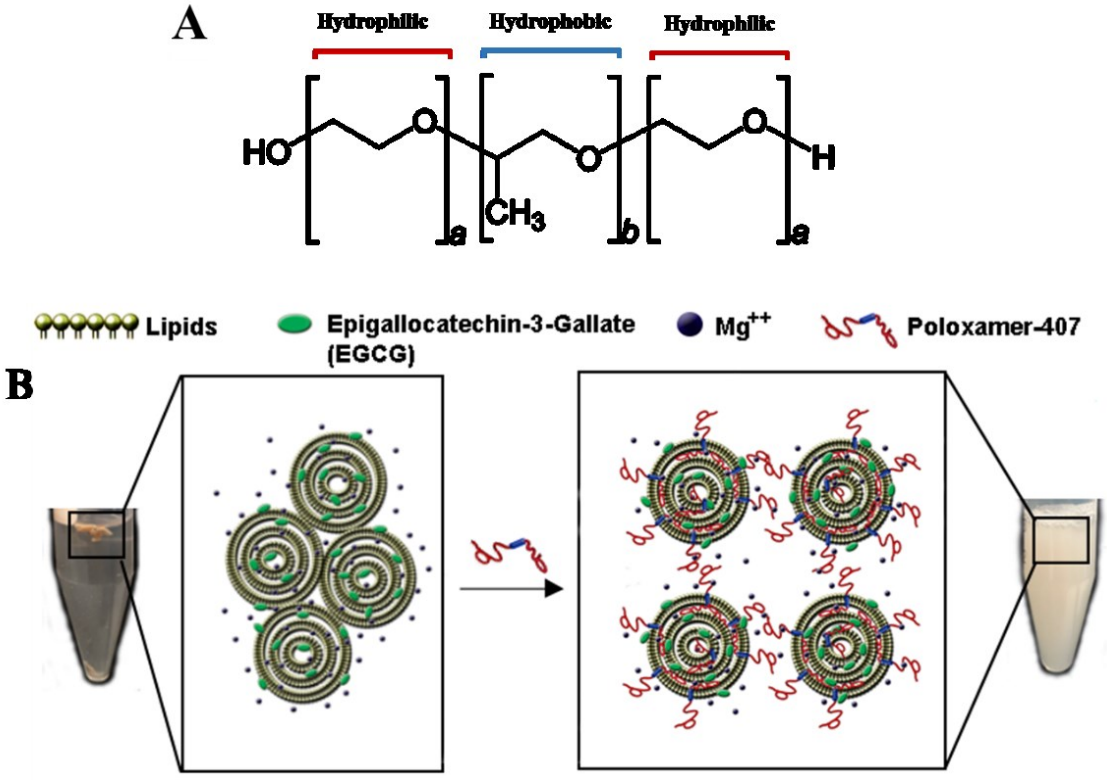

Figure 27. Stabilizing effect achieved in presence of Poloxamer-407. (A) Structure of Poloxamer-407; **(B)** Photography of MLV liposomes in the presence of magnesium salt and EGCG before and after addition of Poloxamer-407.

5.4. Characterization of bulk and nanodispersed liposomal phase

5.4.1. X-ray diffraction measurements

With the aim to study the influence of EGCG and magnesium cations on the supramolecular properties of the self-assembled nanoparticles, X-ray diffraction experiments were carried out on L, ML, L-EGCG and ML-EGCG systems, prepared both in the absence and in the presence of Poloxamer-407.

X-ray diffraction is a powerful tool, which can be used for the structural characterization of crystalline or crystalline liquid materials and can be applied for investigating the structure of nano drug delivery system. X-rays are electromagnetic radiation with a wavelength (λ) between approximately 10^{-8} and 10^{-11} m, comparable to the interatomic distances typical of crystals. Their production takes place when electrons accelerated by a high potential electric field interact with matter. The crystalline molecular structures are able to absorb the electromagnetic radiation and to refract them according to particular angles that depend on the position of the atoms in the analyzed system. Given a crystal, the direction of the diffracted radiation depends on the symmetry and dimensions of the unit cell in the lattice and its intensity depends on the distribution of the atoms in the cell itself. The analysis of the corresponding X-ray diffraction profile, which results in a graph showing the intensity of the diffracted beam as a function of the diffraction angle, allows to obtain two types of information:

- the crystal lattice symmetry of the sample from the position of diffraction peaks
- the profiles of electronic density relative to the unit cell from the integrated intensity of the diffraction peaks. The electronic density profiles allow to obtain important structural parameters, for example, for a lamellar phase, the values of the thickness of the aqueous layer (dW) and of the lipid layer (dHH).

The X-ray diffraction profiles obtained in the absence of Poloxamer-407 are reported in **Figure 28.**

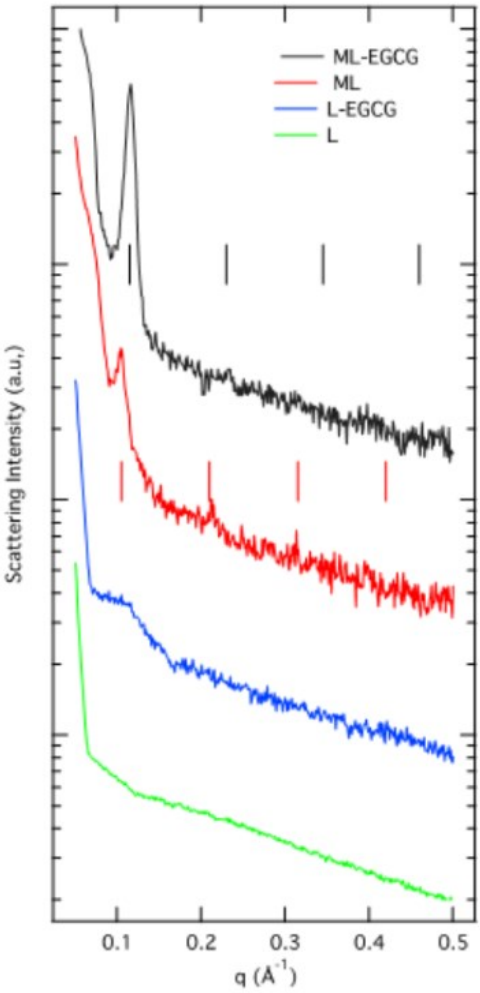

Figure 28: X-ray diffraction profiles from L, ML, ML-EGCG, L-EGCG systems. The temperature was 25 °C.

Depending on the composition, different characteristics are observed: for L and L-EGCG samples, a very large band (centered at about 57 Å) occurs in the low-Q region, suggesting the formation of a disordered system, probably unordered MLVs or LUVs; on the other side, 3 or 4 Bragg peaks characterize the diffraction profiles of ML and ML-EGCG samples, indicating that the presence of Mg^{2+} induces the formation of a rather ordered structure. As the peak spacing ratios scale as 1:2:3..., a 1-D lamellar organization is proposed: the well-known rearrangement of the lipidic carbonyl region (Binder and Zschörnig, 2002), which accompanies Mg^{2+} binding and which involves hydration and conformational changes, appears to stabilize the lamellar structure, even in the presence of EGCG. ML and ML-EGCG samples then show the same multilamellar structure, the main difference being the unit cell dimension (e.g., the

repeat distance among the lamellae, d), which is larger for ML (59.8 ± 0.5 Å) and smaller for ML-EGCG (54.6 ± 0.5 Å). The 10% reduction observed in the presence of EGCG can be related to a different lipid hydration induced by the presence of the active molecule or to changes in the hydrocarbon chain conformation, which is more disordered when EGCG is present.

To disentangle the different structural effects, low-resolution electron density profiles have been calculated, as reported by Di Gregorio et al. (Di Gregorio et al., 2010). Electron density maps, reported in **Figure 29**, show small differences in the position of the maxima corresponding to the head-group location and in the form of the electron density in the hydrocarbon region (see the differences between the full and the dashed lines).

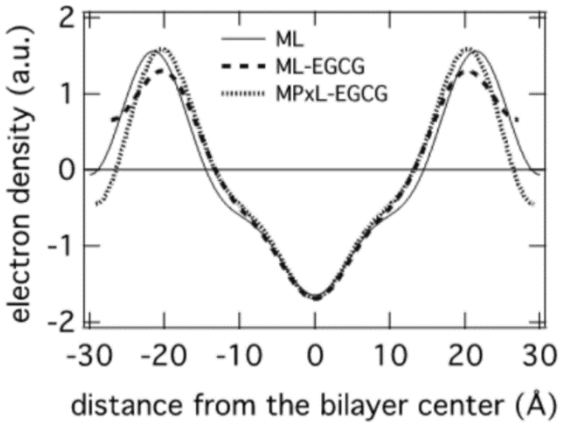

Figure 29. Reconstructed electron density profiles for the lamellar phase of ML (full line), ML-EGCG (dashed line) and MPxL-EGCG (dotted line) systems at 25 °C.

From the head-to-head electron density peak distance, the lipid bilayer thickness was obtained and, according to the decomposition of the sample in the hydrophobic and hydrophilic regions (Pabst t al., 2000), the average lipid cross sectional area, S_{lip}, and the lipid-associated intermembrane water volume, $V_{w,lip}$, were derived using equations reported in the Material and Methods section.

Table 4. Structural and molecular parameters for ML, ML-EGCG and MPxL-EGCG

System	***d*** **(Å)**	d_{HH} **(Å)**	d_{wat} **(Å)**	S_{lip} **(Å^2)**	$V_{w/lip}$ **(Å^3)**	$n_{w/lip}$
ML	59.8	44	15.8	43.6	345	11
ML-EGCG	54.6	40	14.6	48.0	350	12
MPxL-EGCG	58.1	40	18.2	48.0	436	-

The results shown in **Table 4** are compatible with the location of EGCG near the lipid head-group, so as to induce an increase in the area-per-lipid at the polar/apolar interface and an increased disorder of the lipid hydrocarbon chains. Of note is that hydration is not modified, as indicated by the rather constant lipid-associated intermembrane water volume (e.g., the number of water molecule-per-lipid is practically the same); consequently the formation of aggregates has to be ascribed to the strong interaction between EGCG and lipid-head group rather than to dehydration phenomena, as just underlined by MD simulations.

This result can be related to the high encapsulation efficiency observed in our liposomal system but also to the occurrence of precipitates in the liposome formulation containing both Mg^{2+} and EGCG. Indeed, the interaction network is complex. On the one hand, EGCG can behave both as H-donor with lipid oxygen groups and as H-acceptor with ethanolamine groups in DOPE; on the other hand, the presence of magnesium ions enhances the interaction possibilities between EGCG and the lipid bilayer. In fact, at physiological pH, EGCG is partially deprotonated (its pKa is 7.75) so that magnesium divalent ions can serve as cross-bridge to bind phosphate or oxygen lipid groups. Moreover, the presence of CHEMS, which is a negatively charged steroid molecule, increases the electrostatic interactions with Mg^{2+} ions, indirectly promoting the interaction of EGCG with the lipid bilayer (Laudadio et al., 2018).

X-ray diffraction profiles related to samples prepared in the presence or absence of Poloxamer-407 were very similar. **Figure 30** shows the results obtained from ML-EGCG and MPxL-EGCG carriers as a function of temperature: in both cases the multilamellar structure is confirmed by the Bragg peak sequence. Furthermore, the peak reciprocal intensities are maintained even at 45 °C, so guaranteeing the antioxidant liposome stability at physiological temperature.

If the two carriers show the same structural stability on heating, the polymer has an ordering effect on the supramolecular organization of liposomes and induces a change in the unit cell, which increases from 54.6 to about 58 Å. According to the unit cell temperature dependence reported in **Figure 30**, such an increase is probably determined by the presence of polymer molecules in between the lipid layers. In fact, as reported elsewhere (Djekic et al., 2015), Poloxamer-407 has two water-soluble PEO chains and a more hydrophobic middle block (**Figure 27**) that may be adsorbed at, or incorporated

in, the surface of the lipidic structural elements. As a consequence, steric repulsion between bilayers could occur.

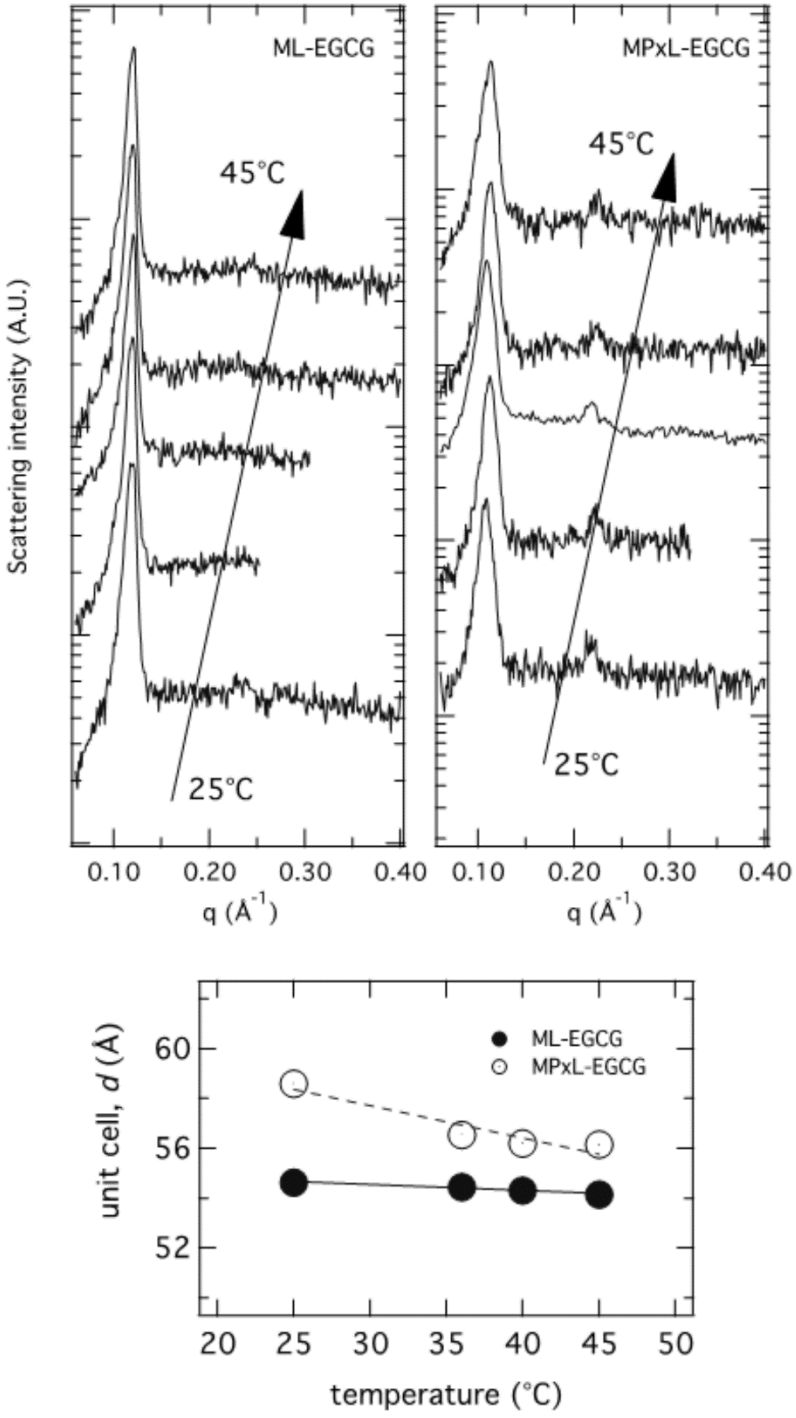

Figure 30. X-ray diffraction profiles observed for ML-EGCG (left frame) and MPxL-EGCG (right frame) samples as a function of temperature, as indicated. The lower frame shows the temperature-dependence of the lamellar repeat distance, as determined from the analysis of the position of the observed Bragg peaks.

Electron density maps confirm this view: the profiles calculated at 25 °C for ML-EGCG and MPxL-EGCG samples and reported in **Figure 29** (compare the dashed and the dotted lines), show that the head-to-head electron density peak distance is practically unaltered by the presence of Poloxamer-407 (hence, no changes in lipid conformation and in average lipid cross sectional area are expected). Moreover, while the inner lamellar part shows very similar features, differences are observed in correspondence of the polar region. Poloxamer-407 does not affect the lipid packing, but steric effects due to adsorption at the polar-head region enlarge the lamellar repeat distance (note the consequent increases of the lipid-associated intermembrane volume, referred as $V_{w,lip}$, in **Table 4**).

In order to verify the time stability, structural studies were also performed on MPxL-EGCG samples after storage at 4 °C for 1 month: X-ray diffraction profiles confirm that the inner multilamellar morphology is preserved, with a very small reduction of the unit cell dimension to 57.1 Å, well inside the experimental error (estimated around 0.5 Å).

5.4.2. Dynamic Light Scattering measurements

In order to investigate the ability of Poloxamer-407 to improve the colloidal stability of our best liposomal formulation, the magnesium poloxamer-407 liposomes loaded with EGCG (MPxL-EGCG) were sonicated and characterized by Dynamic Light Scattering. As controls we prepared also the Poloxamer-407 liposome with (PxL-EGCG) and without EGCG (PxL) and magnesium Poloxamer-407 liposome (MPxL). As shown in **Table 5**, the presence of Poloxamer-407 confers high stability to all the suspensions and prevents aggregation; the intensity mean diameter of MPxL-EGCG, expressed as *Z* average, was about 205 nm with a certain degree of polydispersity (PDI about 0.3) and the size did not change after 24 h.

Table 5. Characterization of sonicated liposomes with Poloxamer-407 [a,b]

Liposomes Formulation	Time of analyses (h)	Particle size ± SD (nm)	PDI ± SD (nm)	ζ-potential ± SD (mV)	Encapsulation Efficiency (EE%)	Loading Drug Capacity (LDC%)
PxL	0	99.8 ± 11.9	0.221 ± 0.004	-40.0 ± 0.2	n.a	n.a.
	24	137.0 ± 12.5	0.268 ± 0.048			
MPxL	0	112.8 ± 6.4	0.329 ± 0.047	-29.5 ± 3.5	n.a	n.a.
	24	123.5 ± 4.2	0.282 ± 0.006			
PxL-EGCG	0	101.2 ± 13.4	0.396 ± 0.008	-43.0 ± 1.9	57.0 ± 4.5	9.2± 2.1
	24	117.4 ± 3.3	0.251 ± 0.025			
MPxL-EGCG	0	205.2 ± 8.9	0.271 ± 0.023	-17.6 ± 4.1	95.0 ± 4.8	15.0 ± 2.3
	24	201.9 ± 9.4	0.245 ± 0.015			

[a] Particle size, PDI and zeta potential were determined by DLS. Encapsulation Efficiency and Loading Capacity were determined as reported in Materials and Methods section. [b] SD: standard deviation.

The analysis per number revealed that the most representative amount of vesicles displayed a mean diameter of 140 nm; a bimodal distribution was highlighted by the intensity and volume based particle size distribution where an additional population of about 370 nm was present. The DLS measurements did not show the presence of micelles. The stability of MPxL-EGCG stored at 4 °C was also evaluated after 1 month. The intensity-based distribution showed the presence of some amounts of aggregates of 0.8-1.0 μm, which are not present in the number-based distribution where the only peak corresponds to a population of about 150 nm. The negative zeta potential of liposomes due to the presence of CHEMS decreased in absolute value in the presence of Mg^{2+} because of the absorption of positive ions; in MPxL-EGCG, the zeta potential is further reduced: the ability of EGCG to chelate positive ions is probably responsible for a major absorption of magnesium ion on the liposome surface. By virtue of the presence of Poloxamer-407, the EGCG magnesium liposomes did not aggregate in spite of their low zeta potential.

The physical stability of the produced liposomes was studied also in the presence of plasma proteins, after their exposure to serum, using DLS and turbidity measurements. For this purpose, liposomes were incubated in PBS supplemented with FBS (50% v/v) at 37 °C and measurements were carried out at 0 and 24 h.

For both MPxL and MPxL-EGCG dispersion, the average dispersed vesicle diameter remained essentially unchanged upon exposure to 50% FBS (t=0), even after 24 h (**Table 6**).

Table 6. Influence of serum on size distribution of Magnesium Liposomes with Poloxamer-407[a,b].

Liposomes Formulations	Time of analyses (h)	Size in serum ± SD (nm)	λ=500 nm		λ=600 nm	
			Serum	PBS	Serum	PBS
MPxL	0	106.3 ± 12	0.086	0.068	0.082	0.066
	24	90.65 ± 14	0.085	0.067	0.081	0.066
MPxL-EGCG	0	210.9 ± 7.4	0.124	0.103	0.108	0.090
	24	189.2 ± 9.1	0.134	0.103	0.116	0.092

[a] Particle size was determined by DLS. Turbidity of the dispersions was determined as OD as reported in Materials and Methods section. [b] SD: standard deviation; PBS: phosphate buffered saline.

We confirmed the liposomal suspension stability by spectroturbidimetry. The optical densities at 600 and 500 nm for particles in PBS and in 50% of FBS are reported in **Table 7**. At these wavelengths, the absorbance for the liposomes in serum, as well as in PBS, increased only slightly or nothing with time, indicating that the dispersions are stable as highlighted from DLS results.

5.4.3. Encapsulation Efficiency studies in presence of Poloxamer-407

The percentage of EGCG encapsulated inside liposomes (PxL-EGCG and MPxL-EGCG) was determined by the Folin-Ciocalteu assay and the results are presented in **Table 5**. For the PxL-EGCG we obtained 57.0 ± 4.5 % of encapsulation efficiency, thus confirming the capacity of EGCG to form phytosomes (Galeazzi et al. 2015; Nakayama et al., 2000). Instead, in the presence of the magnesium salt, we practically reached a complete encapsulation of EGCG (95.0 ± 4.8 %), which decreased by 17 % after storage at 4 °C for 1 month. In **Table 5** the Loading Drug Capacity of both formulations are also reported. These data confirm previous results in which $MgCl_2$ can greatly improve the interaction of EGCG molecules with anionic liposomes (Laudadio et al., 2018) and consequently we chose the anionic formulation MPxL-EGCG, presenting the best encapsulation outcome, for the following experiments.

5.4.4. *In-vitro* drug release

Another important point for drug delivery applications is the ability of liposomes to retain their encapsulated drugs following administration. Therefore, i*n-vitro* antioxidant release from MPxL-EGCG was evaluated by dialysis method at 37 °C in PBS and the results, compared with free EGCG behavior, are presented in **Figure 31** as cumulative percentage release during 24 h.

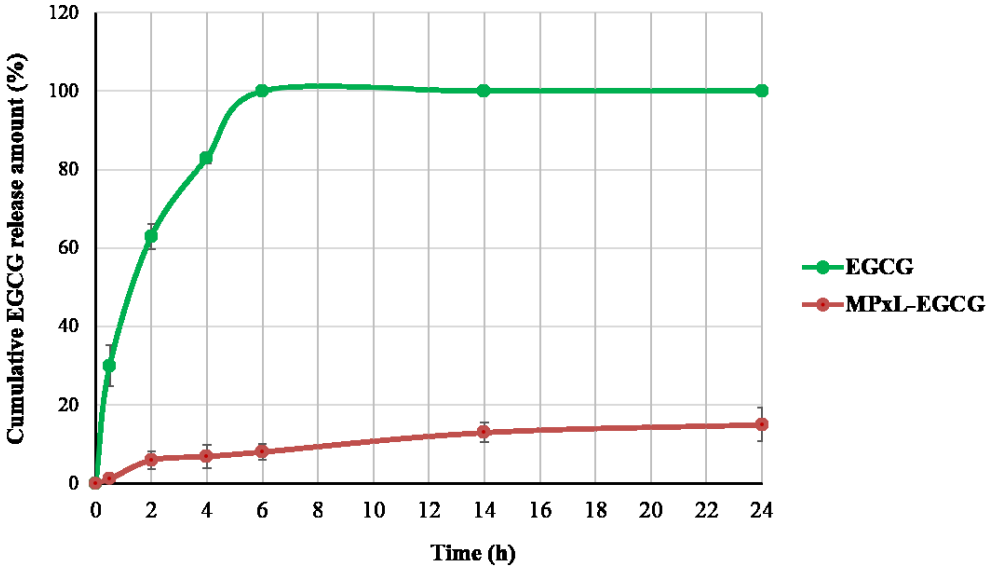

Figure 31. *In vitro* release of EGCG in PBS (pH 7.4) for liposomal and free drug solution. Values are expressed as mean ± SD; n=3 independent experiments.

The diffusion of the free antioxidant through the dialysis membrane from the control was more than 60% in the first 2 h and complete by 6 h, demonstrating that the dialysis membrane did not limit the release of EGCG. The drug encapsulation in liposomes modified its release profile: the MPxL-EGCG release was about 6 % in the first 2 h and reached 15% after 24 h. Evidently, the strong interaction underlined *in silico* (Laudadio et al., 2018) between anionic liposomes and EGCG in the presence of magnesium ions determines the low release of the molecule from liposomes. The presence of Poloxamer-407 on the liposomal surface can contribute to reduce the speed of release of encapsulated EGCG.

5.5. Cellular experiments

Once the structural and stability properties of EGCG-loaded nanoparticles were determined, cellular experiments were performed to assess cytotoxicity and potential activity as antioxidant delivery system.

5.5.1. Cytotoxicity of EGCG-loaded magnesium-poloxamer liposomes in Retinal Pigment Epithelial Cells

The toxicity of MPxL-EGCG was evaluated in ARPE-19 cells by MTT assay and compared with that of corresponding concentrations of free EGCG (**Figure 32**). To exclude both positive and negative Mg^{2+} effect on cells vitality, we tested the EGCG molecule with and without magnesium ions. Moreover, unloaded MPxL were also tested to verify the potential toxicity of the lipid vector used in the present study.

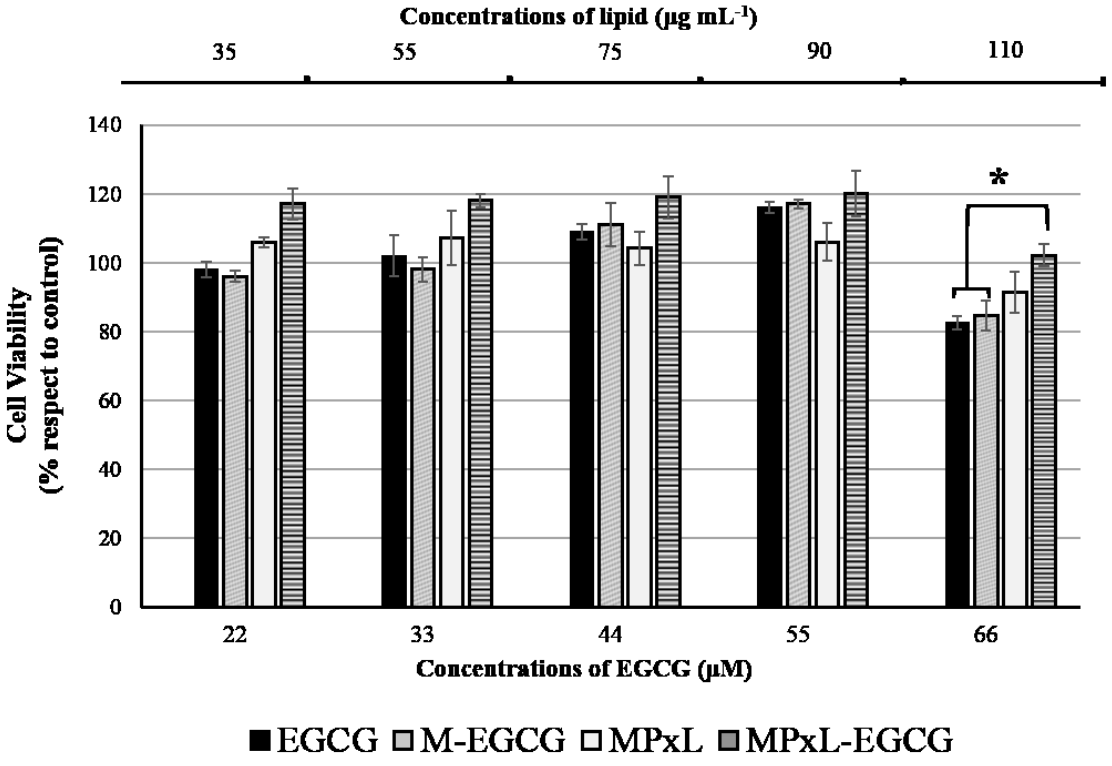

Figure 32. Cytotoxicity of free and encapsulated EGCG liposomes in ARPE19 cells. The cells were treated with various concentrations of MPxL-EGCG, MPxL, EGCG, and M-EGCG (at concentrations equal to the catechin content in the liposomal formulations) for 24 h in complete culture medium. The respective concentration of lipid (µg mL^{-1}) for each EGCG concentration tested in liposomes is reported above the histogram. Cell viability was determined by MTT assay. The values in the figures are expressed as the means ± SD. Significant differences can be observed between cell viability in the presence of MPxL-EGCG vs. EGCG and M-EGCG groups, at 66 µM and 110 µg mL^{-1} of catechin and lipid, respectively (*$p<0.05$).

The free EGCG shows low cytotoxicity in ARPE-19 cells. In detail, EGCG treatment did not decrease cell viability up to 55 μM (**Figure 32**); at this percentage we observed instead an increase in viable cells in relation to the control (55 μM, 115%). At 66 μM EGCG concentration, we observed ca. 20% decrease in cell viability probably due to the pro-oxidative action of molecules at high concentrations (Li et al., 2010) and/or to its strong interaction with cellular membranes (Nakayama et al., 2000) leading to membrane leakage, change in membrane potential, and increase in permeability to protons and potassium ions (Caturla et al., 2003). The same result was obtained with EGCG in presence of magnesium ions, thus demonstrating that the bivalent salt concentrations, used in this study, did not affect cell viability. Empty liposomes showed a similar trend as free EGCG with a decrease in cell survival only at high concentration of lipid (110 μg ml^{-1}, ca. 20% of cell death compared to no-treated cells). In the MPxL-EGCG-treated cells, no decrease in cell viability compared to the control was observed at the highest concentration of EGCG and lipid, despite an overall drop compared to lower concentrations. The employment of liposomes probably allows EGCG internalization thus avoiding massive surface membrane interactions that can alter cell membrane fluidity and permeability. Based on these results, we chose the 55 μM concentration of bioactive molecule which corresponds to 90 μg mL^{-1} of lipids for the experiments described in the next section.

5.5.2. Enhancement of EGCG efficacy by magnesium-poloxamer liposome incorporation

In order to study MPxL-EGCG potential ability to protect ARPE-19 cells from physiological stressors, oxidative damage mediated by hydrogen peroxide was induced. (Iloki-Assanga et al., 2015). MPxL-EGCG activity was compared with that of free EGCG and empty liposomes; in particular, we examined both inhibition of oxidative stress-induced cell death and morphological changes that occur in the cytoplasm, mitochondria and nucleus of cells (**Figure 33**). After pre-treatment of ARPE-19 with EGCG alone, MPxL and MPxL-EGCG for 24 h, cells were washed twice with PBS to avoid direct extracellular interactions between the tested compounds and the oxidant. As shown in **Figure 33A**, the free EGCG treatment, as described above, effectively

protects ARPE19 cells from H_2O_2-induced cell death (15% more cell viability than H_2O_2-exposed cells, $p<0.05$). The results also reveal that empty liposomes MPxL had a protective effect against H_2O_2-induced cell death (12% more cell viability than than H_2O_2-treatedcells, $p<0.05$); lipids play in fact an important role in cellular regulation, as building blocks of membranes but also in transducing intra- or extracellular signals. Consequently, liposomes can have a positive influence on cellular viability and appear suitable for drug delivery application. (Caddeo et al., 2008) The encapsulation of EGCG in magnesium liposomes markedly enhanced their protective effect against oxidative stress with an increase in cell survival of 40% compared to H_2O_2-exposed group cells ($p<0.001$) and up to 25-28% when compared to free EGCG and empty liposomes, respectively.

We also examined, for all samples studied, ultrastructural changes of the mitochondria and other cellular features using TEM and the results are shown in **Fig. 33B**. The control group cells exhibited healthy normal appearing mitochondria, endoplasmic reticulum, presence of villi and normal nuclear membrane (**Fig. 33B, I-II)**. In contrast, H_2O_2-exposed group cells (**III**) and EGCG plus H_2O_2 group cells (**IV**) had almost completely damaged mitochondria and loss of ribosome from endoplasmic reticulum. Nuclear membrane appeared swollen and villi severely reduced. In the empty liposomes plus H_2O_2 cell group (**V**) the phenotype was less severe than in **III** and **IV** but still the nuclear membrane and mitochondria showed major morphological alterations. In the MPxL-EGCG plus H_2O_2 group cells (**VI**) the nuclear membrane appeared normal; likewise, for the untreated cell, the endoplasmic reticulum was in close proximity with mitochondria that were frequently undamaged. Overall, the damage induced by H_2O_2 treatment induced substantial necrosis. Indeed, it is reported that H_2O_2 altered membranes as well mitochondria resulting in oncosis and blebbing, as defined by Majno and Joris (Majno and Joris, 1995). Moreover, we rarely observed aspects of apoptosis in all samples, suggesting that the oxidative insult was far too intense for the cells to trigger that pathway. Thus, our findings of better preserved mitochondria in the MPxL-EGCG treated cells clearly suggests that the liposomes can effectively increase the efficacy of EGCG treatment, maintaining mitochondrial integrity and vitality.

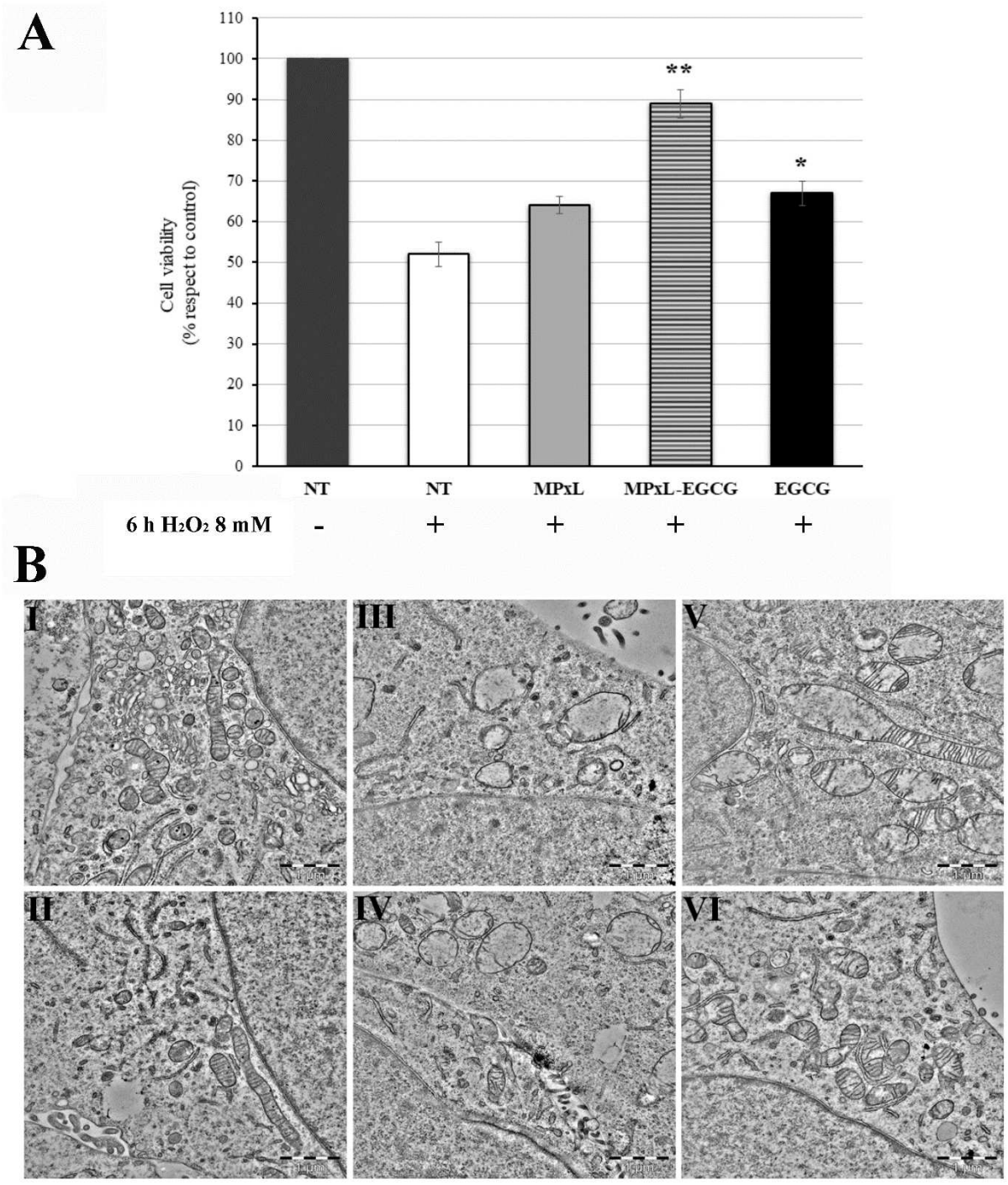

Figure 33. Effect of free EGCG and EGCG loaded in magnesium-poloxamer liposomes in ARPE19 cells after H_2O_2 exposure. The cells were pre-treated with 55μM free EGCG or EGCG encapsulated in MPxL, which correspond to 90 μg mL^{-1} lipid for 24 h, before being exposed to 6 mM H_2O_2 for 6 h. **A)** Cell viability was determined by MTT assay. Data are expressed as means ± S.D. of five independent experiments, each performed in triplicate, **$p < 0.001$, *$p < 0.05$ difference from control, representing cells treated only with H_2O_2.; **B)** Qualitative evaluation of cell morphology was done by TEM analyses. I, II: Control cells with normal mitochondria, nuclear membrane, Golgi, striated endoplasmic reticulum and villies between cells. III: H_2O_2,treated cells with mitochondria bearing no cristae, swollen nuclear membranes, fragmented reticulm with loss of ribosomes; IV: EGCG plus H_2O_2 treated cells, some mitochondria retain some cristae, reticulum retain some ribosomes; V: MPxL plus H_2O_2 treated cells, similar to III; VI. MPxL-EGCG plus H_2O_2 treated cells; many mitochondria retain cristae, a few normal ones observed, normal nuclear membrane.

5.6. Conclusion

First of all, the experimental and *in silico* results show a high correlation, thus confirming the efficiency of the developed combined approach. The encapsulation percentage showed specific ion effects together with influence of the lipid matrix composition. More in details, we found out that the presence of calcium ions hinders the insertion of EGCG in the liposome bilayer in both neutral and anionic systems. This can be explained considering that calcium ions interact more efficiently with lipids' phosphate groups compared to EGCG, so the corresponding percentage of catechin encapsulation observed experimentally is very low. In the anionic system, this phenomenon is more pronounced because the Ca^{2+} interacts more strongly with the negatively charged CHEMS molecules, thus explaining the lowest degree of encapsulation obtained with respect to the neutral vector. From the computational simulations we observed that the 5:1 molar ratio shows a slightly difference in the MD values respect to the other three anionic models. This correlates with the little increase of EGCG encapsulation measured experimentally in these liposomes. On the contrary, $MgCl_2$ can notably improve the degree of encapsulation of EGCG molecules, in particular at the 5:1 molar ratio (Mg^{2+}: EGCG) in both neutral and anionic models. Of particular interest is the result obtained with the anionic lipid system, where we achieved 100% EGCG encapsulation. The high degree of encapsulation is due to the magnesium electrostatic influence that promote the membrane stretching along its major axis and EGCG insertion. Concerning the lipid matrix composition, all the data collected suggest that the anionic vector is more efficient in promoting the catechin insertion within the liposomes. Even if EGCG tends to interact with POPC and DOPE phosphates, the presence of the negative charged steroid CHEMS increases the electrostatic interaction with the cations, thus, it indirectly promotes the catechin insertion. Thus, the combination of this anionic liposomal formulation enriched with magnesium chloride, appears particularly suitable to be optimized for drug delivery applications to avoid time-consuming separation steps of unentrapped bioactive molecules.

However, the simultaneous presence of EGCG and magnesium induces a cluster aggregate formation. The addition of Poloxamer-407 allow us to obtain stable nanodispersions, as demonstrated by DLS and turbidimetric analysis, also in the presence of serum. XRD experiments show the location of EGCG near the lipid head-group and a more ordered lamellar structure obtained by incorporation of Poloxamer-407. Because age-related macular degeneration is also caused by oxidative stress, the ability of the new liposomal system in contrasting H_2O_2-induced cell death was studied. MPxL-EGCG liposomes show superior antioxidant activity compared with free EGCG, as evaluated by MTT assay. Morphological

analysis performed by TEM showed better preserved mitochondria in the MPxL-EGCG treated cells, suggesting that encapsulated EGCG actually results very effective inside cells.

CHAPTER VI

Epigallocatechin-3-gallate (EGCG)-loaded cubic or hexagonal phase gels and its dispersed forms: pre-formulation studies

6.1. Introduction

As described above *(Chapter III, Section 3.3.2.),* cubic and hexagonal liquid crystals are isotropic phases that are physically stable in excess water representing an unique system for the production of pharmaceutical dosage forms; however, the practical use of cubic or hexagonal phase gels as drug carriers is limited by their high viscosity. Their emulsification in water in the presence of a surfactant results in the production of cubosomes and hexosomes that can be defined as nanoparticulate disperse systems characterized by high biocompatibility and bioadhesivity. Because of their properties, these versatile delivery systems can be administrable by different routes (such as orally, parenterally, or percutaneously). Compared to liposomes, they possess high physical and chemical stability and an increased surface area. In addition, they are able to encapsulate several molecules from hydrophilic, hydrophobic and amphiphilic (Salonen et al, 2010; Gordon et al, 2012). Recent studies revealed that the cubosome dispersions were more capable of increasing the corneal penetration by prolonging the drug retention time than the commercially eye drops containing liposomes (Han et al, 2010); therefore, this suggests that the cubosomes have a great potential as ocular delivery system for treating ocular diseases.

In this Chapter, I describe for the first time the preparation of epigallocatechin-3-gallate (EGCG)-loaded cubic or hexagonal phase gels and their dispersed forms. With the aim to maximize the EGCG encapsulation efficiency, I examined the effect of increasing concentrations of catechin on its interaction with the bulk (nondispersed) lipid phases and its dispersed forms. The influence of EGCG on supramolecular organization of systems was investigated by Small Angle Neutron Scattering (SANS). In prevision of cellular studies, Dynamic Light Scattering (DLS) experiments were carried out in order to study the colloidal stability of the produced dispersion both in PBS and in presence of plasma proteins.

6.2. Preparation and Drug Loading Capacity of bulk (Nondispersed) phase and its dispersed forms (Cubosomes and Hexasomes)

The bulk (nondispersed) lipid phases and the corresponding dispersed form are prepared by using GMO (Glycerol monoolein), a polar synthetic unsaturated monoglyceride, consisting mainly of monooleate (**Figure 34**). GMO is a biodegradable and biocompatible material classified as generally recognized as safe (GRAS).

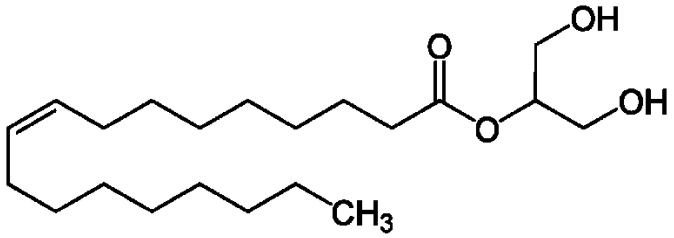

Figure 34. Structure of Glycerol Monoolein (GMO).

The phase diagram of GMO and water is shown in **Figure 35**. It is evident that GMO forms cubic phase with water in a broad area at physiological temperature and therefore it is widely used for the preparation of cubic liquid crystals.

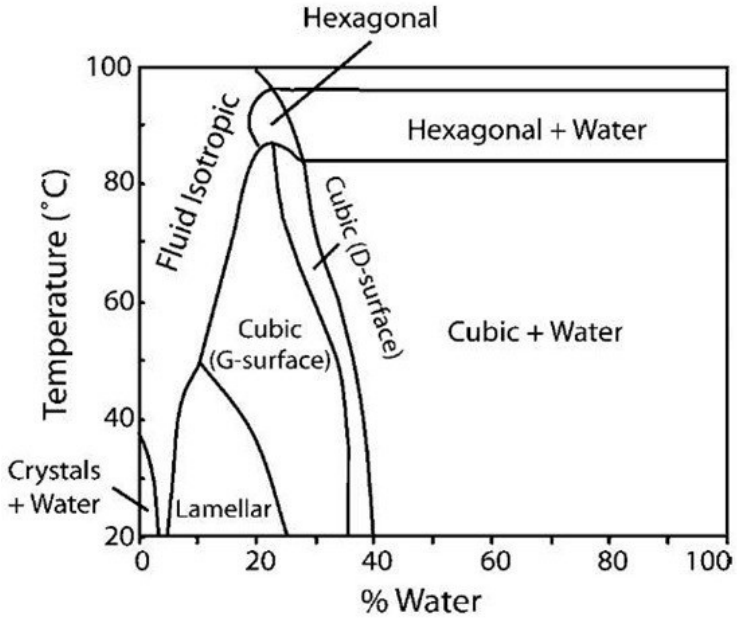

Figure 35. Phase diagram of monoolein/water system.

The dispersion production requires the use of stabilizer: the van der Waals forces driving flocculation, and consequent coalescence to bulk nondispersed phase, are destabilizing factors of the colloidal nature of cubic and hexagonal dispersions. More in details, I used the Poloxamer-407 (**Figure 36**), which had shown to efficiently stabilize dispersions of reversed hexagonal and bicontinuous cubic phases (Gustafsson et al, 1997). As just described, Poloxamer-407 is an amphiphilic triblock copolymer with a structure formula of PEO99-PPO67-PEO99, where PEO and PPO denote poly(ethylene oxide) and poly(propylene oxide), respectively. The hydrophobic middle block (PPO) are anchored in the apolar region or at the surface of the monoglyceride-based bilayers, while the two PEO tails are exposed to water. This disposition can lead to strong steric repulsion between lipid layers thus avoiding the fusion and aggregation phenomena (Minnelli et al, 2018; Gustafsson et al, 1996).

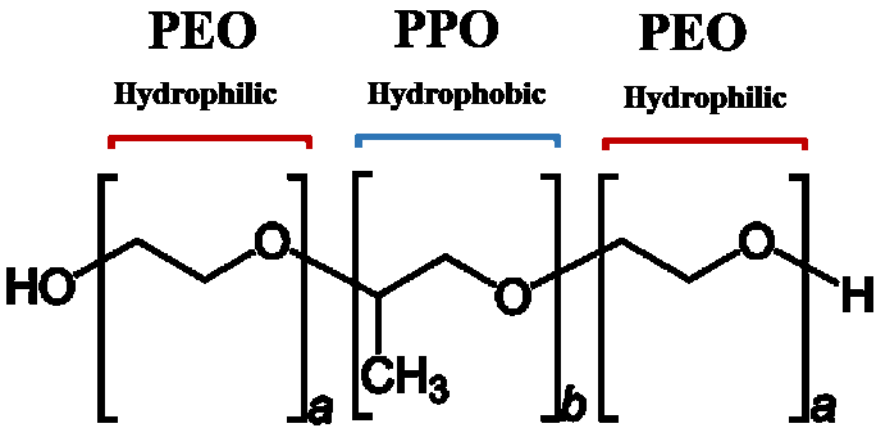

Figure 36. Structure of Poloxamer-407.

With the aim to obtain the cubic structure, the GMO lipid should be hydrated with 20-40% wt/wt of water. As shown in **Figure 35**, the specific phases could be seen, or should be expected, under determined conditions. For example, the pure GMO exists as lamellar phase Lα until 20% water concentration. Instead, by heating there is a transition from the lamellar to cubic and finally into the hexagonal phase which is another type of phase that usually consists of seven rod-like micelles arranged in a hexagonal three-dimensional lattice, that is, in cylinders.

The bulk phases were prepared by hydration of the appropriate amount of GMO (40 mg) with an aqueous solution containing increasing concentrations of EGCG (2, 4, 7 and 10 mg mL^{-1}).

The lipid phase was 4% with respect to the total weight of sample. The EE and DLC were calculated by determining the EGCG concentration in the surnatant (see Material and Methods) by Folin–Ciocalteu assay and the results are presented in **Table 7.**

The EE, shown in green in the table, decreases as the concentration of EGCG increases. The sharp decline is evident in the transition from 7 mg mL^{-1} to 10 mg mL^{-1}. Another important data is o the loading capacity of the system. In this case, we can observe an increase of EGCG amount encapsulated into the lipidic system, until a plateau is achieved at EGCG concentration of 7 mg mL^{-1}. We can therefore conclude that as the concentration of catechins increases, there is a phenomenon of saturation: that is, it does not matter if we use higher concentrations of EGCG, as the loading capacity of the system is exceeded.

Table 7. Composition and properties of bulk phases

Formulations	GMO (% w/w)	EGCG (% w/w)	H_2O (% w/w)	EE (%)	Amount of EGCG entrapped (mg in 1 mL of formulations)	DLC (%)
Blank	4	-	96.0	-	-	-
[EGCG] = 2mg/mL	4	0.2	95.8	44 ± 1.2	0.8 ± 0.2	2.2 ± 0.1
[EGCG] = 4mg/mL	4	0.4	95.6	38 ± 0.8	1.5 ± 0.3	3.8 ± 0.1
[EGCG] = 7mg/mL	4	0.7	95.3	41 ± 0.7	2.9 ± 0.4	7.1 ± 0.1
[EGCG] = 10mg/mL	4	1	95.0	29 ± 7.0	2.9 ± 0.7	7.2 ± 1.7

After having estimate the ability of monoolein to encapsulate EGCG, we proceeded to the obtainment of the corresponding dispersed phases because, as I mentioned, just them are used in ocular drug delivery. Since the EE and DLC did not change in bulk phase with [EGCG] ≥ 7 mg mL^{-1}, the catechins concentrations used in the following experiments were 2, 4 and 7 mg mL^{-1}. The cubosomes were obtained by hydration with PBS of a dry film of monoolein/poloxamer-407 (10:1 w/w) in the presence or not of EGCG, (GMO 40 mg mL^{-1}, 4% w/w). After 48 h of equilibration, optically isotropic gel phases were formed. After ulterior addition of PBS, the bulk phases were disrupted by sonication and the dispersion phase was obtained (GMO 20 mg mL^{-1}, 2.5% w/w). The free EGCG was removed by exclusion chromatography following the procedure previously described for the determination of EGCG entrapment efficiency in liposomes. The formulation details and fundamental properties of the obtained nanoparticle dispersion were listed in **Table 8**.

Table 8. Composition and properties of dispersed phases

Formulations	GMO (% w/w)	EGCG (% w/w)	H_2O (% w/w)	Poloxamer-407 (% w/w)	EE (%)	Amount of EGCG entrapped (mg in 1ml of formulations)	DLC (%)
Blank	2.5	-	97.2	0.3	-	-	-
[EGCG] = 2mg/mL	2.5	0.2	97.0	0.3	74.1 ± 3.5	1.5 ± 0.6	6.0 ± 0.1
[EGCG] = 4mg/mL	2.5	0.4	96.8	0.3	65.2 ± 2.6	2.6 ± 0.8	10.4 ± 0.1
[EGCG] = 7mg/mL	2.5	0.7	96.5	0.3	61.5 ± 4.5	5.3 ± 0.3	21.0 ± 0.1

The EE and DLC values for the dispersed phase were higher compared to those of the bulk system (**Table 7** and **Table 8**). In particular, the EE, highlighted in green, decreases as the concentration of EGCG increases while the DLC doubles and reaches about 6, 10 and 21 %. This different behavior can probably be due to the much larger surface area of the dispersed phase with respect to the bulk phases. Other studies should be performed in order to understand and rationalize these data.

6.3. Nanostructural Characterization

6.3.1. Small Angle Neutrons Scattering (SANS) studies

To investigate the internal structure of the dispersed particles in monooleine-based dispersions and to detect possible variations due to the presence of EGCG, Small Angle Neutrons Scattering (SANS) have been carried out. In particular, SANS experiments have been performed during my experience at the Institut Laue-Langevin (Grenoble, France).

The SANS profiles show that the presence of EGCG into monoolein strongly influenced the supramolecular structure of the systems. More in details, as the EGCG concentration increased, we observed, both in the bulk and dispersed systems, the phase transition from reversed bicontinuous cubic phase Pn3m (Q224, D-surface) to reversed hexagonal phase through the formation of reversed bicontinuous cubic phase 229 (**Figure 37A**). The addition of Poloxamer-407 did not influence the structure of cubosomes and hexosomes and the structure trend observed was the same (**Figure 37B**).

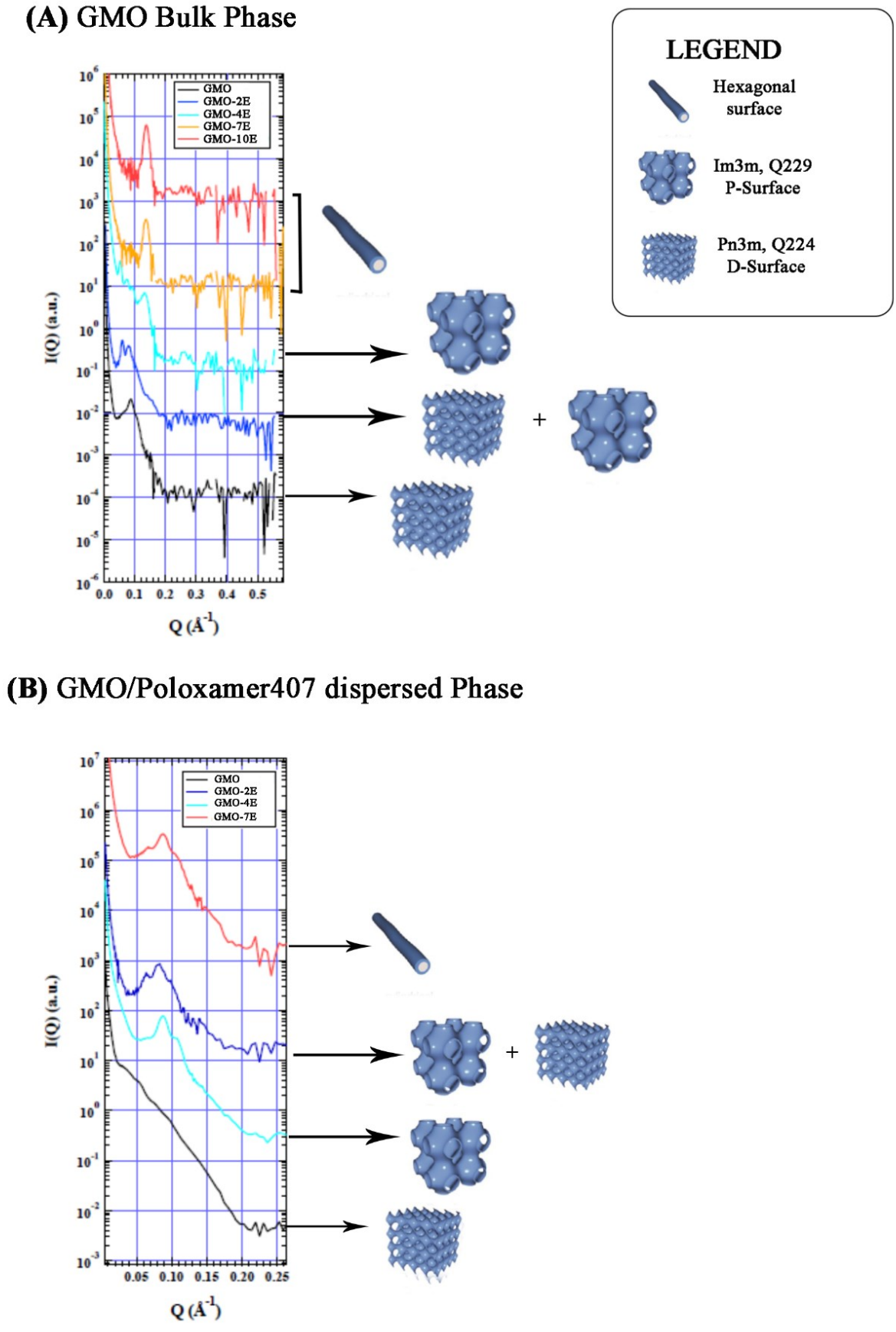

Figure 37. SAXS profiles of a **(A)** bulk GMO phase loaded with EGCG and **(B)** GMO/Poloxamer-407 dispersed phase. GMO-2E, GMO loaded with EGCG 2 mg mL^{-1}; GMO-4E, GMO loaded with EGCG 4 mg mL^{-1}; GMO-7E, GMO loaded with EGCG 7 mg mL^{-1}

6.3.2. Colloidal stability of dispersed phases: Dynamic Light Scattering (DLS)

Since the hexosomes and cubosomes are famous for their extremely stability (also in the far time) I examined by DLS measurement whether the incorporation of increasing amounts of EGCG had altered the colloidal stability of the systems also after 1 month of preparation.

All systems studied (**Table 9**), showed high stability in PBS with a Z average of about 250-300 nm. The polydispersity (PDI) is very low and indicated the presence of highly monodisperse systems, also after 1 month of preparation.

Table 9. Characterization of GMO-dispersed systems [a,b]

Formulation	Time of analyses	Particle size ± SD (nm)	PDI ± SD (nm)
GMO	0 h	263.9 ± 3.9	0.131 ± 0.03
	24 h	253.9 ± 6.6	0.272 ± 0.02
	1 month	290.4 ± 10.4	0.193 ± 0.03
GMO-EGCG 2 mg mL^{-1}	0 h	256.6 ± 2.8	0.213 ± 0.01
	24 h	249.2 ± 4.1	0.224 ± 0.01
	1 month	244.6 ± 5.2	0.131 ± 0.08
GMO-EGCG 4 mg mL^{-1}	0 h	313.7 ± 7.6	0.233 ± 0.06
	24 h	285.8 ± 5.9	0.327 ± 0.05
	1 month	280.1 ± 6.0	0.116 ± 0.01
GMO-EGCG 7 mg mL^{-1}	0 h	226.7 ± 3.8	0.240 ± 0.06
	24 h	225.7 ± 2.1	0.227 ± 0.01
	1 month	277.5 ± 3.8	0.133 ± 0.01

[a] Particle size, PDI and zeta potential were determined by DLS. Encapsulation Efficiency and Loading Capacity were determined as reported in Materials and Methods section. [b] SD: standard deviation

In order to identify the formulation that we will use in the future cellular experiments, the physical stability of the produced dispersion was studied also in the presence of plasma proteins, after their exposure to serum, using DLS. For this purpose, cubosome and hexosomes were incubated in PBS supplemented with FBS (50% v/v) at 37 °C and measurements were carried out at 0 and 24 h. However the presence of serum induces the aggregate formation, which are visible to the naked eye (data not shown), when the EGCG concentration is 7 mg mL^{-1}; therefore, this system is not suitable for drug delivery applications. Probably, its instability is due to the high EGCG concentration.

6.4. Conclusion and future perspective

In this work, GMO and EGCG/GMO systems were prepared and characterized, for their potential use as antioxidant lipid nanoparticles. GMO-based cubosomes and hexosomes containing EGCG were successfully prepared through fragmentation of the bulk cubic and hexagonal phases gel, obtaining nanoparticles with a reproducible and narrow particle size distribution. The more stable systems are the GMO with EGCG concentration of 2 and 4 mg mL^{-1}. The encapsulation efficiency of EGCG is about the same in the two systems but in the systems with 4 mg mL^{-1} of EGCG the loading capacity that is the effective drug content in nanoparticles, is higher than in GMO-EGCG 2 mg mL^{-1}. These systems appears particularly suitable in terms of EE and stability and it will used in the future cellular experiment in order to evaluate its efficacy as antioxidant delivery systems.

CHAPTER VII

A new lipophilic derivative of EGCG

7.1. Introduction

As discussed above, the metabolic and chemical instability in water seems to be responsible of EGCG low bioavailability. Its encapsulation inside the lipid carrier can enhance the amount of catechin that reaches the target site. However, due to its high water solubility, it is difficult to obtain a full encapsulation of EGCG. Previous studies showed that the acetylation of EGCG, masking the hydrophilic OH-groups, increased the solubility of EGCG in fat (Zhu et al, 2014). EGCG was treated with acetic anhydride and pyridine to create peracetate protection of OH-groups and improve its encapsulation into lipid nanoparticles. Despite a partial deacetylation (50% of initially acetylated EGCG), the amount of EGCG in nanoparticles remained constant over 25 days, suggesting improved stability (Barras et al, 2009). Another derivative of EGCG was obtained by esterification of catechin molecule with docosapentaenoic acid (DPA) which has shown an enhanced anti-inflammatory effect compared with free EGCG (Zhong et al, 2012). Therefore, the structural modifications that lead to a reduction of the water solubility of EGCG can modulate its bioavailability as well as its transport by lipid-based nanocarriers.

In light of these considerations, I explored as alternative approach to increase the EGCG bioavailability and cell interaction, the covalent attachment of a lipid moiety to EGCG. With this structural modification I wanted reach a dual goal: to ensure the encapsulation in liposomal carriers of the antioxidant molecule that becomes a constituent of the vector (**Figure 38**) and guarantee the molecule to be retained on the lipid layer of the tear film thus extending its action.

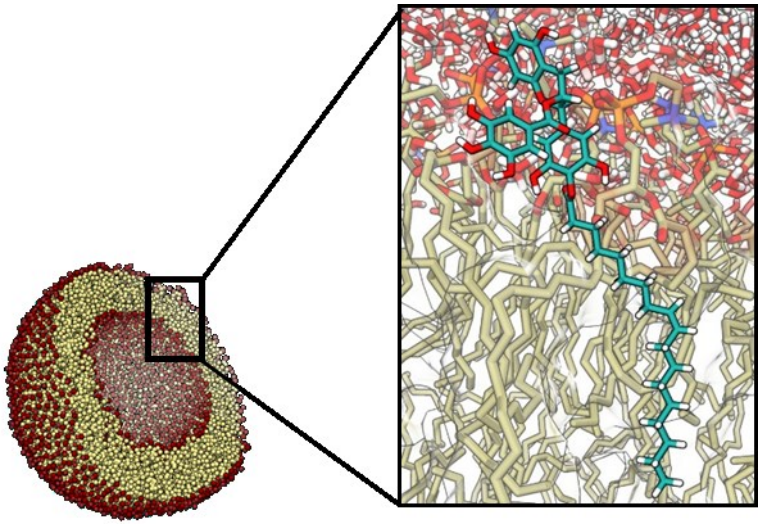

Figure 38. Hypothetical representation of lipophilic derivative organization inside liposome vector

In this way, after administration of eye drops formulation, the molecule may represent the first antioxidant barrier against free radicals and potentially represents an optimal strategy to treat the Dry Eye Disease (Chapter II, section 2.4.).

With the aim to obtain an antioxidant able to strongly interact with phospholipids present in the cells or in the liposome bilayer, my initial strategy was to functionalize EGCG with C-18 chains linked to the phenolic oxygens by ester linker. From the esterification reaction, two main products were obtained, a monoester and a diester, but both the derivatives showed high instability in solution. For this reason, I chose to link the C-18 moiety by an ethereal link.

In this chapter, the synthesis and the structural characterization of a new lipophilic derivative of EGCG will be described. Since the functionalization of EGCG can change the antioxidant properties of the natural molecule, the activity of C18-EGCG ethereal derivative was studied *in vitro* by DPPH and TBARS assays; then, its ability to contrast H_2O_2-induced cell death, was assessed in human retinal cells.

7.2. Synthesis and characterization of an ether derivative of EGCG

C18-EGCG ethereal derivative has been prepared by Williamson ether synthesis. In this reaction, a halide ion is displaced from an alkyl halide by an alkoxide ion in an SN_2 reaction. The alkoxide ion is generally prepared by the reaction of an alcohol with a strong base such as sodium hydride. In the O-alkylation reaction of polyphenols the moderate acidity of phenolic proton allows to employ K_2CO_3 to remove a proton and generate the alkoxide. (Jurd, 1962). In an one-pot reaction, after addition of an equivalent of octadecyl iodide to EGCG in the presence of K_2CO_3, I obtained a principal product (**Scheme 1**) purified by silica gel chromatography (35% yeld).

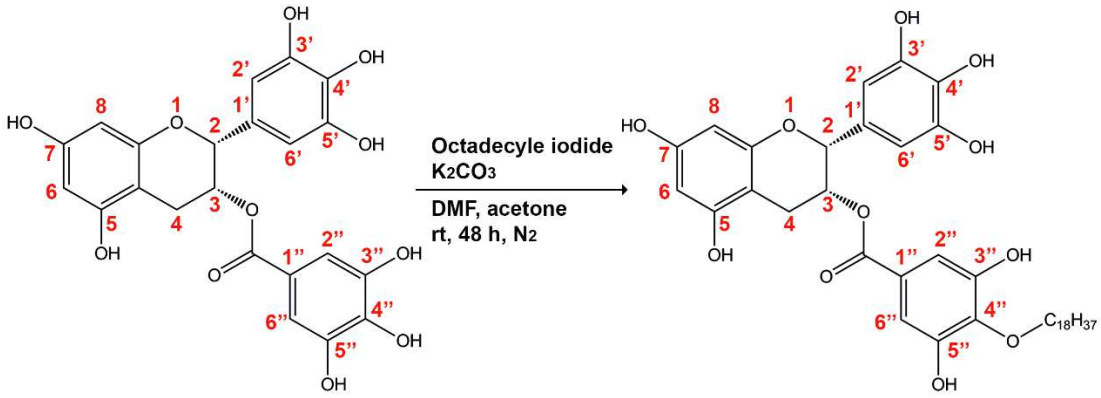

Scheme 1

The nuclear magnetic resonance and mass spectrometry characterization stated the presence of a C-18 chain in the molecule skeleton. The analysis of ^{13}CNMR spectra allows us to affirm that EGCG has been alkylated at the 4" position; according with literature data reported for 4"-alkyl derivatives of EGCG, (Seo et al, 2017), we can observe down-field shifts of C1", C3" and C4" carbon peaks respect to EGCG. To confirm the assignment of 4"-O-octadecyl-EGCG structure to the synthesized derivative of EGCG, a heteronuclear multiple-bond connectivity (HMBC) experiment has been carried out. The HMBC experiment gives correlations between carbons and protons that are not directly connected. In **Figure 39** we can observe a cross-peak between C4" and methylenic protons of C18 chain directly bound to the oxygen in C4".

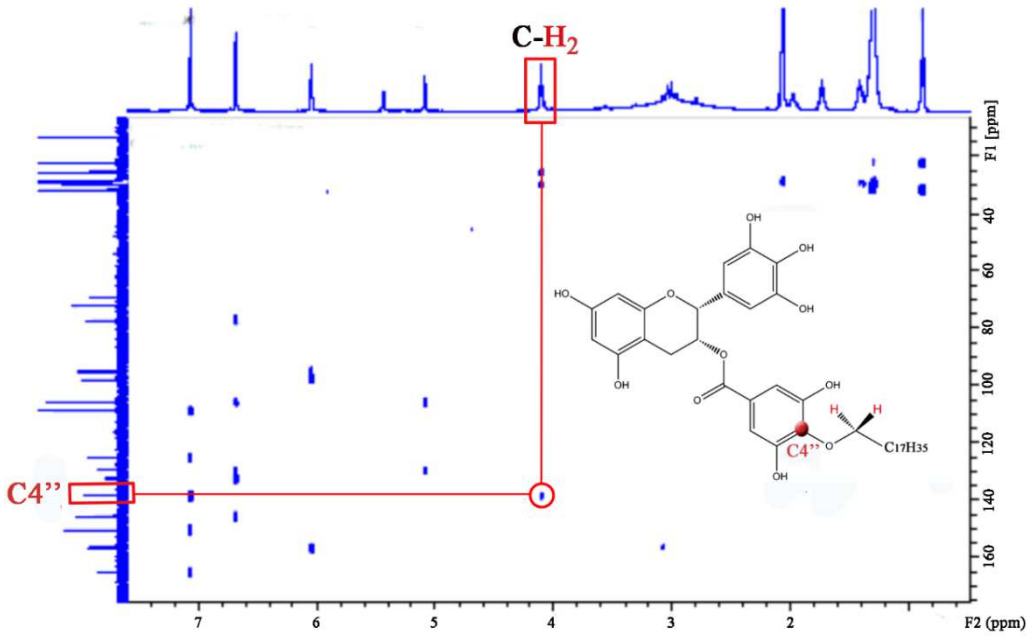

Figure 39. HMBC experiment. Cross-peak between C4" and methylenic protons of C18 chain directly bound to the oxygen in C4".

7.3. Antioxidant properties of new derivative

7.3.1. Scavenging Activity on the DPPH Radical

The scavenging activity of C18-EGCG was evaluated by DPPH assay and compared with that of corresponding concentration of Vitamin E and free EGCG. The Vitamin E has been chosen for its structural similarities with C18-EGCG (**Figure 40**): they both consist of two functional domains: a long hydrocarbon chain, which is responsible for the lipophilicity of the molecule and its proper location within the membrane bilayer; and a head group responsible for their antioxidant activity. Moreover, Vitamin E was found to be beneficial in prevention of cataracts (Tavani et al, 1996; Theodoropoulou et al, 2014) and age-macular degeneration (van Leeuwen et al, 2005; Bibiloni et al, 2014).

In order to verify the antioxidant stability, the DPPH assay was also performed after 24, 48, 72 and 96 h.

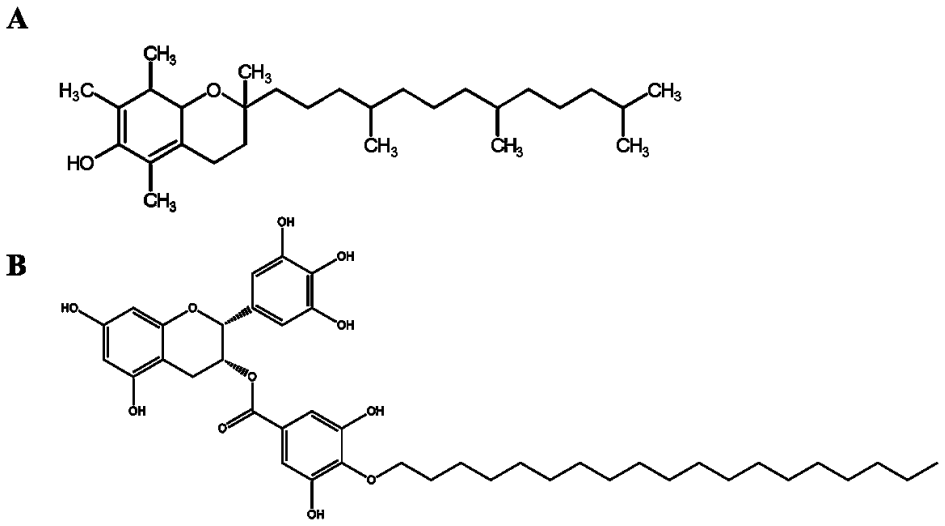

Figure 40. 2D structures of **(A)** Vitamin E and **(B)** C18-EGCG.

DPPH is a stable nitrogen-centered free radical commonly used for testing radical scavenging activity of antioxidant molecules. It possesses a purple color, with a maximum absorption at 519 nm in ethanol; when it accepts an electron (single electron transfer, SET) or a hydrogen atom (Hydrogen atom transfer, HAT) from an antioxidant compound, the DPPH radical scavenging results in a decrease in absorption. The extent of decrease in DPPH absorption can be measured colorimetrically and can be correlated to the concentration of radicals that have being scavenged. DPPH radical scavenging activity of tested molecules is presented in **Figure 41** as percentage inhibition of DPPH radicals at different time of analysis. The samples

were protected from the light with an aluminium foil to prevent photodegradation of EGCG and Vitamin E (Bianchi A. et al. 2011; Sabliov et al, 2009) and were maintained at 25°C.

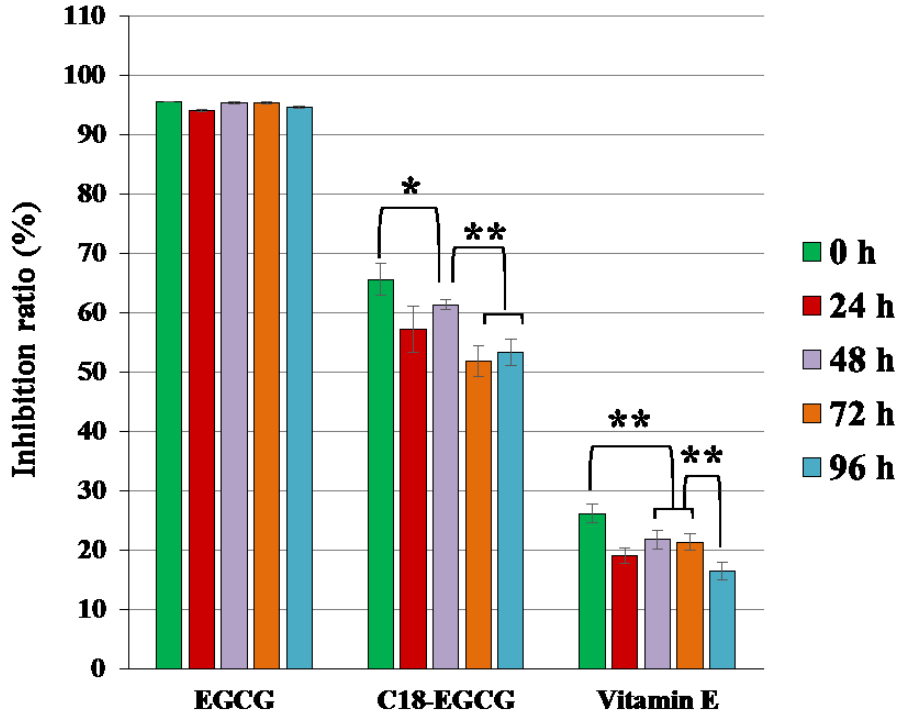

Figure 41. DPPH free radical scavenging activity of EGCG, C18-EGCG and Vitamin E at different time of analyses (0, 24, 48, 72 and 96 h). The values in the figures are expressed as the means ± SD; n=7 independent experiments. Significant differences can be observed between the different time of analyses, as indicated in the figure, *p<0.05; **p<0.001.

All tested compounds had the ability to quench DPPH radical. However, the EGCG was found to be the strongest one at each time analyzed (percentage inhibition, ca. 95%). The presence of C-18 carbon chain in the EGCG determined a reduction in the antioxidant capacity of molecule of about 30% (percentage inhibition, ca. 65%). A probable hypothesis is that the functionalization, masking the OH-group, decreased the number of hydroxyl groups that are able to donate hydrogen atoms and electrons involved in the reduction of free radicals. Finally, the Vitamin E with only one hydroxyl group, showed a low scavenging activity of about 27% at time=0 of analysis.

With regard to antioxidant stability, the functionalization of EGCG seems to be responsible of a certain instability of catechin over time; however, after an earlier decrease (percentage inhibition at 72 h, 53%, p<0.001), the antioxidant capacity did not change in the analyzed time. Also the Vitamin E partially lost its antioxidant activity, but in this case the decrease

occurred already after 48 h (percentage inhibition, 21%; $p<0.001$) and we observed the further reduction after 96 h of incubation (percentage inhibition, 16%; $p<0.001$). As reported by others (Sabliov et al, 2009), the exposition to oxygen, light and/or minerals can degrade the Vitamin E.

Based on these results, the functionalization of EGCG seems to be responsible of a decreased antioxidant capacity of the natural catechin also over time.

.

7.3.2. Protection of liposome oxidation: TBARS assay

As described above (Chapter I, section 1.3.2.), the lipid peroxidation (LPO) is a critical and common damaging process in biological membranes. This damage induced by LPO may also impair the efficiency of liposomal dispersion containing polyunsaturated fatty acids (PUFAs) as drug delivery systems. Thus, prevention of LPO represents an interesting therapy in many diseases and pathologies involving free radicals and is also an important aspect in the preparation and preservation of liposomes to be used as carriers for several agents in medicinal, pharmaceutical, cosmetic and food industry applications.

The antioxidant activity of the synthesized C18-EGCG against radical-induced lipid peroxidation was evaluated in liposomes made up of egg-PC (PC, phosphatidylcholine) containing poly-unsaturated chains susceptible of oxidation and compared with equal concentration of EGCG and Vitamin E. The water-soluble azo-initiator 2,2-azobis(2-amidinopropane)dihydrochloride (AAPH) was used as the radical generating system since it thermally decomposes at a constant rate producing a continuous flux of radicals.

The antioxidant activity of the samples was evaluated by measuring the percentage inhibition of aldehydic breakdown products (Thiobarbituric Reactive Species, TBARS) formed during the peroxidation process and shown in **Figure 42**. Even if TBARS assay is not so specific and may give overestimated results, it remains however the simplest, cheapest and widely used method for identifying the presence of lipid peroxide products (malondialdehyde and other aldehydes). As showed in **Figure 42**, all compounds were able to inhibit lipid peroxidation in high percentage (percentage inhibition, 78–90%), with natural and functionalized EGCG being a little more active than the Vitamin E. No significative difference was observed between EGCG and its derivative.

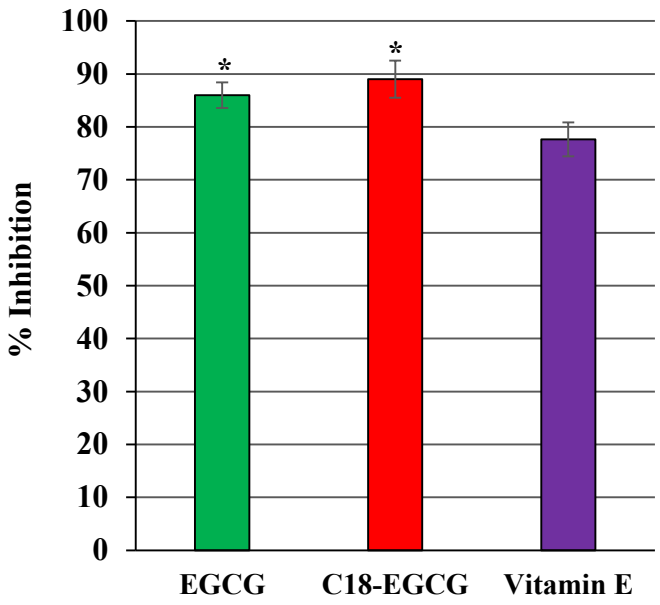

Figure 42. % Inhibition of TBARS formation in PC (3 mM) liposomes peroxidation by EGCG, C18-EGCG or Vitamin E (0.05 mM) induced by thermal decomposition (310 K, 1 h) of AAPH (5 mM). The values in the figures are expressed as the means ± SD; n=5 independent experiments. *p<0.05, C18-EGCG and EGCG vs. Vitamin E.

As described previously, the EGCG as well as the Vitamin E acts as ‘‘chain blocker’’ thus inhibiting the lipid peroxidation. The hydrophobic nature of C18-EGCG and Vitamin E makes them able to insert into the lipid bilayer; therefore, they blocked TBARS formation by interrupting the propagation of lipid peroxidation in the membranes. Even though the EGCG is able to interact with lipid bilayer (Laudadio et al, 2017; Laudadio et al, 2018; [b]Minnelli et al, 2018), a part of it also lie in the water phase thus scavenging a portion of AAPH radical before its interaction with membrane lipids. Consequently, although the percentage inhibition observed for the lipid peroxidation is about the same for the samples studied, the contribution of these two mechanisms can be different. It is interesting to observe that, although the functionalization had decrease the radical scavenging activity of EGCG, the protection of lipid peroxidation was similar for these two molecules.

7.3.3. Cellular Experiments

First of all, I evaluated the toxicity of the new derivative in ARPE-19 cells by MTT assay and compared with that of corresponding concentrations of Vitamin E and free EGCG. As shown in the **Figure 43**, the studied molecules did not decrease the cell viability after 24 h of treatment. Importantly, the methanol, which I used as vehicle, did not affect the cell viability at the concentration used in the experiments (data not shown). In particular, the treatment whit C18-EGCG in 10-240 μM range did not decrease the cell viability after 24 h of treatment increasing instead the cell proliferation. The mitogens effect may be explained as a function of its C-18 saturated tails that leads to a lipid accumulation in the cell membrane, thus enabling

them to play a role in cell proliferation. Similar results were obtained after treatment of ARPE19 cells with exogenous phospholipids, added as liposomes ([b]Minnelli et al, 2018).

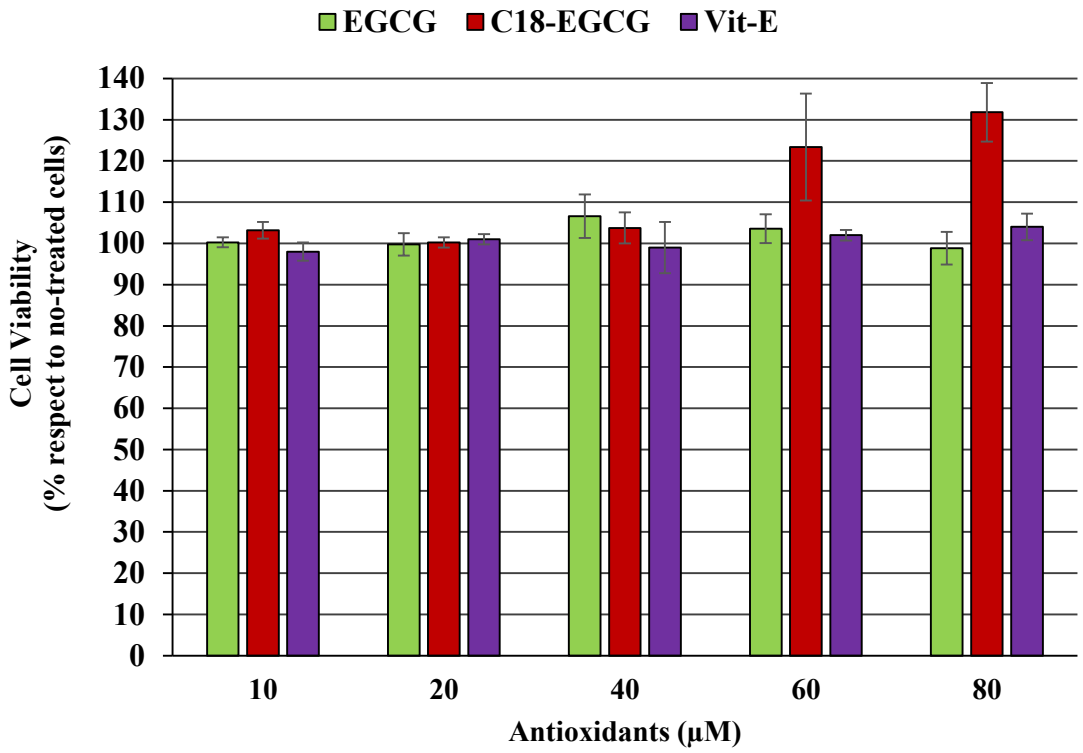

Figure 43. Cytotoxicity of C18-EGCG in ARPE19 cells. The cells were treated with various concentrations of EGCG, C18-EGCG, and Vitamin E for 24 h in complete culture medium. The viability of treated-cells as reported as percentage respect with no-treated cells, which are considered as 100% of cell viability. The values in the figures are expressed as the means ± SD.

Next, in order to study C18-EGCG potential ability to protect ARPE-19 cells from physiological stressors, oxidative damage mediated by hydrogen peroxide was induced (Iloki-Assanga et al, 2015). After pre-treatment of ARPE-19 with EGCG, C18-EGCG and Vitamin E for 24 h, cells were washed twice with PBS to avoid direct extracellular interactions between the tested compounds and the oxidant. In this way, only the molecules that entry in cells or that strongly interact with lipid bilayer may protect the cells from oxidative stress induced-cell death.

As in the previous work (Chapter V), the cells were treated with hydrogen peroxide for 6 h and the results are showed in **Figure 44A**. All the antioxidant studied protected the cells from oxidative stress induced-cell death although with different efficacies (EGCG < Vitamin E < C18-EGCG). The protection provided by EGCG was dose-dependent with the best result

obtained at 40 µM concentration (ca. 20% more cell viability than H_2O_2-exposed cells) while, after treatment with EGCG concentrations up to 40 µM I did not observe significant differences in cell viability respect to H_2O_2-exposed cells. On the contrary, C18-EGCG and Vitamin E continued to have a protective effect even at high concentrations (60-80 µM). However, the Vitamin E showed the similar protection capacity of EGCG inducing a maximum increase of viability cells of about 25% respect to H_2O_2-exposed cells at 40 µM concentrations. The functionalization of EGCG markedly enhanced the protective effect of molecule against oxidative stress with an increase in cell survival in a range of 40-50% compared to H_2O_2-exposed group cells ($p<0.001$). In particular, at 40µM concentration, the C18-EGCG protected the 41% of cells from oxidative stress-induced cell-death and therefore the protection capacity was about 16-20% higher than to Vitamin E and EGCG at the same concentration, respectively.

Probably, the hydrophobic carbon chain effectively increased the interaction of C18-EGCG's with lipidic tails of cellular membrane: after the washing step the lipophilic molecules remain inserted inside bilayer while the portion of hydrophilic EGCG that lies in water phase will be brought away. Consequently, the lipid moiety increased the antioxidant protection of new derivative.

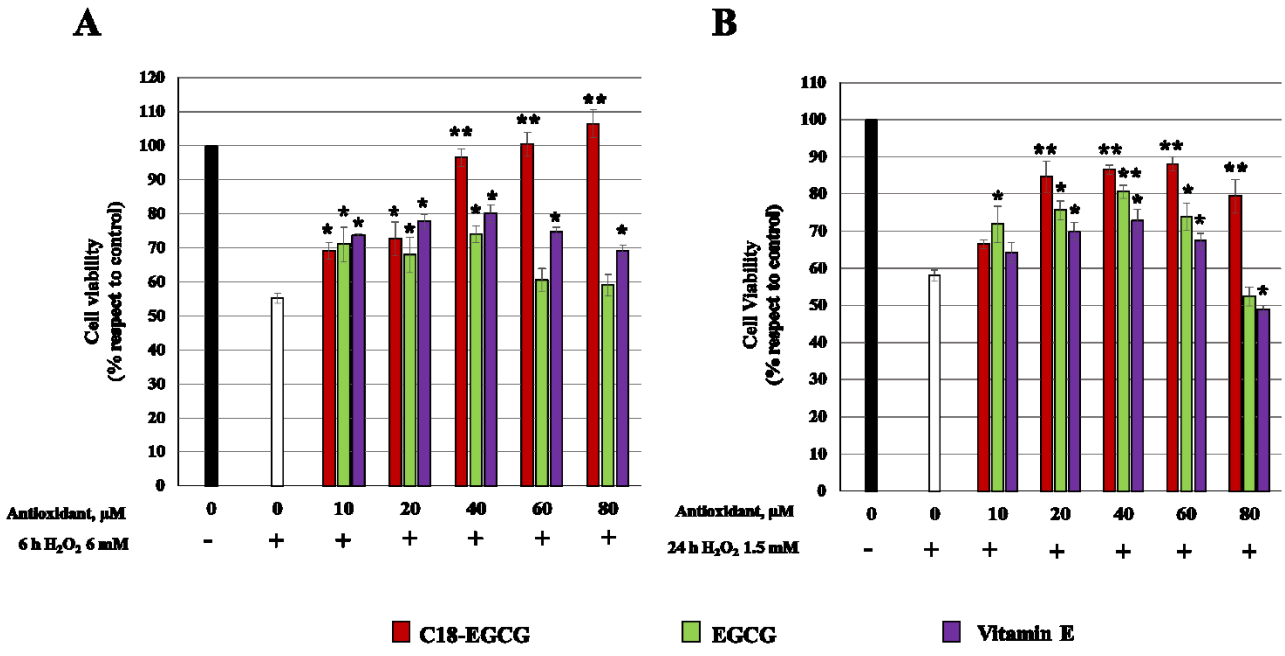

Figure 44. Effect of C18-EGCG in ARPE19 cells after H_2O_2 exposure. The cells were pre-treated with increasing concentrations of C18-EGCG, EGCG or Vitamin E for 24 h, before being exposed to **(A)** 6 mM H_2O_2 for 6 h or **(B)** 1.5 mM H_2O_2 for 24 h. Cell viability was determined by MTT assay. Data are expressed as means ± S.D. of five independent experiments, each performed in triplicate. Significative differences between samples and H_2O_2-exposed cells, as reported in the figure. *$p<0.05$ and **$p<0.001$.

From a clinical perspective, it is highly desirable having a compound that could protect against oxidative stress over an extended period in the presence of an oxidant. Therefore, in an additional experiment, the ARPE19 cells, pre-treated with the antioxidant compound for 24 h as described above, have been exposed to H_2O_2 for 24 h. As showed in **Figure 44B**, the three antioxidants molecules protected the cells from oxidative stress. However, C18-EGCG provided a higher degree of protection than the others did. Moreover, while the increase of EGCG and Vitamin E concentrations produced the known cytotoxic effect with a decrease of cell viability of respectively 10% and 8% than H_2O_2-exposed group cells ($p<0.05$), EGCG-C18 had a protective effect even at high concentrations (80 μM, 22% more cell viability than H_2O_2-exposed cells, $p<0.0001$).

7.4. Conclusion and future perspective

Although the functionalization strategy seems to be responsible of a decreased antioxidant capacity of the natural EGCG also over time, the protection towards the lipid peroxidation was similar for these two molecules. In addition, C18-EGCG significantly reduced oxidative stress-induced retinal damage more strongly than free EGCG. The hydrophobic nature of C18-EGCG makes it able to insert into the cell membrane lipid bilayer: in this environment, the molecule can act as ‘‘chain blocker’’ thus inhibiting the lipid peroxidation and therefore increasing the antioxidant protection of molecule. These data suggest that C18-EGCG may be promising as a novel therapeutic drug candidate in the treatment of disease associate with oxidative stress.

It is important to underlying that the new lipophilic antioxidant molecule needs solvent vehicle and could not be used for the eye drops development without a carrier. The development of Drug Delivery Systems is therefore needed. Future studies will performed in order to study the effective ability of lipid moiety to increase the encapsulation efficiency of the antioxidant inside lipid-based nanocarriers.

PART III – A new lipophilic derivative of Edaravone: antioxidant properties and liposomal formulations

"One child, one teacher, one book, one pen can change the world"
-Malala Yousafzai-

CHAPTER VII

Edaravone Derivative

8.1. Introduction

Edaravone (3-methyl-1-phenyl-2-pyrazolin-5-one) (**Figure 45**) has been used in Japan to treat acute cerebral infarction since 2001, and was approved (Radicava® and Radicut®) for amyotrophic lateral sclerosis (ALS) treatment at June 2015 in Japan and at May 2017 in U.S. (Petrov et al, 2017; Watanabe et al, 2018). The molecule was discovered during a research program aimed at develop antioxidants for the treatment of acute cerebral infarction and with a phenol-like free radical-scavenging activity. The basic idea was to synthesize an aromatic heterocycle structure where a hydroxyl group would be generated by keto-enol tautomerization in order to obtain the key functional group responsible for the radical-scavenging activity of phenol derivatives. A variety of heterocyclic ring containing an amide or a ketone moiety were synthesized and 3-methyl-1-phenyl-2-pyrazolin-5-one (edaravone) was identified as an active compound.

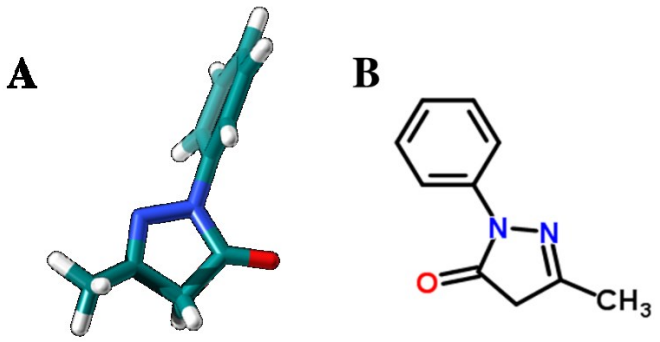

Figure 45. Edaravone **(A)** 2D structure and **(B)** 3D structure.

The mechanism action of Edaravone (EdV) is mainly based on its free radical scavenging activity by which it protects against oxidative stress and neuronal apoptosis (Watanabe et al, 2018). The EdV quenches hydroxyl radicals (·OH) and strongly inhibits lipid peroxidation (Yamamoto et al, 1996); it also scavenges the superoxide anion (O_2^{-}·), hydrogen peroxide (H_2O_2) and peroxynitrite ($ONOO^-$) (George, 1947; Fridovich, 1978). In addition, the chemical structure makes Edaravone able to cross the blood-brain barrier, unlike other free

radical scavengers. These properties may be important for its neurovascular protective effects observed in patients with acute ischemic stroke.

The EdV has an acid constant dissociation (pKa) of 7.0 showing the properties of a weak acid and its dissociation affords the anion with release of a proton. Therefore, at physiological environment (pH, 7.4), the percentage of the neutral and anionic forms is about 29% and 71%, respectively (Watanabe et al, 2018). The neutral form of the Edaravone shows keto-enol tautomerism with three isomeric structures and, in the same way, the Edaravone anion possess three resonance structures (**Figure 46**). All these forms are present at pH 7.4. The keto-enol tautomerism and the presence of the anionic form are the basis of the antioxidant activity of Edaravone in the body.

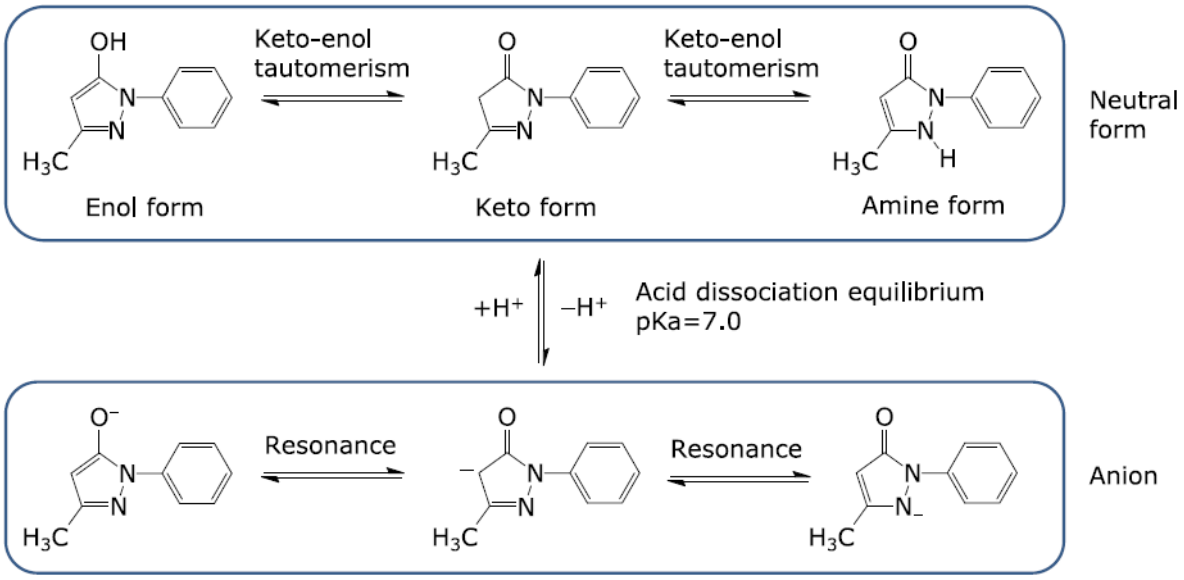

Figure 46. Edaravone tautomerism and acid dissociation equilibrium. From Watanabe et al, 2018.

In particular, the preponderant mechanism of radical scavenging by Edaravone is shown in **Figure 47**. Edaravone anion scavenges radicals (·X) to produce anion molecules (X−), Edaravone radicals and oxidation products. Thus, the radical scavenging activity of this molecule can be attributed to scavenging by single electron transfer (SET) mechanism, and the major product of this reaction is 2-oxo-3-(phenylhydrazono)-butanoic acid (OPB). Another mechanism is based on allylic hydrogen abstraction (AHA) that produces an unpaired electron delocalized at 2, 4, and 6 positions (**Figure 48**).

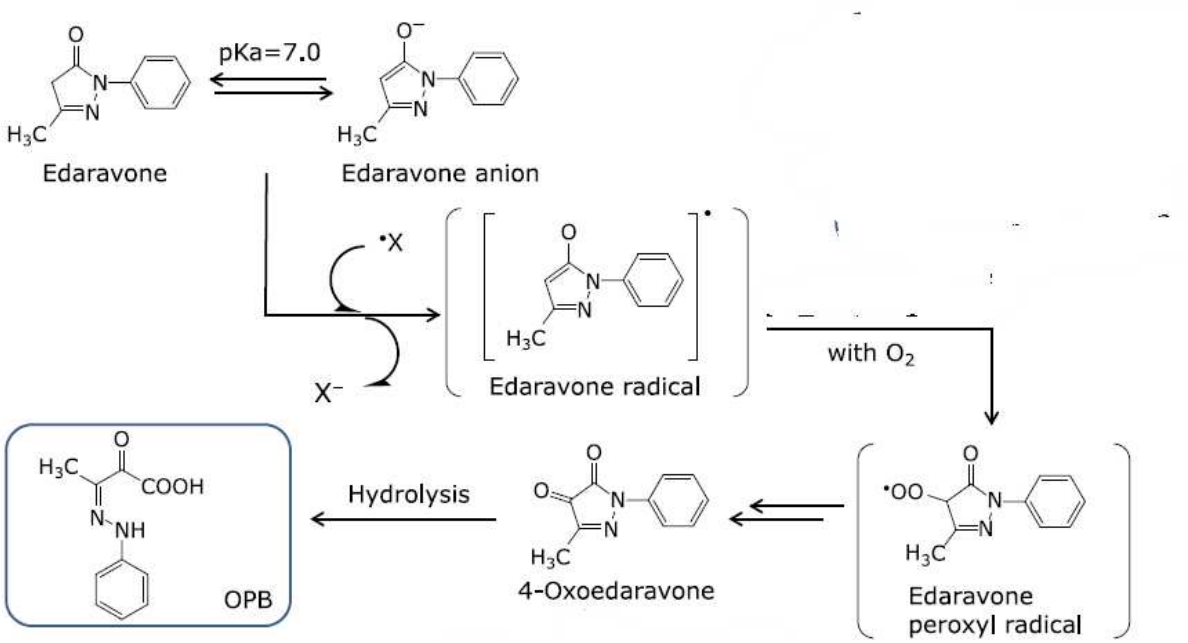

Figure 47. Single electron transfer (SET) mechanism for the scavenging activity of Edaravone. From Watanabe et al, 2018.

Therefore, the Edaravone reactivity, and consequently its antioxidant activity, might be controlled by tuning the acid–basic equilibrium. In addition, the lipophilicity of the neutral form and its low molecular weight makes the EdV able to enter lipid environments such as cell membranes, and scavenge peroxyl radicals generated from lipids in radical chain reactions.

As well as being bioactive in stroke treatments, the Edaravone is also a promising candidate for the treatment of retinal diseases associated with oxidative stress including age-related macular degeneration (AMD), glaucoma, diabetic retinopathy (DR), and retinal vein occlusion (RVO) (Masuda et al, 2017). However, the EdV is a substrate of P-glycoprotein (P-gp). Thus, despite its lipophilic nature, poor intestinal and ocular permeability was reported (Shimazaki et al, 2011; Rong et al, 2014). The P-gp plays a major role in limiting drug absorption by enhancing Pgp-mediated efflux and consequently reducing the oral and ocular adsorption of EdV (Rong et al, 2014). Moreover, the aqueous formulations of Edaravone are very unstable because the presence of Edaravone anion, which is capable of transferring an electron to radicals including oxygen, and becomes Edaravone radical.

For these reasons, the development of eye drops containing EdV can take advantage from the use of lipid-based nanocarriers, which can increase its residence time and its permeation through the ocular barriers. In fact, *in vivo* and *in vitro* studies showed that the protective effects against visual dysfunction and apoptosis induced by light exposure were higher for edaravone-loaded liposome than to free drug (Shimazaki et al, 2011). Therefore, I believe that EdV specific delivery by liposomes may be a promising way to treat ocular disorder with high efficiency and extended intervention time-window (Shimazaki et al, 2011; Hironaka et al, 2011).

Since the Edaravone-loaded liposomes show a low degree of molecule encapsulation of about 25% (Shimazaki et al, 2011; Hironaka et al, 2011), I decided to synthesize an analog that possess a great lipophilic character in order to be easily incorporated inside lipid matrix and/or into lipid layer of the tear film. In addition, it has been shown that the introduction of lipophilic group at C-4 or C-3 position of 2-pyrazolin-5-one ring (**Figure 48**) seems to increase the lipid peroxidation-inhibitory activity in biological systems (Watanabe et al, 1997; Watanabe et al, 2018).

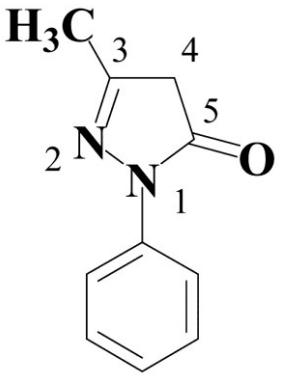

Figure 48. Numbering of Edaravone functionalization sites

Based on these considerations, I introduced a C-18 chain at C-4 position of Edaravone. The synthesis and the structural characterization of this new lipophilic derivative of Edaravone will be described. After having studied its new radical scavenger ability by DPPH assay, I determined the antioxidant effect of the new derivative on lipid peroxidation of artificial lipid membrane. With the aim to investigate if the functionalization strategy allow me to increase the Edaravone interaction with lipid vector, liposomal formulations were developed and the encapsulation efficiency studies were performed. After evaluation of the colloidal

stability, the ability of these liposomes to contrast oxidative stress induced cell death was assessed in human retinal cells and compared whit that of free C18-EdV.

8.2. Synthesis and characterization of C18- Edaravone

To synthesize the 3-metil-4-ottadecil-1-fenil-1H-pirazol-5(4H)-one, alkylation of ethyl acetate was carried out using sodium ethoxide in ethanol as base and octadecyl bromide as alkylating agent. The condensation reaction of the alkylation product with phenylhydrazine allowed me to obtain Edaravone-C18 (**Scheme 2, Figure 49**).

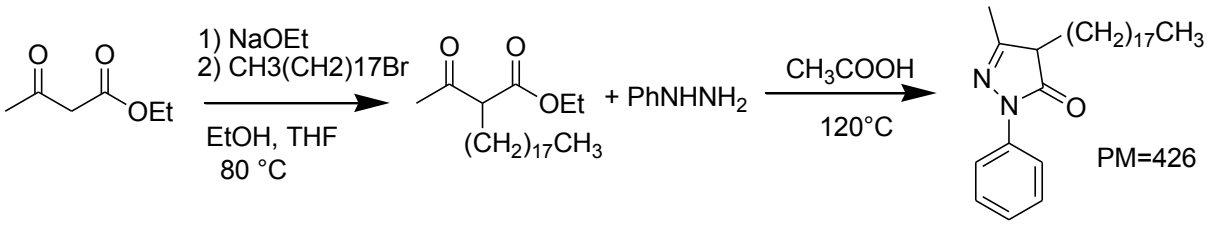

Scheme 3

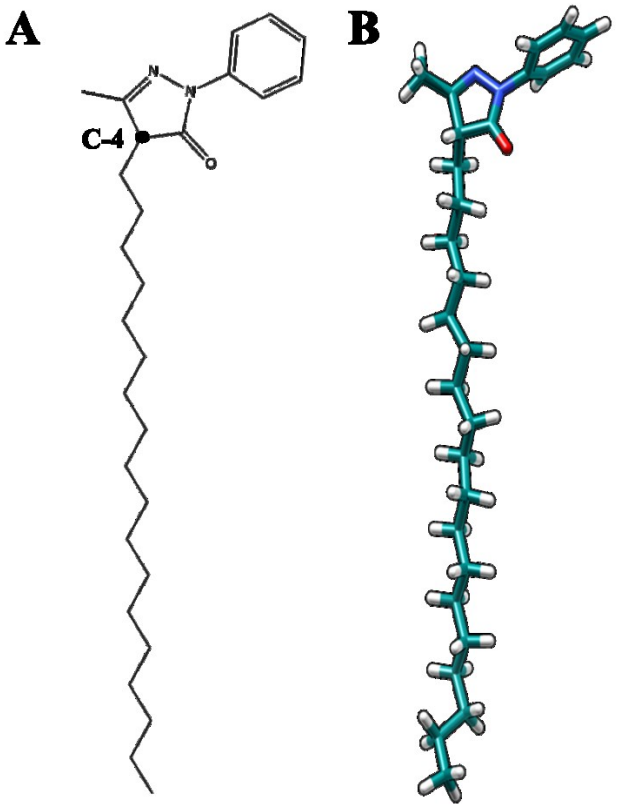

Figure 49. 3-metil-4-ottadecil-1-fenil-1H-pirazol-5(4H)-one (Edaravone-C18, EdVC18) structure. **(A)** Shows 2D structure and **(B)** shows 3D structure.

The structure of the synthezised molecule has been confirmed by mass spectrometry (MS), infrared spectroscopy (IR), elemental analysis and nuclear magnetic resonance spectroscopy (NMR). The analysis of ^{1}HNMR spectra, carried out in $CDCl_3$ (**Figure 50**) and in DMSO (**Figure 51**), has shown that the Edaravone-C18 can exist in at least two tautomeric forms, in analogy to what reported in for Edaravone (Pérez-González and Galano, 2011). In fact, the solvent structure in which the ^{1}HNMR spectrum is recorded allows the stabilization of the ketonic or enol form depending on the ability of the solvent itself to give hydrogen bond with the molecule.

In the two spectra, registered in $CDCl_3$ and DMSO, the existence of the tautomerization is evident. In the chetonic form ($CDCl_3$) I can found the proton bound to the alpha carbon (Cα) at about 3.25 ppm, but it disappears when the enolic form is present and a more deshielded proton appear at about 10.5 ppm. The results indicate that the functionalization of Edaravone with a long carbon chain does not prevent the keto-enol tautomerism which seems to be one of fundamental causes of the antioxidant activity of Edaravone in the body.

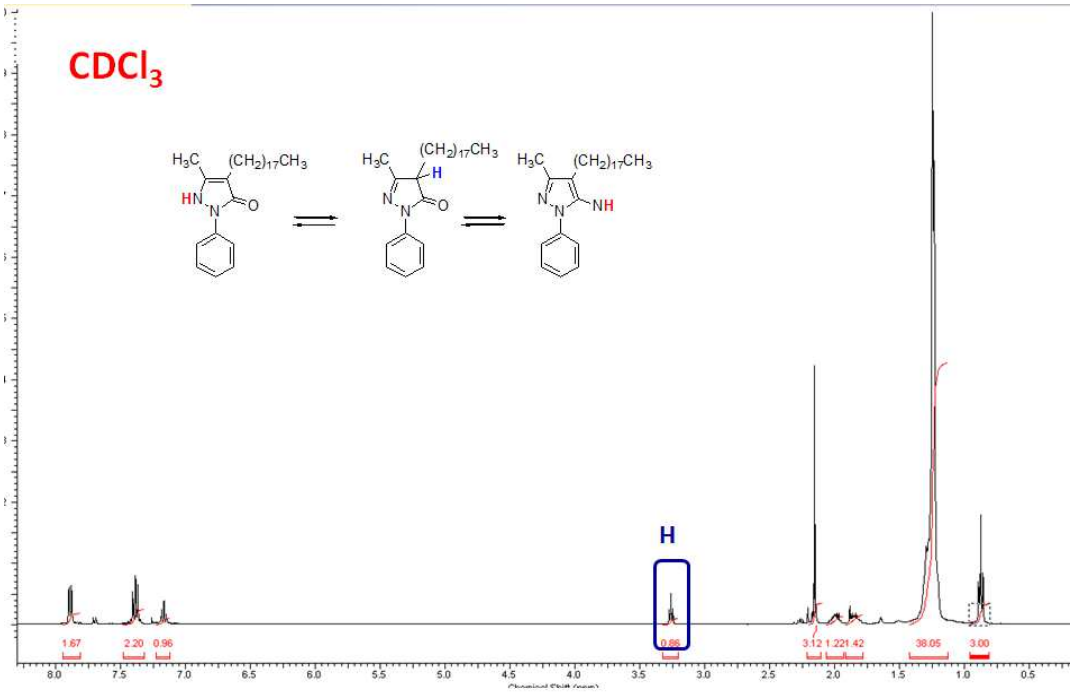

Figure 50. ^{1}HNMR spectra of C18-Edaravone, carried out in $CDCl_3$.

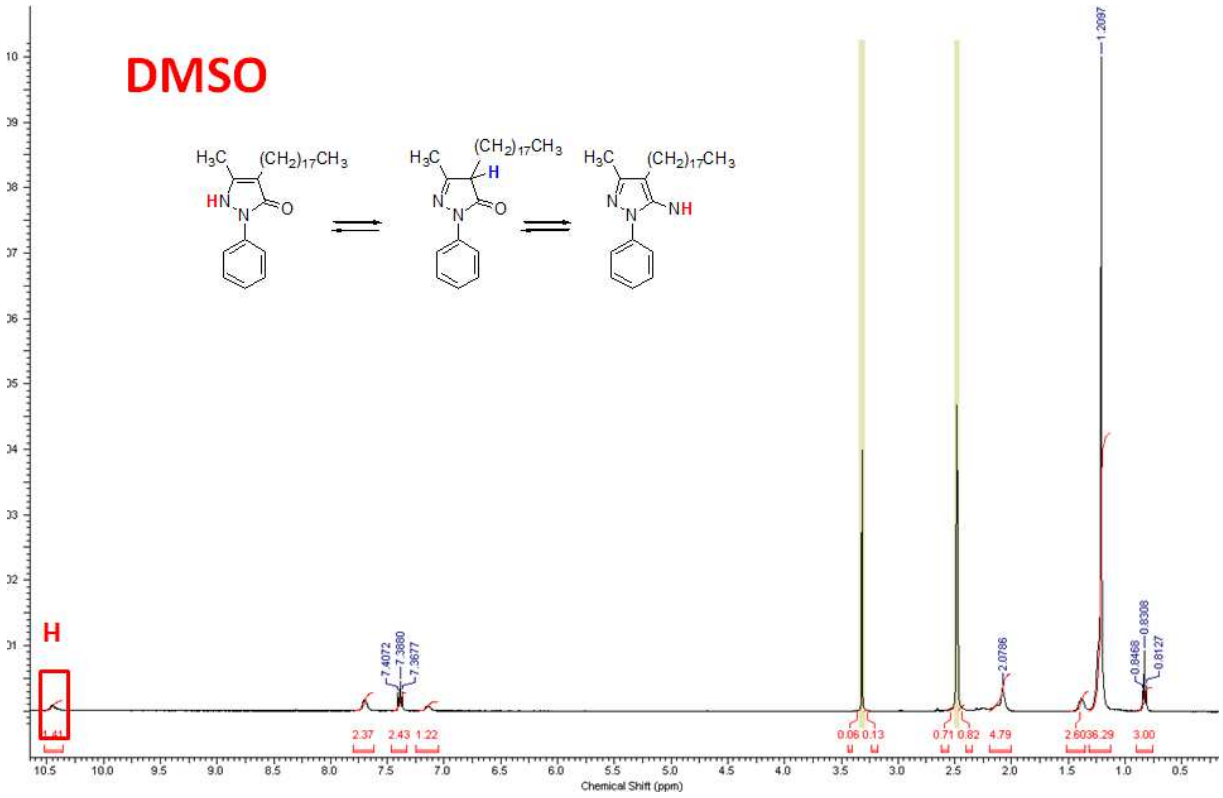

Figure 51. [1]HNMR spectra of C18-Edaravone, carried out in DMSO.

8.3. Antioxidant activity of C18-Edaravone (C18-EdV)

8.3.1. Scavenging Activity on the DPPH Radical

The scavenging activity of C18-Edaravone (C18-EdV) was evaluated by DPPH assay and compared with that of corresponding concentration of free Edaravone. DPPH radical scavenging activity of the tested molecules is presented in **Figure 52** as percentage inhibition of DPPH scavenging activity. During the preparation, the vials containing samples were protected from the light with an aluminum foil and were maintained at 25°C.

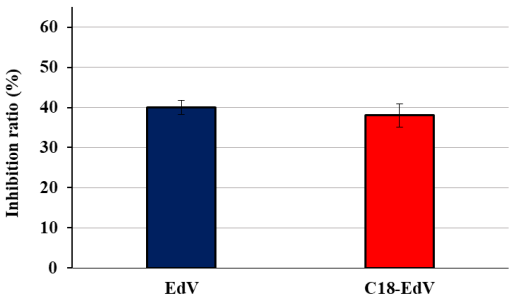

Figure 52. DPPH free radical scavenging activity of Edaravone (EdV) and C18-Edaravone (C18-EdV).

As described above (see Material and Methods), the DPPH is a stable nitrogen-centered free radical commonly used for testing radical scavenging activity of antioxidant molecules. As shown in the histogram, the EdV-C18 retains the same scavenging activity of the parent compound and this means that the structural modification did not influences the antioxidant capacity of the molecule.

8.3.2. Protection of liposome oxidation: TBARS assay

As widely discussed, the lipid peroxidation is responsible of damage and functional impairment of biological membranes; therefore, particular attention is given to the development of drugs that suppress such oxidation.

The antioxidant activity of the synthesized C18-EdV against radical-induced lipid peroxidation was evaluated in liposomes made up of egg-PC (PC, phosphatidylcholine) containing poly-unsaturated chains susceptible of oxidation and compared with that of an equal concentration of Edaravone. The oxidation was initiated with either a water-soluble initiator (AAPH) or a lipid-soluble initiator (AMVN), in order that the initiator radicals were generated inside in the aqueous phase or in the lipid bilayer, respectively **(Figure 53)** (see Material and Methods).

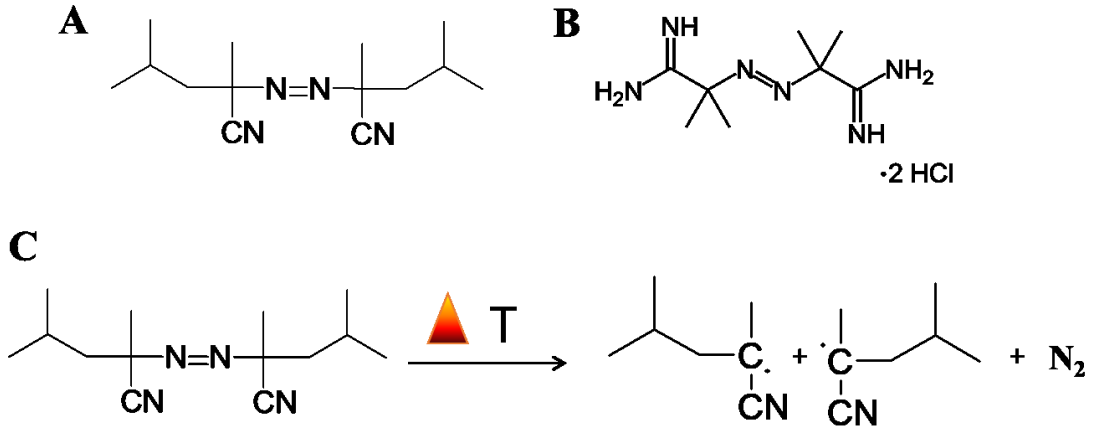

Figure 53. Chemical structure of the azocompounds **(A)** 2,2-azobis(2,4-dimethylvaleronitrile) (AMVN) and **(B)** 2,2-azobis(2-amidinopropane hydrochloride) (AAPH). **(C)** Generation of carbon-centered radicals by thermal decomposition of the water-soluble azo-compound.

The antioxidant activity of Edaravone and Edaravone C-18 was evaluated during AAPH and AMVN-induced lipid peroxidation of PC liposomes, by measuring the percentage inhibition of aldehydic breakdown products (TBARS) produced during lipid peroxidation, using the TBA assay.

As shown in the **Figure 54**, both molecules were able to inhibit lipid peroxidation although with different efficacies with respect to the use of AMVN (**Figure 54A**) or AAPH (**Figure 54B**). More in details, in presence of water-soluble azo-initiator, the Edaravone shows the best performance (percentage inhibition, 82%): since the free radical is produced initially in the aqueous phase, this result suggests that Edaravone is not completely encapsulated and the free Edaravone is able to scavenge oxygen radicals in the aqueous phase before the initiation of lipid peroxidation.

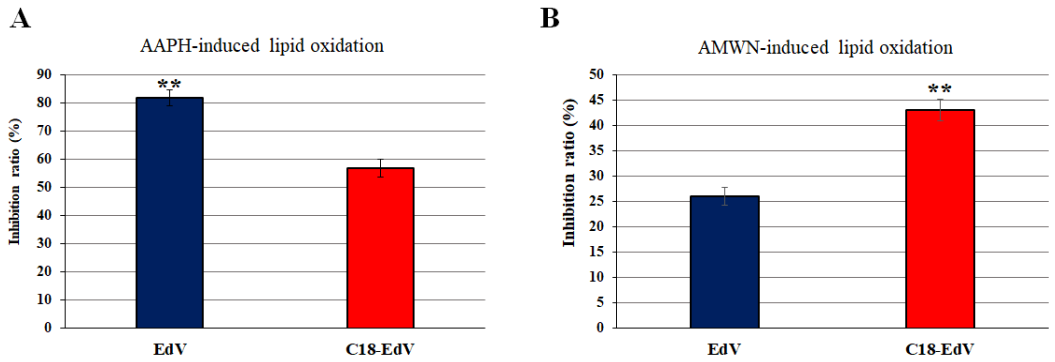

Figure 54. % Inhibition of TBARS formation in PC (3 mM) liposomes peroxidation by Edaravone (EdV) or C18-Edaravone (C18-EdV) (0.05 mM) induced by thermal decomposition of **(A)** water-soluble AAPH and **(B)** lipid-soluble AMWN. The values in the figures are expressed as the means ± SD. Significative differences between two molecules, **p<0.001.

Figure 54B shows the results when the lipid-soluble initiator (AMVN) was used to start the oxidation of PC liposomes. In this system, C18-EdV exhibits the best antioxidant activities because the oxidation-initiating radicals are present in the lipid phase; the lipophilic C-18 effectively leads to an increase of the derivative concentration in the lipid phase thus blocking the propagation of lipid peroxidation in the membranes.

In line with other works (Watanabe et al, 1997; Watanabe et al, 2018), I demonstrated that the lipophilic groups seems to increase the lipid peroxidation-inhibitory activity when the oxidation is induced in the lipid phase.

8.3.3. Cellular experiments

The toxicity of C18-EdV was evaluated in ARPE-19 cells by MTT assay and compared with that of corresponding concentrations of Edaravone (**Figure 55**). The EdV shows low cytotoxicity in ARPE-19 cells; in particular, the Edaravone treatment did not decrease cell viability after 24 h of treatment, while after 48 h I observed a significative decrease of survival cells up to 100 µM. The C-18 lipid moiety increases the cytotoxicity of Edaravone molecule inducing a decrease of viable cells both 24 h and 48 h after treatment. Although there are differences in the degree of cytotoxicity, both modified and unmodified molecule induced a marked cell death after 48 h of treatment in presence of concentrations up to 100 µM. For this reason, I have chosen the 50 and 100 µM concentration of bioactive molecules for the experiments described in the next section.

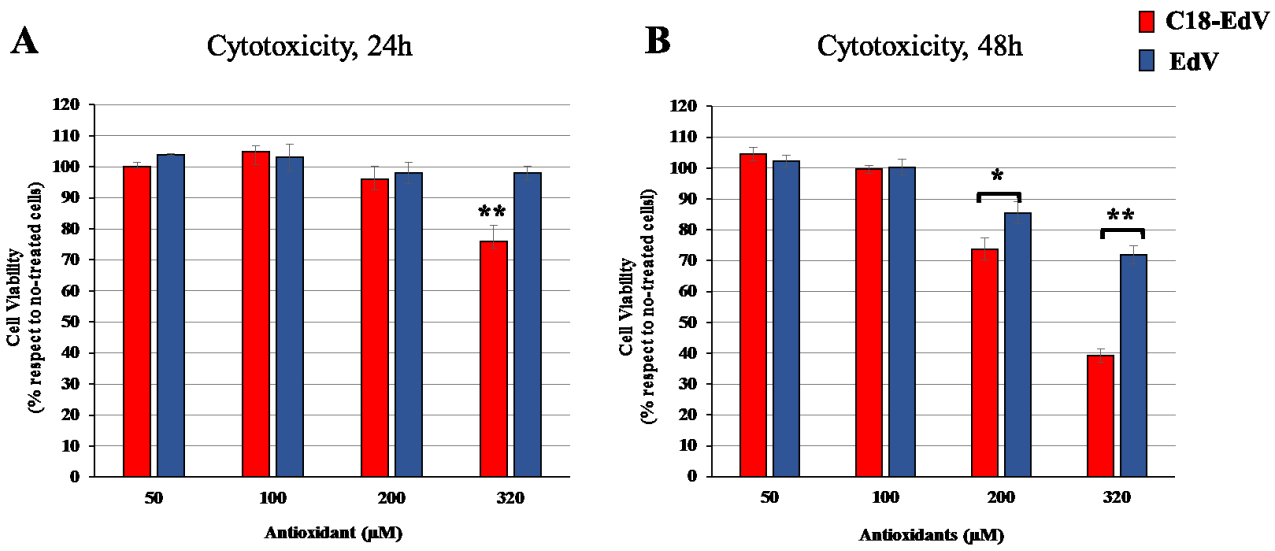

Figure 55. Cytotoxicity of C18-EdV in ARPE19 cells. The cells were treated with increasing concentrations of Edaravone, C18-Edaravone for **(A)** 24 h and **(B)** 48 h in complete culture medium. The viability of treated-cells as reported as percentage respect with no-treated cells, which are considered as 100% of cell viability. The values in the figures are expressed as the means ± SD. *p<0.05 and **p<0.001.

Now, we studied the ability of the molecules to act as antioxidant in cellular system. More in details, in order to mimic chronic oxidative stress, the AAPH was used as stressor agent. As described above, this molecule is an azo compound that decomposes forming alkyl, peroxyl and alkoxyl radicals at physiological temperature; consequently, the AAPH has been widely used to trigger the oxidative stress in cell culture system (Duan et al, 2016; He et al, 2009).

ARPE19 cells were pre-treated with increasing concentrations of C18-EdV and EdV for 24 h and then, incubated with 10 mM of AAPH, in order to induce 50% of cell death after 24 h of incubation and the results are showed in **Figure 56**. As in the previous studies (Chapter VII) the washing steps with PBS ensure that only the molecules that entry the cells, or that strongly interact with lipid bilayer may protect the cells from oxidative stress induced-cell death. Finally, the methanol, used as vehicle, was used as control and did not induce toxicity in the cell cultures (data not shown).

In accordance with other studies, which demonstrated multiple roles of Edaravone on the protection of retinal cells against oxidative stress (Lee et al, 2010; Hironaka et al, 2011; Masuda et al, 2017), I demonstrated that EdV administration effectively decreases the oxidative stress-induced cell death in ARPE19 cells (ca. 18% more cell viability than AAPH-exposed cells, $p<0.001$), at concentration of 100 μM or less. However, the oxidative damage induced by AAPH was mostly attenuated by C18-EdV than to EdV. In particular, the treatment with C18-EdV, at 100 μM concentration, induces an increase in cells survival of about 38% compared to AAPH-exposed cells ($p<0.0001$) and up to 15% when compared to unmodified molecule ($p<0.05$). The superior performance of C18-EdV respect to EdV is due to the washing step before the addition of AAPH in the culture medium: the Edaravone amount that lie in the water phase will be brought away with the PBS while the C18-EdV with its hydrophobic chain is probably well inserted into the bilayer thus increasing the antioxidant protection of retinal cells.

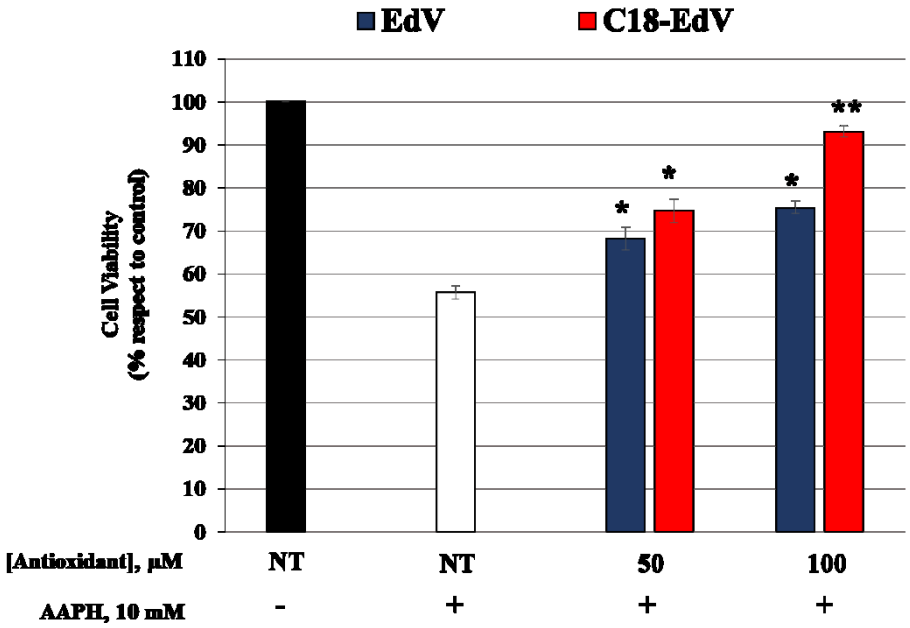

Figure 56. Effect of C18-Edravone in ARPE19 cells after AAPH exposure. The cells were pre-treated with 50 and 100 µM concentrations of C18-Edaravone and Edaravone for 24 h, before being exposed to 10 mM AAPH for 24 h. Cell viability was determined by MTT assay. Data are expressed as means ± S.D. of five independent experiments, each performed in triplicate. Significative differences between treated and no-treated cells, *p<0.05 and **p<0.001.

Next, in order to guarantee a good bioavailability of Edaravone-C18 in the ocular tissues, I studied the effective ability of lipid moiety to increase the encapsulation efficiency of the antioxidant inside lipid vector.

8.3. C18-EdV loaded liposome: characterization

8.3.1. Fluidity of lipid bilayer: *in silico* studies

With the aim to investigate the behavior of C18-EdV inside the liposomal vector and therefore evaluate the more opportune C18-EdV concentrations to be employed for the liposome preparation, *in silico* studies were performed by the molecular modeling unit of our group. A model membrane containing different amount of C18-EdV in a POPC matrix was prepared and properly equilibrated, corresponding to 10, 20 and 40% w/w with respect to phospholipid molecules, namely POPC-10%C18EdV, POPC-20%C18EdV and POPC-40%C18EdV respectively. After Molecular

Dynamics simulations, C18-EdV's molecules reached stability in membrane, but with different results depending on the concentration of synthetic lipid added.

In particular, we found that in the model with 10% of C18-EdV concentration, the molecules had a great freedom of movement. As shown in the representative structures of the steady state of POPC matrix with C18-EdV, some of antioxidant molecules operated the flip-flop phenomena during MD simulations (**Figure 57**). Area per lipid and membrane thickness values calculated on last 20 ns (steady state) were respectively 0.58 ± 0.03 nm^2 and 4.04 ± 0.02 nm. Area per lipid calculations showed a little decrease comparing by POPC pure system and membrane thickness value showed that the picks were very tight and defined; this means a great order of the phosphate groups, and thus for the POPC molecules, that were all in a very orderly way at a determined distance from the center of box.

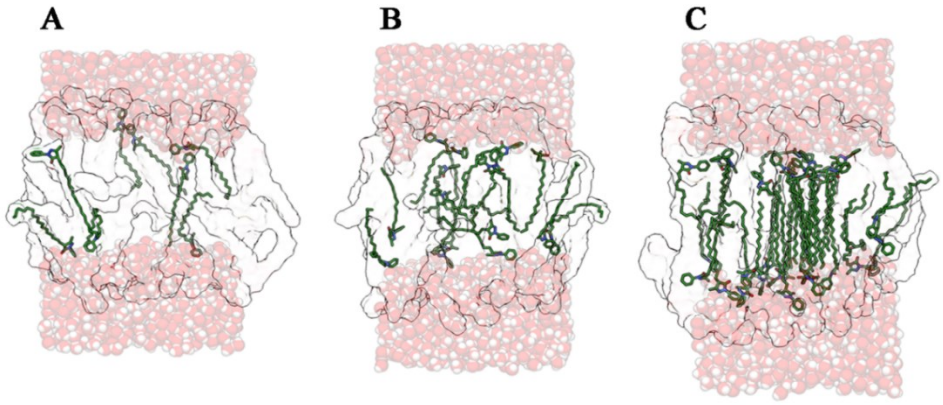

Figure 57: POPC-C18-EdV in water. **A)** C18-EdV 10%; **B)** C18-EdV 20%; **C)** C18-EdV 40%; Highlighted in green C18-EdV carbon atoms, in blue Nitrogen atoms and red Oxygen atoms of C18-EdV molecules. In transparence, we highlighted water molecules.

At 20% of C18-EdV concentration, we again observed a massive fluidity of EdV derivatives in POPC membrane, with a major trend to expose aromatic heads towards the solvent. Area per lipid and membrane thickness values (respectively 0.54 ± 0.02 nm^2 and 4.06 ± 0.01 nm) confirmed that increasing C18-EdV concentration did not induce substantial modifications on physical-chemical properties of the liposome, preserving its fluidity. However, as concentration of antioxidant molecules increased at 40%, we observed many differences. Analyzing MD trajectories for the reported

structures, we noted an increased rigidity degree: the resulting overcrowding present in POPC matrix prevented to maintain the fluidity of system. The Area per lipid value is 0.5 $nm^2 \pm 0.02$, and membrane thickness is very similar to the first two model, but the phosphate groups seems to be disposed in a more disordered manner **Figure 57**). Therefore, the membrane order and parameters were strongly influenced by an excess of the C18-EdV molecules.

8.4.2. Colloidal stability of liposome formulations

A major limitation in the use of liposomes as drug delivery system is their colloidal instability. If liposomes are developed for marketing use, they must be stable maintaining an appropriate size during the storage period. Therefore, as in our previous work (Chapter V), considerable attention has been given to study the physical stability of our liposome formulations.

In particular, I tried to examine whether the incorporation of increasing amounts of C18-EdV may alter the colloidal stability of lipid bilayer also for 1 month after the preparation. Based on *in silico* studies, I prepared POPC-C18-EdV liposomes at a final concentration of lipid of 3 mg mL^{-1} and 10, 20 and 40% w/w of C18-EdV respect to the lipid molecules. The systems were sonicated and their size measured by Dynamic Light Scattering. As shown in **Table 10**, the POPC-40%C18EdV formulation showed high colloidal instability: 24 h after preparation, I observed the presence of large units of liposome material with a mean diameter, expressed as Z average, of about 600 nm with a certain degree of polydispersity (PDI about 0.42).

Table 10. Characterization of sonicated liposomes with C18-EdV [a,b]

Formulation	Time of analyses	Particle size ± SD (nm)	PDI ± SD (nm)	ζ-potential ± SD (mV)
POPC	0 h	117.5 ± 3.9	0.41 ± 0.01	-9 ± 0.8
	24 h	109.8 ± 3.2	0.43 ± 0.04	
	1 month	134.7 ± 5.6	0.52 ± 0.13	
POPC-10%C18 EdV	0 h	103.9 ± 1.3	0.25 ± 0.01	-6 ± 0.5
	24 h	107.8 ± 0.7	0.26 ± 0.04	
	1 month	111.9 ± 1.2	0.24 ± 0.01	
POPC-20%C18 EdV	0 h	156.2 ± 2.3	0.35 ± 0.02	-5 ± 0.2
	24 h	170.3 ± 1.1	0.36 ± 0.01	
	1 month	246.5 ± 1.7	0.37 ± 0.02	
POPC-40%C18 EdV	0 h	158.0 ± 1.2	0.24 ± 0.06	-6 ± 0.7
	24 h	601.9 ± 30.6	0.42 ± 0.01	
	1 month	435.3 ± 15.9	0.83 ± 0.05	

[a] Particle size, PDI and zeta potential were determined by DLS. Encapsulation Efficiency and Loading Capacity were determined as reported in Materials and Methods section. [b] SD: standard deviation

Based on the *in silico* results, I think that this high C18-EdV concentration induces the formation of a disordered system that can result in the aggregation phenomena. Therefore, I decided not to use this formulation in the following experiments. The POPC-10%C18EdV and POPC-20%C18EdV liposome formulations showed high stability with a Z average of about 106 and 150 nm, respectively and the particle size did not change after 24 h. Notably, the differences in the mean diameter of liposomes are probably due to the concentration of C18-EdV. The DLS measurements showed that the POPC-10%C18EdV formulation is the more stable system with a low polydispersity (PDI about 0.24) also after 1 month of preparation. I can conclude that as the concentration of C18-EdV increases the stability of lipid vesicles decreased.

In order to make sure that liposome formulations were usable for the cellular experiments, the physical stability of the produced liposomes was studied by DLS analysis, also in the presence of plasma proteins, after their exposure to serum (**Table 11**). For this purpose, liposomes were incubated in PBS supplemented with FBS (50% v/v) at 37 °C and measurements were carried out at 0 and 24 h. For POPC-10%C18EdV dispersion, the average dispersed vesicle diameter remained essentially unchanged upon exposure to 50% FBS (t=0), even after 24 h, while for the POPC-20%C18EdV formulation only a slightly increase in liposome size was observed. The

physical instability of system with high C18-EdV concentration was confirmed also in presence of plasma proteins.

From the overall obtained results, I used both POPC-10%C18EdV and POPC-20%C18EdV in the following cellular experiments.

Table 11. Influence of time on size distribution of liposomes with EdV-C18 in presence of plasma proteins [a,b]

Liposomes Formulation	Time (hours)	Z Average ± SD (nm)	PDI ± SD (nm)
POPC	0	108.6 ± 1.1	0.413 ± 0.014
	24	121.3 ± 0.7	0.268 ± 0.048
POPC-10%C18 EdV	0	89.1 ± 1.8	0.206 ± 0.020
	24	90.0 ± 1.3	0.206 ± 0.021
POPC-20%C18 EdV	0	145.7 ± 2.2	0.339 ± 0.040
	24	221.1 ± 3.2	0.251 ± 0.025
POPC-40%C18 EdV	0	145.8 ± 1.1	0.172 ± 0.044
	24	396.5 ± 0.6	0.598 ± 0.035

[a] Particle size was determined by DLS. Turbidity of the dispersions was determined as OD as reported in Materials and Methods section. [b] SD: standard deviation; PBS: phosphate buffered saline.

8.4.3. Encapsulation efficiency studies

With the aim to investigate if the functionalization strategy allows to increase the Edaravone interaction with the lipid vector, encapsulation efficiency studies were performed. After liposome preparation, the free C18-EdV was separated from POPC-10%C18EdV and POPC-20%C18EdV by gel exclusion chromatography method as described in Material and Methods. As for poloxamer-407 magnesium liposome loaded with EGCG, the Stewart test was used to determine the phospholipids concentration in the eluates after separation. As controls, I prepared also liposomes containing the no-functionalized molecule at the same concentrations used for the C18EdV liposomes. According to data from literature (Hironaka et al, 2011), I found very low encapsulation efficiencies for Edaravone, of about 36% and 20% for the POPC-10%EdV and POPC-20%EdV, respectively (**Table 12**). On the contrary, the strong interaction between the C18 EdV hydrophobic chain and lipidic tails of phospholipids allows me to obtain a full encapsulation.

Table 12. Encapsulation efficiency (%) of liposomes loaded with EdV or C18-EdV; standard deviation (SD) is also reported.

Formulations	Particle Size ± SD (nm)	PDI ± SD (nm)	Encapsulation Efficiency ± SD (%)
POPC-10%C18EdV	103.9 ± 1.3	0.41 ± 0.01	100.5 ± 2.5
POPC-20%C18EdV	156.2 ± 2.3	0.35 ± 0.02	91.3 ± 3.3
POPC-10%EdV	91.2 ± 8.5	0.22 ± 0.03	36.2 ± 2.5
POPC-20%EdV	80.2 ± 2.6	0.20 ± 0.01	20.1 ± 3.3

8.5. Cellular Experiments: the effect of liposomal encapsulation

In order to investigate the effect of POPC-C18EdV formulations on inhibition of oxidative stress induced-cell death, cellular experiments were performed. In particular, I selected the concentrations of C18-EdV and EdV in which I observed the highest cellular protection, corresponding to 100 μM (**Figure 56**). In order to compare the liposome efficacy, ARPE19 cells were pre-treated with both POPC-10%C18EdV and POPC-20%C18EdV for 24 h and the chronic oxidative stress was induced by the AAPH stressor agent. The washing steps were carried out before the addition of oxidant, as just described. Liposome activities were compared with that of free C18-EdV, free EdV and empty liposomes (POPC). As shown in **Figure 58A**, the treatment with POPC-10%C18EdV significantly increased the cell viability (20% more cell viability than AAPH-exposed cells, $p<0.05$) but to a lesser extent compared to free C18-EdV. Interestingly, the POPC-20%C18EdV reduced the oxidative stress induced-cell death more strongly than POPC-10%C18EdV treatment (40% more cell viability than AAPH-exposed cells, $p<0.05$) but there was no significant difference between the effects of free C18EdV.

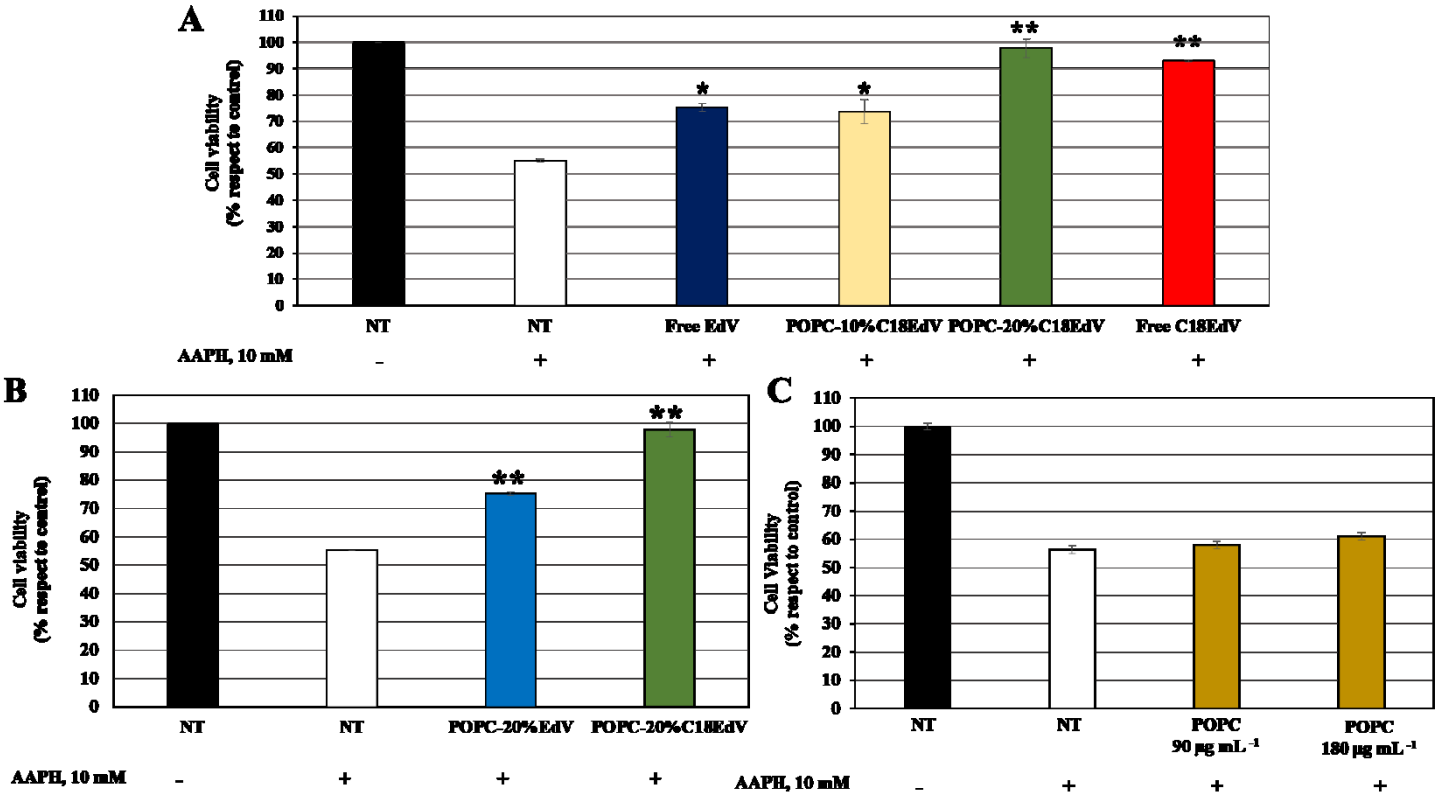

Figure 58. **Effect of free C18-EdV and C18-EdV incorporated in liposomes in ARPE19 cells after AAPH exposure** by **MTT assay**. **(A)** The cells were pre-treated with 100 µM free C18-EdV, free EdV or POPC-10%C18EdV and POPC-20%C18EdV, which correspond to 180 and 90 µg mL^{-1} lipid for 24 h, before being exposed to 10 mM AAPH for 24 h. **(B)** The same experiment was carried out comparing the POPC-20%EdV and POPC-20%C18EdV formulations. **(C)** The experiments were carried out with the empty liposomes at lipid concentrations of 180 and 90 µg mL^{-1}. Data are expressed as means ± S.D. of five independent experiments, each performed in triplicate. *p<0.05 and **p<0.001.

Since the serum stability of POPC-10%C18EdV and POPC-20%C18EdV was about the same, the degree of cellular protection observed may be explained by the differences in the rate of cellular uptake of drug leakage of these two liposomal formulations. Other experiments were necessary to understand the reason of this different behavior. Next, I compared the antioxidant effect of our best C18Edaravone-loaded liposome formulations (POPC-20%C18EdV) with the POPC-Edaravone which was prepared at the same antioxidant concentration (POPC-20%EdV). As shown in the **Figure 58B**, POPC-20%C18EdV reduced oxidative stress-induced retinal death more strongly than POPC-20%EdV (20% more cell viability than AAPH-exposed cells, p<0.05). Notably, I did not observe differences between the antioxidant protection provided by Edaravone loaded and non-loaded in POPC liposome, probably because the very low encapsulation efficiency observed for the POPC-20%EdV (**Table 10**)

Finally, the antioxidant activity of POPC used at the same lipid concentrations of POPC-10%C18EdV and POPC-20%C18EdV (180 and 90 μg mL^{-1}, respectively) was negligible (**Figure 58C**).

8.6. Conclusion and Future perspective

Although the functionalization strategy did not influence the radical scavenging activity of Edaravone, the protection of lipid peroxidation was more different for modified and unmodified molecules. More in details, I found out that the presence of lipophilic C-18 chain increases the bilayer protection when the radicals are generated in the lipid phase while with the use of the water-soluble initiator AAPH the inhibition of lipid peroxidation decreased when compared to the Edaravone. This can be explained considering that lipophilic substituents make C18EdV able to insert into the lipid matrix; therefore, it can block TBARS formation by interrupting the propagation of lipid peroxidation in the membranes. The strong interaction between the hydrophobic carbon chain and lipid tails of cellular membrane seems to be responsible of the high ability of Edaravone derivative to protect retinal cells, thus confirming the TBARS assay results.

Moreover, the functionalization method yielded a full C18EdV entrapment in all liposomal formulations studied while the encapsulation efficiency of the Edaravone was very low (20-35%). Since the high concentration of drug (C18EdV, 40% w/w with respect to the lipid molecules) markedly decreased the colloidal stability of liposomes both in PBS and in presence of plasma proteins, I identified the model bilayer containing 10% and 20% of EdV-C18 as the suitable systems to be used in cellular experiments. C18-Edaravone-loaded liposomes (POPC20%-C18EdV) significantly reduced oxidative stress-induced retinal damage more strongly than free EdV and EdV-loaded liposomes (POPC20%-EdV). Interestingly, there were no significant differences between the effects of free C18EdV and related liposome formulation. However, it is important to underlying that the new lipophilic antioxidant needs solvent vehicle and could not be used for the eye drops development without a carrier.

These data suggesting that C18-EdV and its liposomal formulation may be promising as a novel therapeutic drug candidate in the treatment of disease associate with oxidative stress.

Materials and Methods

Materials

Glyceryl monooleate (monoolein, GMO), 1,2-dioleoyl-sn-glycero-3-phosphoethanolamine (DOPE), 1-palmitoyl-2-oleoyl-sn-glycero-3-phosphocholine (POPC) and cholesteryl hemisuccinate (CHEMS) and cholesterol (Chol) used for liposomes preparation, were purchased from Avanti Polar Lipids Inc. (Alabaster, AL, USA). Commercial phosphatidylcholine from egg yolk (PC), the α,α-diphenyl-β-picrylhydrazyl (DPPH), the azocompound 2,2-azobis(2-amidinopropane hydrochloride) (AAPH), Sephadex G-50, Poloxamer-407, $MgCl_2$ and $CaCl_2$ salts, 3-(4,5-dimethylthiazol-2-yl-2,5-diphenyl tetrazolium bromide (MTT), hydrogen peroxide and all solvents were obtained from Sigma Aldrich Co. (Stenheim, Germany). The 2,2-azobis(2,4-dimethylvaleronitrile) (AMVN) was purchased from Santa Cruz Biotechnology, Inc. (Dallas, USA) used after purification by recrystallisation in cold methanol. Epigallocatechin 3-Gallate was purchased from Cayman Chemical Company (Ann Arbor, MI, USA). All the other reagents and chemicals were of analytical grade for biochemical purposes or HPLC grade.

In order to prevent metal contamination, all the solutions were prepared in ultrapure MilliQ water. All materials and reagents employed in the synthetic procedures were purchased from SigmaAldrich Co. (Stenheim, Germany) unless otherwise stated and used without purification. All solvents were analytically pure and dried before use. The reactions are performed under argon. TLC were carried out on aluminium sheets precoated with silica gel 60 F254 (Merck). Column chromatography was performed using silica gel 60 (230–400 mesh). Mass spectra (MS) were obtained by electron impact on a Hewlett-Packard spectrometer 5890, series II. The ^{1}H and ^{13}C NMR spectra were recorded at 400 and 100 MHz, respectively, on a Varian Gemini 200 spectrometer, using $CDCl_3$, acetone or DMSO as solvents. Chemical shifts (δ) are reported in ppm relative to TMS and coupling constants (J) in Hz.

Adult human retinal pigment epithelial (ARPE-19) cells were a kind gifted from Dr. Dario Rusciano (Sooft Italia spa). All cell culture reagents were purchased from Euroclone (Euroclone, Italy). All other chemicals and buffer components were analytical grade preparations.

Computational Methods

Parameterization of Epigallocatechin-3-Gallate and cholesteryl-hemysuccinate

Epigallocatechin-3-gallate (EGCG) and cholesteryl-hemysuccinate (CHEMS) molecules were firstly parametrized following the same protocol previously reported (Laudadio et al, 2017). Thus, we explored their conformational potential energy surface (PES) in order to localize the main stationary points, i.e. lowest energy minimum and the most populated conformers. Then, molecular mechanics energy calculations were performed using the AMBER force field implemented in the Maestro/MacroModel (Schrodinger Inc., Portland, OR, USA) software framework (Mao et al, 2013), and the torsional space of the molecules was randomly varied with the usage-directed Monte Carlo Multiple Minimum (MCMM) conformational search approach (Migalska-Zalas et al, 2008). For each search, 1000 starting structures for each variable torsion angle were generated and then minimized until the gradient was less than 0.05 kJ Å-1 mol^{-1}. We used quantum mechanical calculations (DFT, B3LYP/6-311G**) to calculate EGCG and CHEMS's Mulliken charges. The solvent effect was included by using the implicit water GB/SA solvation method (Goodman et al, 1994), and duplicate conformations and those with an energy in excess of 6.0 kcal mol^{-1} above the global minimum were discarded. The cluster analysis was performed within the Macromodel package using X-cluster following a protocol already reported (Goodman et al, 1994; Mao et al, 2013; Onufriev and Sigalov, 2011). Then, for each compound (EGCG and CHEMS), we carried out the clustering considering the RMSD of the main carbons skeleton (threshold value RMSD=0.5) as filter. We found out for both molecules one most populated cluster (about 90-95 %) that corresponds also to the global minimum's cluster. The resulting lowest energy conformers, together with the representative structures of the most populated clusters, were optimized and the charges re-calculated by DFT calculation using G09 suite of Gaussian 09, Revision D.01 software at B3LYP/6-311G** level of theory (Raghavachari, 2000), in order to better take into account the electronic effects in the conformer's stabilization and populations (Becke, 1996). For the lowest energy conformers of EGCG and CHEMS, we then fitted the missing CHARMM parameters using the VMD toolkit/G09 and we added the corresponding topology file using Xleap tool (Mayne et al, 2013). For POPC, DOPE (1,2-Dioleoyl-sn-glycero-3-phosphoethanolamine), Chol (Cholesterol), TIP3P water molecules we used the already included CHARMM parametrization.

Molecular Dynamics of EGCG and in Mixed Lipid Bilayers

All the molecular dynamics (MD) simulations of the mixed lipid bilayer were carried out on the isothermal–isobaric (N, P, T) ensemble at 1 atm and 310 K (37 °C). The GROMACS 5.0.4 suite

of programs was used with CHARMM force field (Mao et al, 2013) parameter sets, using EGCG and CHEMS's charges and parameters previously calculated (Raghavachari, 2000; Becke, 1993). This force field results particularly accurate for lipid bilayer dynamics (Weiner et al, 1984). The membrane leaflets are composed by a total of 144 lipid molecules hydrated by 4758 water molecules within an initial simulation box (corresponding to a pre-equilibrated mixed bilayer) that was 8 nm (Z) normal to the bilayer and 7 nm long in each of the two dimensions of the bilayer plane (XY). We started from neutral mixed composition lipid system (POPC, DOPE and Cholesterol in molar ratio 1:1:1 between them) was obtained by membrane builder tool of CHARMM-GUI website (www.charmm-gui.org/?doc=input/membrane) with an extension of 10 ns to equilibrate systems by NPT ensemble simulation. To generate the anionic mixed lipid model, we substituted all Cholesterol molecules with CHEMS compounds. We added 30 EGCG molecules at every mixed composition bilayer considered in this study, corresponding to the EGCG molar concentration used experimentally. We carried out MD simulation putting 30 molecules of the catechin in water, starting from a casual and not ordered molecules' orientation. Mixed composition bilayers considered in this study were built adding the antioxidant molecules in the same configuration as found out in the equilibrated solvated model. All the simulations were conducted in presence of divalent metal salts $CaCl_2$ and $MgCl_2$ at different concentrations (1:1, 3:1, 5:1 and 6:1 in molar ratio between salt and EGCG). The TIP3P model for solvent has been used and ions were added to reach salt concentrations. Water and ions overlapping the membrane bilayer were removed before proceeding to system minimization (Domanski et al, 2010). The chosen system dimensions were based on literature reports concerning the smallest representative size that can be used to accurately reproduce the occurring intermolecular interactions in lipid bilayers (Soper et al, 1997). In particular, MD simulations have been extensively carried out by Klauda and co-workers on different sized systems (72 up to 288 lipids) to examine system size dependence on dynamical properties associated with the Particle Mesh Ewald (PME) treatment of electrostatic interactions. Each bilayer system was energy minimized under periodic box conditions (re-modulated starting cell unit in nm, X = 7.00, Y = 7.00, Z = 8.00) applied in all directions using a neighbour searching grid type, and also setting at 1.4 nm the cut-off distance for the short range neighbour list. The Verlet cut-off scheme was used for neighbour searching, combined with PME for electrostatics. Cut-off for the calculation of Van der Waals forces was set to 1.2 nm, with the force smoothly switched to zero between 1.0 and 1.2 nm. Electrostatic were taken into account implementing a fast smooth particle-mesh Ewald (SPME) algorithm (Klauda et al, 2006) with a 1.4 nm distance for the Coulomb cut-off, since this method is considered to be both efficient and accurate for the evaluation of long-range electrostatic interactions in large

macromolecular systems (Onufriev et al, 2011). For all the MD trajectories, we used the NPT ensemble maintaining the weak coupling also for pressure control (i.e. Berendsen barostat). Velocities were first generated at 310 K in the NVT ensemble, using a Maxwell distribution function with random seed; a weak temperature coupling (Berendsen thermostat), with time constant of 1 ps, was applied to maintain the reference temperature (310 K) for the whole run; no water was observed inside the bilayer. At this point a 200 ns dynamics has been set up for each of the built system. An accurate leap-frog stochastic dynamics integrator was used as the main run control option; we used a time step of 0.002 ps, and the coordinates were written out every 10 ps, while energy data were collected every 2 ps. The first 2 ns MD simulation for each lipid system was simulated in the NVT ensemble using Langevin thermostat while the subsequent nanoseconds in the NPT ensemble (T= 310 K, P= 1 atm) using Berendsen thermostat and semiisotropic pressure coupling. A time constant for coupling of 0.5 ps and an optimal compressibility for water of 4.5 x 10^{-5} bar-1 were implemented to obtain the best control on pressure. The MD trajectories were collected until the equilibration period achieved a convergence of the dimensions of the system and the steady state was reached according to Porasso et al. (Porasso and Cascales, 2012). Computation of each MD trajectory was performed in parallel at a speed of 11 ns per day on a GALILEO IBM workstation (CINECA-HPC ISCRA project). All the MD run were carried out in triplicate to allow performance and reproducibility of analysis.

MD Simulation Analyses

We collected all the MD trajectories (Porasso and Cascales, 2012) and mean values and standard deviations (SD) of characteristics were estimated for last 40 ns of each trajectory; the mean values and SD were averaged over the three replicated simulations unless otherwise stated. The analysis of the simulations' trajectories was performed using GROMACS's standard analysis tools, the VMD and CHIMERA software (Pronk et al, 2013).

Synthetic methods

Synthesis of EGCG-C18

To a stirred solution of EGCG and K_2CO_3 (210 mg, 1,52 mmol) in DMF (10 mL, 20 mmol) octadecyl iodide in cyclohexane (3 mL, 1,5 mmol) was slowly added in 1 h under a flow of inert gas. The solution was heated at 40°C for 8 h. Then the mixture was exctracted with ethyl acetate, the organic layers collected, combined, dried over anhydrous Na_2SO_4 and concentrated. The product was then purified by silica gel column chromatography (cyclohexane-EtOAc, 75 : 25) to afford C18-EGCG (4 g, 28%) as a brown solid.

^{1}H NMR (acetone, 400 MHz): δ = 0.87 (t, J= 7.4 Hz, 3H), 1.20-1.35 (m, 30H), 1.35-1.45 (m, 1H), 1.62-1.75 (m, 1H), 2.97 (dd, J= 2.4 Hz, 13.9 Hz, 1H), 3.03 (dd, J=3.9 Hz, J=13.9 Hz, 1H), 4.05-4.15 (m,2H), 5.07 (s, 1H), 5.42 (s,1H), 6.03 (m, 2H), 6.67 (s, 2H), 7.05 (s, 2H).

^{13}C NMR (acetone, 100 MHz): δ = 13.5, 22.4, 25.7, 30.8, 31.7, 62.3, 69.3, 70.2, 73.3, 78.3, 95.9, 96.5, 98.9, 106.8, 109.9, 126.2, 129.6, 130.5, 133.5, 139.6, 146.6, 151.4, 157.1, 157.5, 157.8, 166.3.

ESI-MS: (m/z.) 823 [M + CF3COO-]

Synthesis of ethyl 3-oxo-2-octadecyl-butanoate (ethyl 2-octadecyl-acetoacetate)

To a stirred solution of sodium ethoxyde in ethanol (21% wt, 22 mmol) ethyl acetoacetate (2.53 mL), 30 minutes octadecyl bromide (6.83 mL, 20 mmol) in THF (4 mL) was slowly added in 2 h. After refluxing for 12 hours, the mixture was cooled and acidified with HCl 1M with vigourous stirring until neutral pH. Then the mixture was exctracted with ethyl acetate (3 x 10 mL). The organic layers were collected, combined and washed with brine (2 x 10 mL), dried over anhydrous Na_2SO_4 and concentrated. The residue was purified by silica gel column chromatography (cyclohexane:ethyl acetate 95:5) to give the desired product (5.56 g, 72.7%).

^{1}H NMR (CDCl3, 400 MHz): δ = 0.86 (t, J = 6.4 Hz, 3H), 1.16-1.33 (m, 32H+3H ,7.2 Hz), 1.76-1.88 (m, 2H), 2.20 (s, 3H), 3.37 (t, J = 7.2 Hz, 1H), 4.17 (q, J = 7.2 Hz, 2H).

^{13}C NMR ($CDCl_3$, 100 MHz): δ = 14.1, 22.7, 27.4, 28.2, 28.7, 29.3, 29.5, 29.6, 29.7, 31.9, 59.9, 61.2, 169.9, 203.4.

Synthesis of 3-methyl-4-octadecyil-1-phenil-1H-pirazol-5(4H)-one (Edaravone C-18)

Ethyl 3-oxo-2-octadecyl-butanoate (2 mmol) was added to phenilhydrazine (2 mmol) against a flow of inert gas. The mixture was heated at 140 °C and after 5 hours cooled in an ice-water bath. A portion of 3 mL of diethyl ether was added to obtain pyrazolone precipitation. The obtained product was filtered and washed thoroughly with diethyl ether to obtain a white solid (72%).

^{1}H NMR (DMSO, 400 MHz): δ = 0.85 (t, J = 7.2 Hz, 3H), 1.17-1.31 (m, 32 H), 1.37-1.44 (m, 2H), 2.10 (bs, 3H), 7.12-7.19 (m, 1H), 7.41 (t, J = 8.0 Hz, 2H), 7.68-7.75 (m, 2H), 10.47 (bs, 1H, NH). 1H NMR (CDCl3, 400 MHz): δ 0.87 (t, J = 6.8 Hz, 3H), 1.14-1.37 (m, 32 H), 1.78-1.90 (m, 1 H), 1.94-2.05 (m, 1 H), 2.15 (s,3H), 3,26 (t, J = 5.6 Hz, 2H), 7.17 (t, J = 7.2 Hz, 1H), 7.39 (t, J = 8.1 Hz, 2H), 7.89 (d, J = 8.1 Hz, 2H),

^{13}C NMR (CDCl3, 100 MHz): δ = 14.1, 15.7, 22.7, 25.4, 27.5, 29.2, 29.3, 29.5, 29.6, 29.6, 29.7, 31.9, 52.4, 118.7, 124.8, 128.8, 138.1, 160.0, 173.4. ESI-MS: (m/z.) 424.7 [M-H]-. IR (KBr, cm-1): 2918, 2851, 1591, 1555, 1531, 1502.

Evaluation of free radical scavenging activity: DPPH assay

The 2,2-diphenyl-1-picryl-hydrazyl (DPPH) is a free radical scavenging method widely used to evaluate radical scavenging activity of antioxidants (Kedare and Singh, 2011).

DPPH is a stable free radical by virtue of the delocalization of the unpaired electron over the DPPH structure. The delocalization also gives rise to the deep violet colour, with an absorption in ethanol or methanol solution at around 517 nm. The mixing of DPPH solution with a substance that can donate a hydrogen atom, gives rise to its reduced form with the loss of violet colour (although there would be expected to be a residual pale yellow colour from the picryl group still present) (**Figure 59**). The resulting decolorization is stoichiometric with respect to the number of electrons taken up.

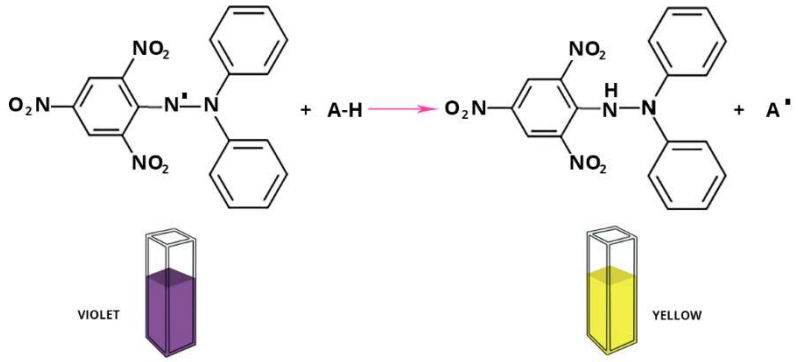

Figure 59. Principle of DPPH radical scavenging capacity assay: reaction of DPPH stable radical with antioxidant compound (A-H).

Once the DPPH accepts an electron or a hydrogen radical, it become a stable, diamagnetic molecule and the reaction is irreversible.

The assay was performed according to the following procedure. A solution of DPPH in methanol was stirred for 40 min. Then, appropriate aliquots of antioxidants solutions in methanol were mixed with to a 1 mM DPPH solution (antioxidant final concentration 0,025 mM) and incubated for 30 min in the dark covered with aluminum foil. Control sample is prepared by adding a methanol aliquot equal to the antioxidant solution volume added. Decrease of absorbance was monitored at 517 nm at 30 min.

The absorbance measured at the addition of the tested antioxidant was expressed as A_{sample}, the absorbance at the addition of methanol instead of the sample as $A_{control}$, and the inhibition ratio (%) was calculated from the following equation:

$$\text{Inhibition ratio (\%)} = [(A_{control}-A_{sample})/A_{control}] \times 100$$

Each sample was measured in triplicate. Mean and standard deviation (n = 5) were calculated.

Peroxidation of Egg-PC liposomes and assessment of % inhibition (TBARS assay)

Thiobarbituric acid reactive substances assay (TBARS assay) is probably the oldest and one of the most widely used assays for measuring malondialdehyde, a reactive aldehyde, which is the major product of lipid oxidation. Malondialdehyde forms an adduct with two thiobarbituric acid (TBA) molecules to produce a pink color species that absorbs at 532–535 nm (**Figure 60**).

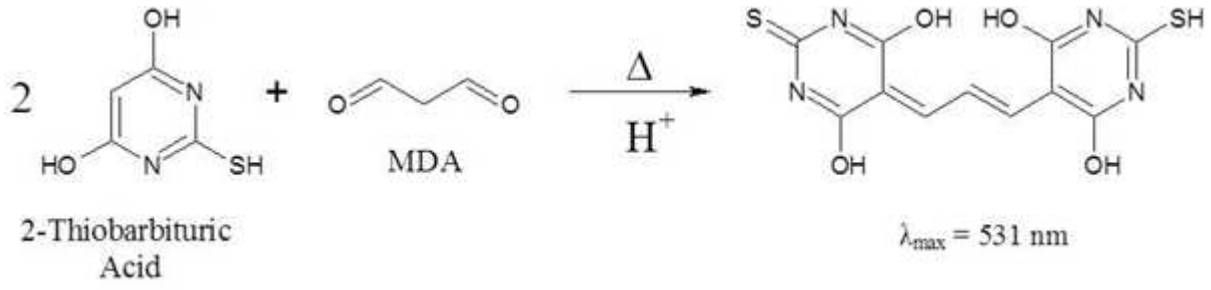

Figure 60. Reaction between 2-thiobarbituric acid and MDA under acidic conditions

Lipid peroxidation studies were carried out on egg yolk PC liposomes as membrane models. All calculations were made by considering an average molecular weight of egg yolk PC of 768 u.m.a. Liposomes were prepared by the "thin film hydration" method. Chloroform stock solutions (5 mM) were prepared for each tested compound. Appropriate amounts of chloroform solutions of PC (100 mg mL^{-1}) and tested compound were mixed in a 50:1 molar ratio. When required,

appropriate aliquots of stock solutions in chloroform of the lipophilic additives 2,2-azobis(2,4-dimethylvaleronitrile) (AMVN) (1mM) were added (**Figure 61A**). The solvent was slowly evaporated with a stream of nitrogen and the thin film obtained was dried for at least 2 h under reduced pressure. This dried film was then resuspended by vortex agitation in the required amount of 5 mM PB (pH 7.4) to a 3 mM Egg-PC and 0.06 mM antioxidant final concentration and incubated overnight to swell and stabilize. Controls were carried out without antioxidant addition. The resulting MLV (Multi Lamellar Vesicles) were incubated overnight to swell and stabilize. When the type of initiator is the lipophilic AMVN, the MLV were directly used for the experiment: 600 µL of each MLV suspension (with and without antioxidant) containing AMVN were incubated at 56°C for 2 h, whereas other 600 µL were added with 10 µL of 10 mM ethanolic BHT to be used as controls (non-oxidized samples). After this time, 10 µL of 10 mM ethanolic BHT were added to stop the reaction and to prevent possible peroxidation of PC during the TBA assay; 900 µL of TBA–TCA–HCl (0.375% w/v TBA, 15% w/v TCA, 0.2M HCl) were then added and the samples were heated for 15 min at 95°C followed by cooling and centrifugation at 1000 g for 10 min.

In the experiment in which the liposomes oxidation was induced by 2,2-azobis(2-amidinopropane hydrochloride) (AAPH) (**Figure 61B)**, the MLV were sonicated for 12 min with a Sonic Vibracell sonicator to obtain SUV (Small Unilamellar Vesicles). Oxidized samples were obtained by taking up 600 µL portions of each dispersion, adding 50 µL AAPH 65 mM (5 mM final concentration) and incubating for 2 h at 37 °C. Addition of 10 µL of 10 mM ethanolic BHT to the oxidized liposomes stopped the reaction and prevented further Egg-PC peroxidation during the TBARS assay. Other 600 µL of the liposome dispersions were added to 50 µL of PBS (instead of AAPH) and 10 µL of 10 mM mM methanolic BHT to make sure that during incubation, also in the absence of radical initiator, no oxidation occurs and incubated at 37 °C for the same time. Finally, as in the experiment with AMVN, 900 µL of TBA–TCA–HCl reagent (0.375% w/v TBA, 15% w/v TCA, 0.2 M HCl) were added to all samples, oxidized and non-oxidized, which were then heated for 15 min at 95°C, cooled and centrifugated at 1000 g for 10 min. The absorbance of the pink chromophore of the supernatant developed upon heating was measured at 532 nm for the determination of the aldehydic breakdown products of lipid peroxidation (TBARS) (Buege and Aust, 1978).

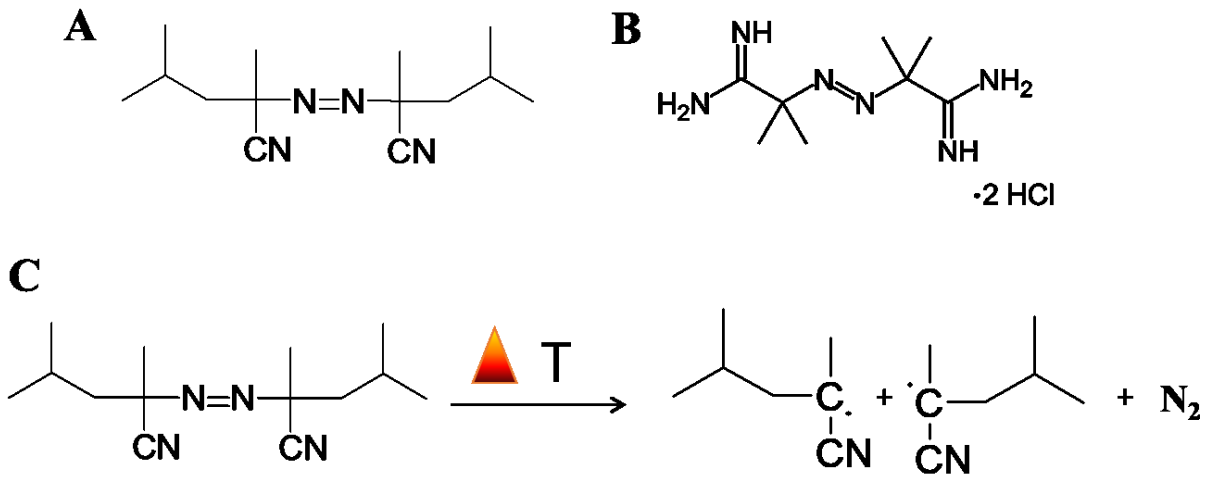

Figure 61. Chemical structure of the azocompounds **(A)** 2,2-azobis(2,4-dimethylvaleronitrile) (AMVN) and **(B)** 2,2-azobis(2-amidinopropane hydrochloride) (AAPH). **(C)** Generation of carbon-centered radicals by thermal decomposition of the water-soluble azo-compound.

The antioxidant activity of the studied compounds was expressed as % inhibition according to the following equation:

$$\% \text{ inhibition} = (1 - \Delta A_{\text{sample}} / \Delta A_{\text{PC}}) \times 100$$

Where, ΔA_{sample} is the difference of the absorbance between the oxidized and non-oxidized sample and ΔA_{PC} is the difference of the absorbance between the oxidized and non-oxidized PC. All the experiments were repeated at least three times and measurements were run in triplicate.

Preparation of lipid-based nanocarriers

Liposome loaded with EGCG

Multilamellar liposomes (MLVs) were obtained by Reverse Phase Evaporation (REV) (Szoka and Papahadjopoulos, 1978). Appropriate amounts of chloroform solutions of DOPE, POPC, CHEMS or Chol and methanol solution of EGCG were mixed to obtain a lipid equimolar ratio. The solvent was removed under reduced pressure at room temperature to prevent EGCG degradation (Sanga et al, 2007). The residual solvents were removed under nitrogen flow and lipids were dissolved in 3 mL of ether/methanol mixture (2:1, v/v). Then, 1 mL of water or, when necessary, of salt solution at different concentration (1, 3, 5, 6 mM) in phosphate-buffered saline (PBS 10 mM, pH 7.4) was added to reach different molar ratios of $CaCl_2$ or $MgCl_2$ salts to EGCG (1:1, 3:1, 5:1, 6:1). With

the aim to obtain an initial water in oil emulsion (W/O), the resulting two-phase system is briefly sonicated (2 min) with a sonicator (Sonics Vibra Cell Mod. VCx130) equipped with a tapered micro tip. The organic solvent was removed under vacuum (Rotavapor, Büchi) to cause a phase inversion that gave an O/W emulsion. We obtained MLV suspensions with a final concentration of 3 mg mL^{-1} of total lipids and 1 mM of EGCG which were used for the determination of the EGCG affinity toward all system studied.

The anionic MLVs loaded with and without EGCG, hydrated with, and without $MgCl_2$ salt ($MgCl_2$/EGCG, 5:1 mol/mol) were used for further experiments. In particular, the obtained liposomes L, ML (magnesium containing liposomes), L-EGCG (EGCG loaded liposomes) and ML-EGCG (magnesium containing liposomes loaded with EGCG) were characterized fresh and/or after equilibration for 24 h. The liposomal suspensions containing Poloxamer-407, PxL (poloxamer liposomes), MPxL (magnesium-containing poloxamer liposomes), PxL-EGCG (poloxamer liposomes loaded with EGCG) and MPxL-EGCG (magnesium-containing poloxamer liposomes loaded with EGCG) were prepared in the same way, but Poloxamer-407 was added in PBS to obtain a polymer final concentration of 0.8 mg mL^{-1}. Note that the MLV suspensions were directly used for X-ray diffraction experiments, while samples for DLS characterization, turbidimetric analysis, encapsulation efficiency determination, in vitro release and cellular assays, were sonicated (sonic Vibracell) before being used for 30 min in pulse mode (30 sec on; 2 sec off, 50%) at 0 °C, until the liposome dispersion was completely clear.

Liposome loaded with C18-Edaravone (C18-EdV)

Liposomes loaded with Edaravone and C18-Edaravone were prepared by "thin film hydration" method. Appropriate amounts of chloroform solutions of POPC and methanol solutions of the tested compounds were mixed in order to obtain liposomes with 10, 20 and 40% w/w of antioxidant with respect to lipid molecule, namely POPC-10%C18EdV, POPC-20%C18EdV and POPC-40%C18EdV, respectively. The solvent was removed slowly by evaporation under reduced pressure and the thin film obtained was dried under vacuum for 4 h. This dried film was then resuspended under stirring in the required amount of sterile PBS (pH 7.4). The resulting multilamellar vesicle dispersions were sonicated (10 min, 50%) with a vibra cell sonicator (Sonics Vibra Cell Mod. VCx130) equipped with a tapered micro tip, until the liposome dispersion was completely clear. The liposomes formulations were employed in DLS and encapsulation efficiency studies.

Preparation of EGCG-loaded bulk (Nondispersed) phase and its dispersed forms (Cubosomes and Hexasomes)

The samples of GMO bulk phase were prepared by hydration of the appropriate amount of GMO (40 mg) with PBS solution (pH 7.4) containing increasing EGCG amount at 25°C for 48h. For blank bulk phase, only PBS was added to GMO. The samples were left to equilibrate for 48h. The monoolein concentration was 4 % w/w. The EGCG was in a range between 0.2-1% w/w respect to the water and 5-25% with respect to the moonolein. In particular, the EGCG concentrations used were 2, 4, 5, 7, 8 and 10 mg mL^{-1}.

To prepare the nanodispersed phases the GMO was co-dissolved with Poloxamer-407 (10% w/w of GMO) in chloroform with or without increasing concentration of EGCG in methanol. The solvent was evaporated under a stream of nitrogen and the mixture dried under vacuum. The mixture was vortexed to achieve a homogeneous suspension and equilibrated at 25°C for 48 hours to obtain the phase-gel. PBS was added until a monoolein concentration of 2.5 % w/w was reached; then, the resulting gel phase was sonicated (10 min; 1 sec on; 1 sec off; 50%) with a vibra cell sonicator (Sonics Vibra Cell Mod. VCx130) equipped with a tapered micro tip, until the aggregates were no longer present. The final EGCG concentration in the nanodispersed formulation was 2, 4 and 7 mg mL^{-1}.

During the production, the vials were protected from light with an aluminium foil to prevent photodegradation of EGCG (Bianchi A. et al. 2011). The bulk formulations and the nanodispersed systems were used in Small Angle Neutrons Scattering (SANS) experiments as well as in the encapsulation efficiency determination. Nanodispersions were also characterized by DLS.

Characterization of lipid-based nanocarriers

Structural Analyses

The X-ray diffraction (XRD) and the Small Angle Neutron Scattering (SANS) diffraction are two fundamental techniques of molecular biophysics to develop structural models; these methods allow to describe the position of atoms in sample studied, thanks to the interference pattern of radiation scattered from the material. The characteristic of the diffraction is the resolution that can reaches 1.2˚A comparable with the interatomic distances of condensed matter (Glasel and Deutscher, 1995). Usually the diffraction techniques are applied to crystals because they are samples well ordered but this method are also useful for the description of Liquid Crystal phases as reported in this thesis in the next chapters.

The differences between neutron and X-ray diffraction methods can be summarize in advantages and disadvantages. The first advantage of neutron diffraction is that the neutron scattering by atoms is not a function of their atomic number so atoms with similar atomic number as nitrogen, oxygen and carbon, that usually are undifferentiated on the basis of the electron density maps, can be distinguish through neutron experiments. The refractive index is related to the Scattering Length Density (SLD) as a measure of the interaction strength between a neutron and the nucleus of a particular element. This important characteristic is helpful also for the distinction of hydrogen from deuterium; indeed hydrogen is one of the few elements that has a negative scatter, this means that the scattering from hydrogen is 180 °C out of phase with the scattering of all other atoms. This distinction is used to define the position of hydrogen in macromolecule to understand their particular functions and to analyze the molecular dynamics by the deuterium exchange. These features are important for the technique of contrast variation where the change of water (H_2O) and heavy water (D_2O) content in the sample can highlight particular feature of the structure. On the contrary, the disadvantages are that heavy atoms cannot be used to determine phases, the neutron source are few expensive to maintain and the flux is low so that a measure can last until a lot of hours, the perfect opposite of the X-rays (Glasel and Deutscher, 1995).

X-Ray Diffraction (XRD) experiments

The X-Ray Diffraction (XRD) experiments were carried out on bulk phase corresponding to MLV's containing EGCG with $MgCl_2$ salt ($MgCl_2$/EGCG, 5:1 mol/mol) and related controls. The experiments were performed using a 3.5 kW Philips PW 1830 X-ray generator (Amsterdam, Netherlands) provided with a bent quartz crystal monochromator (λ = 1.54 Å) and a Guinier-type focusing camera (homemade design and construction, Ancona, Italy). Diffraction patterns were recorded on GNR Analytical Instruments Imaging Plate system (Novara, Italy). MLV suspensions and nondispersed Liquid Crystal phase were measured in a tight vacuum cylindrical cell equipped with thin mylar windows. Experiments, for MLV samples, were performed as a function of temperature, at 25, 36, 40 and 45 °C.

In each experiment, a few Bragg peaks were detected. Peak indexing was performed considering the usually observed lipidic phases and the unit cell dimension of the phases, *d*, calculated from the averaged spacing of the observed peaks.

According to the decomposition of the sample in the hydrophobic and hydrophilic regions (Pabst et al., 2000), a simple equation relates the unit cell dimension to the lipid head-to-head distance,

d_{HH}, that can be measured from electron density maps (Di Gregorio et al. 2010), and the thickness of the water layer d_w (Eq. 21):

$$d_w = d - d_{HH} \qquad \text{(Eq. 21)}$$

Therefore, the area-per-lipid at the water/lipid interface S_{lip} and the averaged number of water molecules associated with one lipid molecule $n_{w/lip}$ can be determined if v_{lip} and v_{wat}, the averaged lipid molecular volume (in this case estimated by MD simulations to be around 960 Å^3) and the water molecular volume (30 Å^3) are known (Eq. 22):

$$S_{lip} = 2v_{lip} / d_{HH} \qquad \text{(Eq. 22)}$$

and (Eq. 23),

$$n_{w/lip} = V_{w/lip} / v_{wat}$$

with (Eq. 24)

$$V_{w/lip} = d_w S_{lip} / 2.$$

Small Angle Neutrons Scattering (SANS) experiments

Neutrons experiments were carried out on EGCG-loaded nondispersed and nanodispersed Liquid Crystalline Systems (LCS) with relative controls. SANS experiments were executed at Institut Laue-Langevin (Grenoble, France) at D22 beamline with a 1 mm quartz cuvette; the neutron wavelenght λ was 6 ˚A. The Q range investigated was 0.001-0.35 ˚A−1 with a CERCA 3He Multi-detector placed at 8 and 1.2 meters. All measures were made at room temperature. The samples for SANS were prepared as described in section *Liposome loaded with EGCG* but replacing H_2O with D_2O.

Dynamic Light Scattering (DLS)

The intensity-based diameter (Z-average) and the zeta potential of all formulations were measured by Dynamic Light Scattering (DLS) and Electrophoretic Light Scattering using a Malvern Zetasizer Nano ZS (Malvern Instruments GmbH). An aliquot of every liposome suspension, obtained by sonication, was diluted at a final concentration of 2.5 x 10^{-2} mM with ultra-purified water. Measurements were performed at 25 °C with a fixed angle of 173°. Size particle polydispersity index were calculated from the autocorrelation function by cumulant analysis (Dispersion Technology Software V7.11 provided by Malvern Instruments). Zeta potentials were determined by the Zetasizer software from the electrophoretic mobility applying Henry's equation

and using Smoluchowski's approximation. For all samples investigated, the data represent the average of at least three different autocorrelations carried out for each sample.

Determination of encapsulation efficiency on MLVs loaded with EGCG

The unentrapped EGCG in the aqueous phase was separated by centrifugation from the MLV suspension and its concentration determined by UV spectroscopy to calculate the encapsulation efficiency (EE) of EGCG liposomes. Briefly, a 0.5 mL of MLV liposomal suspension was spun at 25000 g for 90 min at 4°C; after having verified by the Stewart assay (Pignatello et al, 2008), the absence of phospholipids in every supernatant, the concentration of free EGCG was determined spectrophotometrically at 280 nm using a UV-visible spectrophotometer (Multi-Mode Sinergy, HT BioTeck). The EGCG encapsulating efficiency (EE) was calculated as percentage according to Equation 25:

$$\mathbf{EE\ (\%)} = 100 \times [C_{int} / C_{total}] \qquad \text{(Eq. 25)}$$

where C_{total} refers to the total concentration of the antioxidant measured in the unfiltered liposomes, C_{int} refers to the concentration of the encapsulated antioxidant (which was the amount of EGCG measured inside purified liposomes after lysis), and C_{lipid} is the total lipid concentration. All the experiments were repeated at least three times and measurements were run in triplicate.

Determination of encapsulation efficiency on downsized nanocarriers with gel filtration method

Liposomes were separated from non-encapsulated EGCG, Edaravone or Edaravone-C18 by size exclusion chromatography. The same method was used to separate the EGCG-loaded nanodispersed Liquid Crystalline Systems from free EGCG. The disposable syringes **(**2.5 mL), packed with hydrated Sephadex G-25 resin were placed in 15 mL plastic test tubes. After preconditioning with PBS, 0.8 mL of EGCG-loaded liposomes were gently added on the top of the syringes and centrifuged at 500 g for 10 min. Empty liposomes and free EGCG were also used as control. The eluates were collected at the bottom of the test tubes and the Stewart assay was carried out to determine the lipid content in the liposome preparation after gel filtration (Pignatello et al, 2008). To evaluate the encapsulation efficiency, 150 μL samples of purified and unpurified liposomes were lysed by addition of Triton X-100 to a final concentration of 1% (v/v) and the complete release of the antioxidant was obtained. After lysis, the EGCG as well as the EdV and C18-EdV concentration was estimated by the Folin-Ciocalteu assay. The Folin-Ciocalteu reactive

is a mixture of phosphomolybdate and phosphotungstate used for the colorimetric *in vitro* assay of phenolic and polyphenolic antioxidants (Singleton et al, 1999). The reagent does not measure only phenols, but will react with any reducing substance. Therefore, 0.150 mL of 10% Folin-Ciocalteu reagent was added to 0.05 mL of every sample into a 96-well microplate and shaken. After 10 min 0.100 mL of a 7.5% sodium carbonate solution was added and the mixtures were allowed to incubate in the dark for 1 h at room temperature for colour development. After incubation, the absorbance was measured at 765 nm on a BioTek Synergy HT MicroPlate Reader Spectrophotometer using a blank containing all the appropriate components except molecule encapsulated. The calibration curve was plotted using the correspondent molecule. The encapsulation efficiency (EE) (Eq. 25) and the drug loading capacity (DLC) (Eq. 26) were calculated using the following formulae:

$$\textbf{DLC (\%)} = 100 \times [C_{int} / C_{lipid}] \qquad \text{(Eq. 26)}$$

where C_{total} refers to the total concentration of the antioxidant measured in the unfiltered liposomes, C_{int} refers to the concentration of the encapsulated antioxidant (which was the amount of EGCG measured inside purified liposomes after lysis), and C_{lipid} is the total lipid concentration. All the experiments were repeated at least three times and measurements were run in triplicate.

***In vitro* EGCG release**

The *in vitro* antioxidant release from EGCG-liposomes was studied by the dialysis method. Dialysis bags were soaked in PBS at room temperature for 2 h before use to remove the preservative, and then rinsed thoroughly in the same buffer solution. 1 mL of MPxL-EGCG (1 mM, EGCG) was placed in the dialysis bag (12,000 MW cut off; Sigma-Aldrich) and dialyzed against 10 mL of release buffer (PBS). Control bags, containing EGCG with $MgCl_2$ were prepared and dialyzed. The dialysis process was performed under stirring at 100 rpm at 37 °C and kept away from bright light. At appropriate time intervals, 1 mL of the outer aqueous solution was withdrawn for analysis and immediately replaced by an equal volume of fresh release buffer. The cumulative amount of EGCG released was analyzed by the Folin−Ciocalteu assay as described above. The profiles of *in vitro* EGCG release from liposomes and the accumulative release percentage of catechin (RE %) was expressed according to Equation 27:

$$\textbf{RE \%} = 100 \times (C_{0\text{-}t} / C_0) \qquad \text{(Eq. 27)}$$

Where C_{0-t} is the amount of drug released from liposome suspension from the beginning to the scheduled time, and C_0 is the total amount of drug in liposome suspension. The data represent the average of at least three different analyses carried out for each sample.

Cell treatments

Cell culture

ARPE19 cells were routinely maintained in 25 cm^2 flasks in complete DMEM/F12 medium at 37 °C, 5% CO_2 and 95% relative humidity. Complete DMEM/F12 medium was prepared by adding 10% (v/v) heat-inactivated fetal bovine serum (FBS), 2 mM glutamine and 100 U/ml penicillin-streptomycin. Culture medium was changed every 2 days until cells grew to 90% confluence. The cell cultures were detached by trypsinization with 0.5% trypsin in PBS containing 0.025% EDTA and counted using trypan blue exclusion assay.

For treatments, ARPE19 cells were seeded in 24-well plates at 8×10^4/well to reach 50-60% of confluence at 24 h.

In the cytotoxicity assays, the cells were incubated for 24 h and 48 h with increasing concentrations of tested sample and the cell viability was assessed by the MTT assay.

In the cytoprotection assays, the cells were pre-treated with selected samples for 24 h; then, the cells were washed twice with PBS (pH, 7.4) to avoid direct extracellular interaction between oxidant and antioxidant. For C18-EGCG, magnesium poloxamer-407 liposome loaded with EGCG (MPxL-EGCG) and related controls the stressor used was hydrogen peroxide (H_2O_2). More in details, the cells were treated with 6 mM H_2O_2 for 6 h and, in the antioxidant studies of C18-EGCG, also after for 24 h. The combination of dose/time of H_2O_2 treatments was established according to previous MTT viability assay for cytotoxicity studies (data not shown). For C18-EdV and liposome loaded with C18-EdV (POPC-20%C18-EdV and POPC-10%C18-EdV) after pre-treatment with liposome formulations and related controls, the oxidative damage was induced by 10 mM of 2,2-azobis(2-amidinopropane hydrochloride) (AAPH) for 24 h.

Assay of mitochondrial viability (MTT assay)

The 3-(4,5-dimethylthiazol-2-yl)-2,5-diphenyltetrazolium bromide (MTT) assay is a sensitive and reliable indicator of the cellular metabolic activity (Mosmann, 1983). The method is based on the ability of nicotinamide adenine dinucleotide phosphate (NADPH)-dependent cellular oxidoreductase enzymes to reduce the yellow tetrazolium MTT to its insoluble formazan, which has a purple color (**Figure 62**). A solubilization solution (usually either dimethyl sulfoxide, an

acidified ethanol solution, or a solution of the detergent sodium dodecyl sulfate in diluted hydrochloric acid) is added to dissolve the insoluble purple formazan product into a colored solution. The absorbance of this colored solution can be quantified by measuring at a certain wavelength (usually between 500 and 600 nm) by a spectrophotometer and the amount of color produced is directly proportional to the number of viable cells.

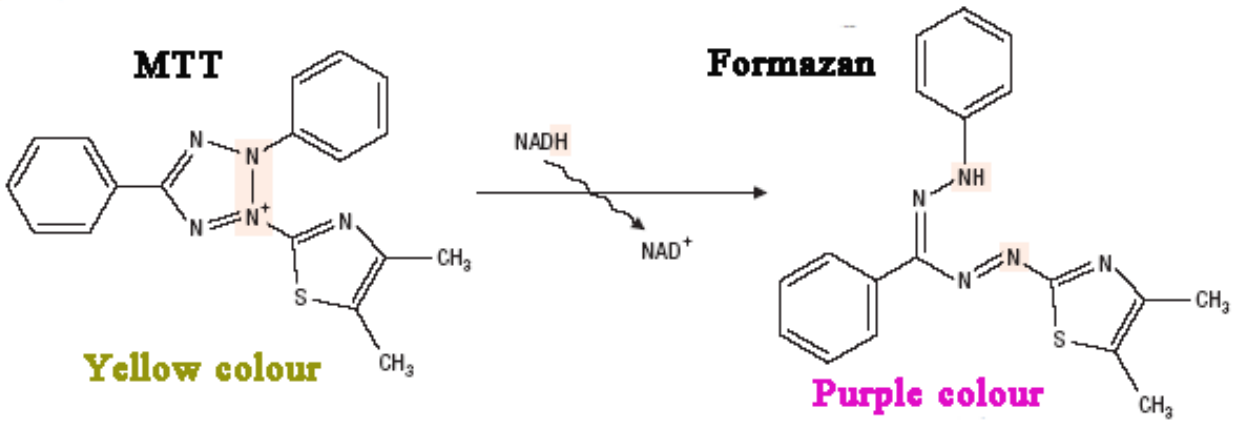

Figure 62. Chemical structures of Yellow MTT and Purple Formazan product in Living Cells.

At the time of analyses, the medium from each well was removed and replaced with fresh medium supplemented with 100 µg MTT (50 µL from the 2 mg mL-1 stock); samples were incubated for 3 h at 37 °C in 5% CO2 atmosphere, until formazan crystals were formed. Next, 400 µL of DMSO was added to each well and mixed thoroughly by shaking to solubilize the MTT formazan crystals. Absorbance was read on a multiwell scanning microplate reader (BioTek Synergy HT MicroPlate Reader Spectrophotometer) at 570 nm using the extraction buffer as blank. The optical density in the control group (untreated cells) was considered as 100% viability. The relative cell viability (%) was calculated as (A570 of treated samples/A570 of untreated samples) x 100. Each experiment was performed at least five times in triplicate.

Transmission Electron Microscopy (TEM)

ARPE19 cells were plated on Aclar films (Ted Pella CA, USA) for flat embedding and were treated as in the cytoprotection assay. After H_2O_2-treatment the cells were fixed for 1 hat room temperature (rt) with a solution of 2.5 Glutaraldeyde in 0.1 M cacodylate buffer (pH 7.4) then post fixed in 1% osmium tetroxide in 0.1 M cacodylate buffer for 30 min at rt followed by dehydration in acetone series and embedded in epoxy resin (Sigma #43359). Ultrathin (40 nm) section were stained with lead citrate and uranyl acetate and imaged on a Philips CM12 TEM at 100 KV. Images

were digitally captured using Olympus Veleta or Megaview G2 digital camera that were previously calibrated for every magnification used.

Qualitative evaluation of cell morphology was done considering the normal cell morphology of nucleous, nuclear membrane, endoplasmic reticulum, mitochondria and villi (Kamogashira, 2017).

Statistical analysis

Data are presented as mean ± S.D. Statistical comparison of differences among groups of data was carried out using Student's t-test. p-values ≤ 0.05 were considered statistically significant, p-values ≤ 0.001 were considered highly significant.

Bibliography

Abe T, Tohgi H, Isobe C, Murata T, Sato C. Remarkable increase in the concentration of 8-hydroxyguanosine in cerebrospinal fluid from patients with Alzheimer's disease. J Neurosci Res. 2002;70 (3): 447–50

Al-Guborya KH, Fowler PA, Garrelc C. The Roles of Cellular Reactive Oxygen Species, Oxidative Stress and Antioxidants in Pregnancy Outcomes. The International Journal of Biochemistry & Cell Biology 2010;42: 1634–50

Andreoli CM, Miller JW. Anti-vascular endothelial growth factor therapy for ocular neovascular disease. Curr Opin Ophthalmol, 2007; 18(6):502–508

Ayala A, Muñoz M F, Argüelles S. Lipid Peroxidation: Production, Metabolism, and Signaling Mechanisms of Malondialdehyde and 4-Hydroxy-2-Nonenal. Oxid Med Cell Longev. 2014; 2014: 360438

Babior B M, Lambeth J D, Nauseef W. The neutrophil NADPH oxidase. Arch Biochem Biophys 397: 342–344, 2002

Babior B M: NADPH oxidase: an update. Blood 1999,93: 1464-1476

Bahorun T, Soobrattee M A, Luximon-Ramma V, Aruoma O I. Free radicals and antioxidants in cardiovascular health and disease. Internet J. Med. Update. 2006; 1: 1-17

Barja G. The flux of free radical attack through mitochondrial DNA is related to aging rate. Aging (Milano). 2000;12 (5):342–55

Bedard K, Krause KH. The NOX family of ROS-generating NADPH oxidases: physiology and pathophysiology. Physiol Rev. 2007 Jan; 87(1):245-313

Bedwell S, Dean RT, Jessup W. The action of defined oxygen centered free radicals on human low density lipoprotein. Biochem J. 1989;262 (3):707–12

Becke A D. Densityfunctional thermochemistry. III. The role of exact exchange. J Chem Phys, 1993, 98, 5648-5652

Beebe DC, Holekamp NM, Shui YB. Oxidative damage and the prevention of age-related cataracts. Ophthalmic Res, 2010; 44(3):155–65

Ben-Shabat S, Parish CA, Hashimoto M, Liu J, Nakanishi K, Sparrow JR. Fluorescent pigments of the retinal pigment epithelium and age-related macular degeneration. Bioorg Med Chem Lett. 2001, 18;11(12):1533-40

Berthoud VM, Beyer EC. Forum review article oxidative stress, lens gap junctions, and cataracts. Antioxid Redox Signal. 2009; 11(2):339–53

Bhutto I, and Lutty G. Understanding age-related macular degeneration (AMD): relationships between the photoreceptor/retinal pigment epithelium/Bruch's membrane/choriocapillaris complex. Molecular Aspects of Medicine, 2012, 33 (4):295–317

Bibiloni Mdel M, Zapata ME, Aragon JA, Pons A, Olea JL, Tur JA. Estimation of antioxidants dietary intake in wet agerelated macular degeneration patients. Nutr Hosp. 2014;29: 880-8

Binder H, Zschörnig O. The effect of metal cations on the phase behavior and hydration characteristics of phospholipid membranes. Chem. Phys. Lipids, 2002, 115:39–61

Birben E, Sahiner UM, Sackesen C, Erzurum S, Kalayci O. Oxidative stress and antioxidant defense, World Allergy Organ J 2012, 5(1):9-19

Boettner EH, Walter JR. Transmission of the ocular media. GPO Invest Ophthalmol Vis Sci. 1962, 1:776–83

Boulton M, Rozanowska M, Rozanowski B. Retinal photodamage. J Photochem Photobiol B. 2001; 64 (2–3):144–161

Boyd, BJ. Characterization of drug release from cubosomes using the pressure ultrafiltration method. Int. J. Pharm. 2003, 24, 260(2):239-47

Briuglia ML, Rotella C, McFarlane A, Lamprou DA. Influence of cholesterol on liposome stability and on in vitro drug release. Drug Deliv. Transl. Res. 2015, 5:231–242

Brodie E, Reed DJ. Cellular recovery of glyceraldehyde-3- phosphate dehydrogenase activity and thiol status after exposure to hydroperoxide. Arch Biochem Biophys. 1990, 276 (1): 210–2

Butterfield DA, Koppal T, Howard B, Subramaniam R, Hall N, Hensley K, et al. Structural and functional changes in proteins induced by free radical-mediated oxidative stress and protective action of the antioxidants N-tert-butyl-alpha-phenylnitrone and vitamin E. Ann N Y Acad Sci. 1998, 854:448–62

Cadenas E, Davies KJ: Mitochondrial free radical generation, oxidative stress and aging. Free Radic Biol Med 2000, 29:222-230

Cai, Y, Anavy N D and Chow HS. Contribution of presystemic hepatic extraction to the low oral bioavailability of green tea catechins in rats. Drug Metab. Dispos. 30, 1246–1249; 2002

Caturla N, Vera-Samper E, Villalain J, Mateo CR, Micol V. The relationship between the antioxidant and the antibacterial properties of galloylated catechins and the structure of phospholipid model membranes. Free Radic. Biol. Med, 2003, 34:(6):648-662

Chaudhury S, Ghosh I, Saha G, Dasgupta S. EGCG prevents tryptophan oxidation of cataractous ocular lens human γ-crystallin in presence of H_2O_2. Int J Biol Macromol 2015, 77: 287-292

Chang, DP, Barauskas, J, Dabkowska, AP, Wadsäter, M, Tiberg, F, Nylander, T. Non-lamellar lipid liquid crystalline structures at interfaces. Adv Colloid Interface Sci. 2015, 222:135-47

Chen Z, Zhu Q Y, Tsang D, Huang Y. Degradation of green tea catechins in tea drinks. J Agric Food Chem 2001;49: 477–82

Chevion M, Berenshtein E, Stadtman ER. Human studies related to protein oxidation: protein carbonyl content as a marker of damage. Free Radic Res. 2000; 33: S99–108

Choi W, Bum L J, Cui L, Li Y, Li Z, Choi J S, Lee H S, Yoon K C. Therapeutic Efficacy of Topically Applied Antioxidant Medicinal Plant Extracts in a Mouse Model of Experimental Dry Eye. Oxid Med Cell Longev. 2016; 2016: 4727415

Chong, YT, Xavier, M, Boyd, B, Drummond CJ. Steric Stabilizers for Cubic Phase Lyotropic Liquid Crystal Nanodispersions (Cubosomes). Advances in Planar Lipid Bilayers and Liposomes. 2015, 21:131-187

Chow H H S, Hakim I A. Pharmacokinetic and chemoprevention studies on tea in humans. Pharmacol Res 2011; 64:105–12

Conrad M., Friedmann Angeli J.P. Glutathione peroxidase 4 (Gpx4) and ferroptosis: what's so special about it? Mol Cell Oncol 2(3) (2015) e995047

Cooke M S, Evans M D, Dizdaroglu M, Lunec J. Oxidative DNA damage: mechanisms, mutation, and disease. FASEB J. 2013; 17 (10): 1195–214

Craig J P, Purslow C, Murphy P J, and Wolffsohn J S. Effect of a liposomal spray on the pre-ocular tear film. Cont. Lens Anterior Eye. 33:83–87, 2010

Cuia Y, Ohb Y J, Lima J, Youna M, Leec I, Pakd H K, Parke W, Job W, Park S. AFM study of the differential inhibitory effects of the green tea polyphenol (−)-epigallocatechin-3-gallate (EGCG) against Gram-positive and Gram-negative bacteria. Food Microbiology. 2012: 29(1):80-87

Deffert C, Cachat J, Krause KH. Phagocyte NADPH oxidase, chronic granulomatous disease and mycobacterial infections. Cell Microbiol. 2014 Aug;16 (8):1168-78

De Jong, "Age-related macular degeneration," The New England Journal of Medicine, vol. 355, no. 14, pp. 1474–1485, 2006

Del Priore LV, Kuo YH, Tezel TH. Age-related changes in human RPE cell density and apoptosis proportion in situ. Invest Ophthalmol Vis Sci 2002 43:3312–3318

Deng R, Hua X, Li J et al. Oxidative stress markers induced by hyperosmolarity in primary human corneal epithelial cells. PLoS ONE 2015 10: e0126561

Di Gregorio G M, Ferraris P, Mariani P. Wetting properties of dioleoyl-phosphatidyl-choline bilayers in the presence of trehalose: an X-ray diffraction study. Chem. Phys. Lipids. 2010, 163 (6), 601-6

Di Marco E, Jha J C, Sharma A, Wilkinson-Berka J L, Jandeleit-Dahm KA, Haan, J.B. Are reactive oxygen species still the basis for diabetic complications? Clin. Sci. 2015; 129, 199–216

Domanski, J, Stansfeld P J, Sansom M S, Beckstein O. Lipidbook: a public repository for force-field parametersused in membrane simulations. J Membr Biol, 2010, 236, 255-258

Drouault-Holowacz S, Bieuvelet S, Burckel A, Rigal D, Dubray C, Lichon JL, Bringer P, Pilon F, Chiambaretta FR. Antioxidants intake and dry eye syndrome: a crossover, placebo-controlled, randomized trial. Eur J Ophthalmol. 2009 May-Jun;19(3):337-42

Duan W J, Li Y F, Liu F L, Deng J, Wu Y P. A SIRT3/AMPK/ autophagy network orchestrates the protective effects of trans-resveratrol in stressed peritoneal macrophages and RAW 264.7 macrophages. Free Radic Biol Med, 2016, 95: 230-242

Dvorakova K., Dorr R T, Valcic S, Timmermann B, Alberts DS. Pharmacokinetics of the green tea derivatives, EGCG, by the topical route of administration in mouse and human skin. Cancer Chemother. Pharmacol.1999; 43, 331–335.

Elbling L, Weiss R M, Teufelhofer O, Uhl M, Knasmueller S, Schulte-Hermann R et al. Green tea extract and (−)-epigallocatechin-3-gallate, the major tea catechin, exert oxidant but lack antioxidant activities. FASEB J 2005;19:807–9

Fenton HJH. The oxidation of tartaric acid in presence of iron. J Chem Soc Proc 9: 113, 1893

Fine SL, Berger JW, Maguire MG, Ho AC. Age-related macular degeneration. New Engl J Med 2000 342:483–492

Fontell K. Cubic phases in surfactant and surfactant-like lipid systems. Colloid and Polymer Science. 1990, 268 (3): 264–285

Friberg S. Lyotropic liquid crystals. Naturwissenschaften. 1977 64 (12): p. 612-618

Frei B, Higdon J V. Antioxidant activity of tea polyphenols in vivo: evidence from animal studies. J. Nutr. 2003, 133 (10), 3275S-84S

Futerman A H, Van Meer G. The cell biology of lysosomal storage disorders. Nature reviews Molecular cell biology, 2004

Gaillard E R, Atherton S J, Eldred G, et al. Photophysical studies on human retinal lipofuscin. Photochem Photobiol 61:448–53, 1995

Galano A, Alvarez-Idaboy JR. Glutathione: mechanism and kinetics of its non-enzymatic defense action against free radicals, RSC Advances 1 (2011) 1763-1771

Galati G, Lin A, Sultan A M, O'Brien P J. Cellular and in vivo hepatotoxicity caused by green tea phenolic acids and catechins. Free Radic Bio Med 2006;40 :570–80

Galli F, Azzi A, Birringer M, Cook-Mills J M, Eggersdorfer M, Frank J, Cruciani G, Lorkowski S, Ozer N Z. Vitamin E: Emerging aspects and new directions. Free Radic Biol Med 102 (2017) 16-36

Gan L, Wang J, Jiang M, Bartlett H, Ouyang D, Eperjesi F, Liu J, Gan Y. Recent advances in topical ophthalmic drug delivery with lipid-based nanocarriers. Drug Discov Today. 2013: 18(5-6): 290-7

Gaudana R, Ananthula H K, Parenky A, Mitra A K. Ocular drug delivery. AAPS J. 2010, 12(3):348-60

George P. Reaction between catalase and hydrogen peroxide. Nature, vol. 159, no. 4028, pp. 41–43, 1947

Granja A, Frias I, Neves AR, Pinheiro M, Reis S. Therapeutic Potential of Epigallocatechin Gallate Nanodelivery Systems. Biomed. Res. Int. 2017, 5813793.

Fridovich I. Superoxide dismutases: defence against endogenous superoxide radical. Ciba Foundation symposium, no. 65, pp. 77–93, 1978

Giblin F.J. Glutathione: a vital lens antioxidant. J. Ocul. Pharmacol. Ther. 2000; 16: 121–135

Gill SS, Tuteja N. Reactive oxygen species and antioxidant machinery in abiotic stress tolerance in crop plants. Plant Physiol Biochem. 2010;48: 909–930

Glasel J A, Deutscher MP. Introduction to Biophysical Methods for Protein and Nucleic Acid Research. Academic Press, 1995

Goodman, J M, James J J, Whiting A. MM2 force field parameters for compounds containing the diazoketone function J Chem Soc Perk T 2, 1994, 109-116

Gordois A, H. Cutler, L. Pezzullo et al. An estimation of the worldwide economic and health burden of visual impairment. Global Public Health, vol. 7, no. 5, pp. 465–481, 2012

Gordon S, Young K, Wilson R, Rizwan S, Kemp R, Rades T, et al. Chitosan hydrogels containing liposomes and cubosomes as particulate sustained release vaccine delivery systems. J. Liposome Res. 2012; 22(3):193–204

Góth L, Rass P, Páy A. Catalase enzyme mutations and their association with diseases. Mol Diagn. 2004; 8: 141–149

Gubitosi-Klug A R, Ramaprasad T, Yunpeng D, Jerry L N, Timothy S K. 5-Lipoxygenase, but Not 12/15-Lipoxygenase, Contributes to Degeneration of Retinal Capillaries in a Mouse Model of Diabetic Retinopathy

Gupta SK, Trivedi D, Srivastava S, Joshi S, Halder N, Verma SD. Lycopene attenuates oxidative stress induced experimental cataract development: an in vitro and in vivo study. Nutrition. 2003 Sep; 19(9):794-9

Gustafsson J, Ljusberg-Wharen H, Almgrem M, Larsson K. Cubic lipid-water phase dispersed into submicron particles. Langmuir. 1996; 12:4611-4613.

Gustafsson J, Ljusberg-Wharen H, Almgrem M, Larsson K. Submicronparticles of reversed lipid phases in water stabilized by a nonionic amphiphilic polymer. Langmuir. 1997, 13:6964-6971.

Haber F, Weiss J. The catalytic decomposition of hydrogen peroxide by iron salts. Proc R Soc London (A). 1934; 147: 332–51

Haeggström J Z, Funk C D. Lipoxygenase and leukotriene pathways: biochemistry, biology, and roles in disease. Chem Rev. 2011 Oct 12;111(10): 5866-98

Halliwell B, Cross C E. Oxygen-derived species: their relation to human disease and environmental stress. Environ Health Perspect 102 Suppl 10: 5–12, 1994

Halliwell B, Gutteridge J M C. Free radicals in biology and medicine. 4th ed. Oxford, UK: Clarendon Press. 2007

Halliwell B, Gutteridge J M C. 1989. Free Radicals in Biology and Medicine, 2nd ed., Oxfors: Clarendon

Halliwell B, Gutteridge J M C. Role of free radicals and catalytic metal ions in human disease, Methods Enzymol. 1990; 186: 1-85

Ham W T Jr, Ruffolo J J Jr, Mueller H A, et al. Histologic analysis of photochemical lesions produced in rhesus retina by short-wave-length light. Invest Ophthalmol Vis Sci 17:1029–35, 1978

Hammond BR Jr, Johnson EJ, Russell RM, et al. Dietary modification of human macular pigment density. Invest Ophthalmol Vis Sci 38:1795–801, 1997

Hammond BR Jr, Wooten BR, Snodderly DM: Preservation of visual sensitivity of older subjects: association with macular pigment density. Invest Ophthalmol Vis Sci 39:397–406, 1998

Hammond BR Jr, Wooten BR, Snodderly DM: Density of the human crystalline lens is related to the macular pigment carotenoids, lutein and zeaxanthin. Optom Vis Sci 74:499–504, 1997

Hammond BR Jr, Wooten BR, Snodderly DM: Individual variations in the spatial profile of human macular pigment. J Opt Soc Am A Opt Image Sci Vis 14:1187–96, 1997

Han, S, Shen, JQ, Gan, Y, Geng, HM, Zhang, XX, Zhu, CL, Gan, L. Novel vehicle based on cubosomes for ophthalmic delivery of flurbiprofen with low irritancy and high bioavailability. Acta Pharmacol Sin. 2010, 31(8):990-8.

Harman D: The aging process. Proc Natl Acad Sci USA 78:7124–8, 1981

He R R, Yao X S, Li H Y, Dai Y, Duan Y H. The Anti-stress Effects of Sarcandra glabra Extract on Restraint-Evoked Immunocompromise. Chem Pharm Bull. 2009. 32: 247-252

Hegde KR, Varma SD. Protective effect of ascorbate against oxidative stress in the mouse lens. Biochimica Biophysica Acta 2004; 1670: 12–18

Hironaka K, Inokuchi Y, Fujisawa T, Shimazaki H, Akane M, Tozuka Y, Tsuruma K, Shimazawa M, Hara H, Takeuchi H. Edaravone-loaded liposomes for retinal protection against oxidative stress-induced retinal damage. Eur. J. Pharm. Biopharm. 2011 Sep; 79(1):119-25

Hofer T, Badouard C, Bajak E, Ravanat J L, Mattsson A, Cotgreave I A. Hydrogen peroxide causes greater oxidation in cellular RNA than in DNA. Biol Chem. 2005;386 (4): 333–7

Honda M, Asai T, Oku N, Araki Y, Tanaka M, Ebihara N. Liposomes and nanotechnology in drug development: focus on ocular targets. Int J Nanomedicine. 2013;8: 495-503

Huang Y, Gui S. Factors affecting the structure of lyotropic liquid crystals and the correlation between structure and drug diffusion. RSC Adv., 2018, 8, 6978

Hülya Bayır M D. Reactive oxygen species. Crit Care Med 2005 Vol. 33, No. 12 (Suppl.)

Hunter J. J., J. I. W. Morgan, W. H. Merigan, D. H. Sliney, J. R.Sparrow, and D. R. Williams. The susceptibility of the retina to photochemical damage fromvisible light. Progress in Retinal and Eye Research, vol. 31, no. 1, pp. 28–42, 2012

Higdon J V, Frei B. Tea catechins and polyphenols: health effects, metabolism, and antioxidant functions. Crit Rev Food Sci Nutr 2003;43:89–143.

Ho H Y, Cheng M L, Weng S F, Leu Y L, Chiu DT. Antiviral effect of epigallocatechin gallate on enterovirus 71. J Agric Food Chem 57: 6140–6147; 2009

Hsu JP, Nacu A. Behavior of soybean oil-in-water emulsion stabilized by nonionic surfactant. J. Colloid. Interface Sci. 2003, 259(2):374-81.

Ibrahim OM, Dogru M, Matsumoto Y et al. Oxidative stress induced age dependent meibomian gland dysfunction in Cu, Zn-superoxide dismutase-1 (Sod1) knockout mice. PLoS ONE 2014 9: e99328

Ighodaro O M, Akinloye O A. First line defence antioxidants-superoxide dismutase (SOD), catalase (CAT) and glutathione peroxidase (GPX): Their fundamental role in the entire antioxidant defence grid. Alexandria Journal of Medicine (2017). Articles in press

Iloki-Assanga SB. Lewis-Luján LM, Fernández-Angulo D, Gil-Salido AA, Lara-Espinoza CL, Rubio-Pino JL. Retino-protective effect of Bucida buceras against oxidative stress induced by H2O2 in human retinal pigment epithelial cells line. BMC Complement Altern. Med, 2015, 15:254.

Imai S, Inokuchi Y, Nakamura S, Tsuruma K, Shimazawa M, and Hara H. Systemic administration of a free radical scavenger, edaravone, protects against light-induced photoreceptor degeneration in themouse retina. EuropeanJournal of Pharmacology, vol. 642, no. 1-3, pp. 77–85, 2010

Isbrucker R A, Edwards J A, Wolz E, Davidovich A, Bausch J. Safety studies on epigallocatechin gallate (EGCG) preparations. Part 2: dermal, acute and shortterm toxicity studies. Food Chem Toxicol 2006;44: 636–50

Israelachvili J N. Intermolecular: And Surface Forces, 2nd Edn. Academic Press, New York, USA 1992

Jeffrey N K. Age-related neuropathology, cognitive decline, and Alzheimer's disease. Ageing Research Reviews Volume 5, Issue 1, February 2006, Pages 1-13

Kaarniranta K, Salminen A, Haapasalo A, Soininen H, Hiltunen M. Age-related macular degeneration (AMD): Alzheimer's disease in the eye? 2011 J Alzheimers Dis 24:615–631

Kamogashira T, Hayashi K, Fujimoto C, Iwasaki S, Yamasoba T. Functionally and morphologically damaged mitochondria observed in auditory cells under senescence-inducing stress. NPJ Aging Mech. Dis. 2017, 3, 2

Karami Z, Hamidi M. Cubosomes: remarkable drug delivery potential. Drug Discov Today. 2016, 21(5):789-801

Katakam M, Banga AK. Use of poloxamer polymers to stabilize recombinant human growth hormone against various processing stresses. Pharm Dev Technol. 1997, 2(2):143-9.

Kielbassa C, Roza L, Epe B. Wavelength dependence of oxidative DNA damage induced by UV and visible light. Carcinog. 1997; 18:811-816

Kikuchi A, Takeda A, Onodera H, Kimpara T, Hisanaga K, Sato N, et al. Systemic increase of oxidative nucleic acid damage in Parkinson's disease and multiple system atrophy. Neurobiol Dis. 2002;9(2):244–8

Klauda J B, Brooks B R, Pastor R W. Dynamical motions of lipids and a finite size effect in simulations of bilayers. J Chem Phys, 2006, 125, 144710

Kliment CR, Suliman HB, Tobolewski JM, Reynolds CM, Day BJ, Zhu X, McTiernan CF, McGaffin KR, Piantadosi CA, Oury TD. Extracellular superoxide dismutase regulates cardiac function and fibrosis. J Mol Cell Cardiol 2009; 47:730–742

Knorr L. Einwirkung von acetessigester auf phenylhydrain. Ber Deut Chem Ges 1883, 16:2597-2599

Krishnamurthy P, Wadhwani A. Antioxidant enzymes and human health. Antioxidant enzyme. InTech; 2012

Kruft BI, Greer A. Photosensitization reactions in vitro and in vivo. Photochemistry and photobiology. 2011; 87 (6):1204–1213

Kulkarni CV, Vishwapathi VK, Quarshie A, Moinuddin Z, Page J, Kendrekar P, Mashele S. Self-Assembled Lipid Cubic Phase and Cubosomes for the Delivery of Aspirin as a Model Drug. Langmuir. 2017; 26:33(38):9907-9915

Lambert J D, Kennett M J, Sang S, Reuhl K R, Ju J, Yang CS. Hepatotoxicity of high oral dose (−)-epigallocatechin-3-gallate in mice. Food ChemToxicol 2010;48: 409–16

Lakshmi Prabha J. Tear secretion: a short review. Journal of Pharmaceutical Sciences and Research, vol. 6, no. 3, 2014 pp. 155–157.

Larsson K. Aqueous dispersion of cubic lipidYwater phases. Curr. Opin. Colloid Interface Sci. 2000, 5:64Y69

Laudadio, E.; Mobbili, G.; Minnelli, C.; Massaccesi, L.; Galeazzi, R. Salts Influence Cathechins and Flavonoid-Encapsulation in Liposomes: A Molecular Dynamics Investigation. *Mol Inform*, June 21 **2017**, 36 (11) 1700059 (1-13)

Laudadio E, Mobbili G, Minnelli C, Massaccesi L, Galeazzi R. Salts influence cathechins and flavonoids encapsulation in liposomes: a molecular dynamics investigation. Mol. Inform., 2017, 36:11.

Lee B J, Egi Y, van Leyen K, Lo E H, Arai K. Edaravone, a free radical scavenger, protects components of the neurovascular unit against oxidative stress in vitro. Brain Res. 2010 Jan 11; 1307:22-7

Lee V H, Morimoto K W, Stratford R E. Jr. Esterase distribution in the rabbit cornea and its implications in ocular drug bioavailability. Biopharm Drug Dispos. 1982 Oct-Dec;3(4): 291-300

Lee YS, Cheon IS, Kim BH, Kwon MJ, Lee HW, Kim TY. Loss of extracellular superoxide dismutase induces severe IL-23-mediated skin inflammation in mice. J Invest Dermatol 133:732–741, 2013

Lemarie F, Chang C W, Blatchford D R, Amor R, Norris G, Tetley L, et al. Antitumor activity of the tea polyphenol epigallocatechin-3-gallate encapsulated in targeted vesicles after intravenous administration. Nanomedicine 2013;8 :181–92

Lemp M A, Baudouin C, Baum J et al. The definition and classification of dry eye disease: report of the definition and classification subcommittee of the international Dry Eye WorkShop. Ocular Surface, vol. 5, no. 2, pp. 75–92, 2007

Lemp M A. Report of the national eye institute/industry workshop on clinical trials in dry eyes. CLAO Journal, vol. 21, no. 4, pp. 221–232, 1995

Liang H, Ran Q, Jang YC, et al. Glutathione peroxidase 4 differentially regulates the release of apoptogenic proteins from mitochondria. Free Radical Biol Med. 2009; 47:312–320

Li H Y, Lee C J, Wen Y C, Chen S J, Huang K F. EGCG, a major polyphenol in green tea, protects human retinal pigment epithelium (ARPE-19) cells from viable blue light-induced disorders. Life Science Journal, 2014;11(4).

Li N. Liposome coated with low molecular weight chitosan and its potential use in ocular drug delivery. Int. J. Pharm. 2009; 379, 131–138.

Li GX, Chen YK, Hou Z, Xiao H, Jin H, Lu G, Lee MJ, Liu B, Guan F, Yang Z, Yu A, Yang CS. Pro-oxidative activities and dose-response relationship of (−)-epigallocatechin-3-gallate in the inhibition of lung cancer cell growth: a comparative study in vivo and in vitro. Carcinogenesis, 2010, 31(5):902-910

Lin J K, Chen P C, Ho C T, Lin-Shiau SY. Inhibition of xanthine oxidase and suppression of intracellular reactive oxygen species in HL-60 cells by theaflavin-3,3′-digallate, (−)-epigallocatechin-3-gallate, and propyl gallate. J Agric Food Chem 2000;48: 2736–43

Li Y., Zhao S, Zhang W, Zhao P, He B, Wu N, Han P. Epigallocatechin-3-O-gallate (EGCG) attenuate sFFAs-induced peripheral insulin resistance through AMPK pathway and insulin signaling pathway in vivo, Diabetes Res. Clin.Pract. 2011, 93:205–214

Luo KW, Lung WY, Chun-Xie, Luo XL, Huang WR. EGCG inhibited bladder cancer T24 and 5637 cell proliferation and migration via PI3K/AKT pathway. Oncotarget. 2018, 9(15):12261-12272.

Maccarone R, Di Marco S, Bisti S. Saffron supplement maintains morphology and function after exposure to damaging light in mammalian retina. Invest Ophthalmol Vis Sci 2008;49: 1254–61

Mandel S A, Amit T, Weinreb O, Youdim M B. Understanding the broad-spectrum neuroprotective action profile of green tea polyphenols in aging and neurodegenerative diseases. J. Alzheimers Dis. 2011, 25 (2), 187-208

Mandel S, Amit T, Bar-Am O, Youdim MB. Iron dysregulation in Alzheimer's disease: multimodal brain permeable iron chelating drugs, possessing neuroprotective-neurorescue and amyloid precursor protein-processing regulatory activities as therapeutic agents. Prog Neurobiol 2007; 82:348–60

Mannermaa, E. et al. Drug transport in corneal epithelium and blood-retina barrier: emerging role of transporters in ocular pharmacokinetics. Adv. Drug Deliv. Rev. 58, 1136–1163; 2006

Mao Y, Du Y, Cang X, Wang J, Chen Z, Yang H, Jiang H. Binding competition to the POPG lipid bilayer of Ca^{2+}, Mg^{2+}, Na^{+}, and K^{+} in different ion mixtures and biological implication. J Phys Chem B, 2013, 117, 850-8

Martın-Molina A, Rodrıguez-Beas C, Faraudo J. Effect of Calcium and Magnesium on Phosphatidylserine Membranes: Experiments and All-Atomic Simulations. Biophys. J. 2012, 102:2095–2103.

Martinet W, de Meyer G R, Herman A G, Kockx MM. Reactive oxygen species induce RNA damage in human atherosclerosis. Eur J Clin Invest. 2004;34 (5):323–7

Masuda T, Shimazawa M, Hara H. Retinal Diseases Associated with Oxidative Stress and the Effects of a Free Radical Scavenger (Edaravone). Oxid Med Cell Longev. 2017; 2017: 9208489

Masuda T, Shimazawa M, Takata S, Nakamura S, Tsuruma K, and Hara H. Edaravone is a free radical scavenger that protects against laser-induced choroidal neovascularization in mice and common marmosets. Experimental Eye Research, vol. 146, pp. 196–205, 2016

Mayne C G, Saam J, Schulten K, Tajkhorshid E, Gumbart J C. Rapid parameterization of small molecules using the Force Field Toolkit. J Comput Chem, 2013, 34, 2757-2770

Mehrabian M, Allayee H, Wong J, Shi W, Wang X P, Shaposhnik Z, Funk C D, Lusis A J. Identification of 5-lipoxygenase as a major gene contributing to atherosclerosis susceptibility in mice Circ. Res., 91 (2002), pp. 120-126

Mellerio J. Light effects on the retina, in Albert D, Jakobiec F (eds): Principles and Practice of Ophthalmology: Basic Sciences. Philadelphia, W B Saunders Co, 1994, pp1326–45

Michelson A M, McCord J M, Fridovich I. Superoxide and Superoxide Dismutases. London: Academic Press; 1977. p. 320

Migalska-Zalas A, Kityk I V, Bakasse M, Sahraoui B. Features of the alkynyl ruthenium chromophore with modified anionic subsystem UV absorption. Spectrochim Acta A Mol Biomol Spectrosc, 2008, 69, 178-182

[a]Minnelli C, Cianfruglia L, Laudadio E, Galeazzi R, Pisani M, Crucianelli E, Bizzaro D, Armeni T, Mobbili G. Selective induction of apoptosis in MCF7 cancer-cell by targeted liposomes functionalised with mannose-6-phosphate. Journal of Drug Targeting, 2018, 26(3):1-31.

[b]Minnelli C, Moretti P, Fulgenzi G, Mariani P, Laudadio E, Armeni T, Galeazzi R, Mobbili G. A Poloxamer-407 modified liposome encapsulating epigallocatechin-3-gallate in the presence of magnesium: Characterization and protective effect against oxidative damage. International Journal of Pharmaceutics, 2018, 552:225–234.

Mishra G P, Bagui M, Tamboli V, and Mitra A K. Recent applications of liposomes in ophthalmic drug delivery. J. Drug Deliv. 2011, 863734, 2011

Mitchel R E, McCann R. Vitamin E is a complete tumor promoter in mouse skin Carcinogenesis, 14 (4) (1993), pp. 659-662

Mosmann T. Rapid colorimetric assay for cellular growth and survival: application to proliferation and cytotoxicity assays. *J. Immunol. Methods.* 1983, *65*, 55–63

Nakayama T, Hashimoto T, Kajiya K, Kumazawa, S. Affinity of polyphenols for lipid bilayers. Biofactors, 2000, 13:147–151.

Nakazato T, Ito K, Miyakawa Y, Kinjo K, Yamada T, Hozumi N. Catechin, a green tea component, rapidly induces apoptosis of myeloid leukemic cells via modulation of reactive oxygen species production in vitro and inhibits tumor growth in vivo. Haematologica 2005;90:317–25

Nanjo F, Mori M, Goto K, Hara Y. Radical scavenging activity of tea catechins and their related compounds. Biosci. Biotechnol. Biochem. 1999, 63 (9), 1621-1623

Nowicki P T, Flavahan S, Hassanain H, Mitra S, Holland S, Goldschmidt-Clermont P J, Flavahan NA. Redox signaling of the arteriolar myogenic response. Circ Res 89: 114–116, 2001

Nozik-Grayck E, Suliman HB, Piantadosi CA. Extracellular superoxide dismutase. Int J Biochem Cell Biol 37: 2466–2471, 2005

Qanungo S, Das M,Haldar S, Basu A. Epigallocatechin-3-gallate induces mitochondrial membrane depolarization and caspase-dependent apoptosis in pancreatic cancer cells. Carcinogenesis 2005;26 :958–67

Onufriev A V, Sigalov G. A strategy for reducing gross errors in the generalized Born models of implicit solvation. J Chem Phys, 2011, 134, 164104

Organisciak DT, Wang H-M, Li YZ, Tso MOM. The protective effect of ascorbate in retinal light damage of rats. Invest Ophthalmol Vis Sci 1985;26:1580–88.

Pabst G., Rappolt M., Amenitsch H., Laggner P. Structural information from multilamellar liposomes at full hydration: full q-range fitting with high quality X-ray data. Phys. Rev. E: Stat. Phys. Plasmas Fluids Relat. Interdiscip. Topics, 62 (3 Pt B) (2000):4000-4009

Padmaja S, Raju TN. Antioxidant effect of curcumin in selenium induced cataract of Wistar rats. Indian J Exp Biol. 2004, 42(6):601-3.

Peters E, Colby K. The tear film. In: Tasman W, Jaeger EA, eds. Duane's foundations of clinical ophthalmology on CD Rom. 2006. Vol. 2. Chapter 3. Philadelphia: Lippincott Williams & Wilkins

Petrov D, Mansfield C, Moussy A, Hermine O. ALS Clinical Trials Review: 20 Years of Failure. Are We Any Closer to Registering a New Treatment?. Frontiers in Aging Neuroscience. 2017, 9: 68

Pignatello R, Nicolosi D, Nicolosi V M. Fusogenic liposomes as new carriers to enlarge the spectrum of action of antibiotic drugs against Gram-negative bacteria.Science against microbial pathogens: communicating current research and technological advances, 1st ed.; Formatex Research Center: Bajadoz, Spain,2008

Porasso R D, Cascales J J L. A criterion to identify the equilibration time in lipid bilayer simulations. Papers in Physics, 2012, 4, 040005

Pronk S, Pall S, Schulz R, Larsson P, Bjelkmar P, Apostolov R, Shirts M R, Smith J C, Kasson P M, van der Spoel D, Hess B, Lindahl E. GROMACS 4.5: a high-throughput and highly parallel open source molecular simulation toolkit. Bioinformatics, 2013, 29, 845-854

Pryor WA, Jin X, Squadrito GL. One- and two-electron oxidations of methionine by peroxynitrite. Proc Natl Acad Sci USA. 1994;91(23):11173–7

Raghavachari K. Perspective on "Density functional thermochemistry. III. The role of exact exchange. Theor Chem Acc, 2000, 103, 361-363

Ranchon I, Gorrand J-M, Cluzel J, Droy-Lefaix M-T, Doly M. Functional protection of photoreceptors from light-induced damage by dimethylthiourea and ginkgo biloba extract. Invest Ophthalmol Vis Sci 1999;40:1191–99.

Ranchon I, Chen S, Alvarez K, Anderson RE. Systemic administration of phenyl-N-tert-butylnitrone protects the retina from light damage. Invest Ophthalmol Vis Sci 2001;42:1375–79

Reddy, V.N. Glutathione and its function in the lens—an overview. Exp. Eye Res. 1990; 50: 771–778

Rice-Evans C. Implications of the mechanisms of action of tea polyphenols as antioxidants in vitro for chemoprevention in humans. Proc. Soc. Exp. Biol. Med. 1999, 220, 262–266

Riley PA. Free radicals in biology: oxidative stress and the effects of ionizing radiation. Int J Radiat Biol 65: 27–33, 1994

Rojkind M, Domininguez-Rosales J A, Nieto N, Greenwel P. Role of hydrogen peroxide and oxidative stress in healing responses. Cell Mol Life Sci 2002, 59:1872-1891

Rong, W T, Lu, Y P, Tao, Q et al. Hydroxypropyl-sulfobutyl-betacyclodextrin improves the oral bioavailability of edaravone by modulating drug efflux pump of enterocytes. J Pharm Sci. 2014; 103(2):730–742

Salah N, Miller N J, Paganga G, Tijburg L, Bolwell G P, Rice-Evans C. Polyphenolic flavanols as scavengers of aqueous phase radicals and as chain-breaking antioxidants. Arch Biochem. Biophys. 1995, 322, 339–346

Salonen A, Moitzi C, Salentinig S, Glatter O. Material transfer in cubosome-emulsion mixtures: effect of alkane chain length. Langmuir. 2010;26 (13):10670–6

Sanga S, Yangb I, Buckleyb B, Chi-Tang H, Chung S Y. Autoxidative quinone formation in vitro and metabolite formation in vivo from tea polyphenol (−)-epigallocatechin-3-gallate: studied by real-time mass spectrometry combined with tandem mass ion mapping, Free Radic. Biol. Med.,2003; 43: 362–370

Sang S, Lee MJ, Hou Z, Ho CT, Yang CS. Stability of tea polyphenol (−)-epigallocatechin-3-gallate and formation of dimers and epimers under common experimental conditions. J Agric Food Chem 2005;53: 9478–84

Schalk I, Zeng K, Wu S K, Stura E A, Matteson J, Huang M, Tandon A, Wilson I A, Balch W E. Structure and mutational analysis of Rab GDP-dissociation inhibitor. Nature 381: 42–48, 1996

Schrader M, Fahimi HD. Peroxisomes and oxidative stress. Biochim Biophys Acta 1763: 1755–1766, 2006

Seen S, Tong L. Dry eye disease and oxidative stress. Acta Ophthalmol. 2018 Jun;96(4):e412-e420

Sen C K. The general case for redox control of wound repair. Wound Repair Regen 2003. In press

Seo Y, Kim M K, Choo H, Chong Y. Facile synthesis of 4″–O–alkyl (–)-EGCG derivatives through regioselective

deacetylative alkylation. An International Journal for Rapid Communication of Synthetic Organic Chemistry, 2017, 47(7): 655-659

Seth RK, Kharb S. Protective function of alpha-tocopherol against the process of cataractogenesis in humans. Annals of Nutrition and Metabolism 1999; 43: 286–289

Severino J F, Goodman B A, Kay C W, Stolze K, Tunega D, Reichenauer T G, Free radicals generated during oxidation of green tea polyphenols: electron paramagnetic resonance spectroscopy combined with density functional theory calculations. Free Radic. Biol. Med. 2009;46: 1076–88

Shimazaki H, Hironaka K, Fujisawa T et al. Edaravone loaded liposome eyedrops protect against light-induced retinal

damage in mice. Investigative Ophthalmology&Visual Science, vol. 52, no. 10, pp. 7289–7297, 2011.

Pérez-González A, Galano A. OH radical scavenging activity of Edaravone: mechanism and kinetics. J Phys Chem B, 2011, 10; 115(5):1306-14

Simon HU, Haj-Yehia A, Levi-Schaffer F. Role of reactive oxygen species (ROS) in apoptosis induction. Apoptosis 2000; 5, 415–418

Simos YV, Verginadis II, Toliopoulos IK, Velalopoulou AP, Karagounis IV, Karkabounas SC, et al. Effects of catechin and epicatechin on superoxide dismutase and glutathione peroxidase activity, in vivo. Redox Rep 2012;17: 181–6

Singh BN, Shankar S, Srivastava RK. Green tea catechin, epigallocatechin-3-gallate (EGCG): mechanisms, perspectives and clinical applications. Biochem Pharmacol. 2011, 82(12):1807-21.

Singleton, Vernon L, Orthofer, Rudolf, Lamuela-Raventós, Rosa M. Analysis of total phenols and other oxidation substrates and antioxidants by means of folin–ciocalteu reagent. 1999, 299: 152

Soper A K, Bruni F, Ricci M A. Site-site pair correlation functions of water from 25 to 400 °C: Revised analysis of new and old refraction data. J Chem Phys, 1997, 106, 247-254

Sparrow JR, Nakanishi K, Parish CA. The lipofuscinfluorophore A2E mediates blue light-induced damage to retinal pigmented epithelial cells. Invest Ophthalmol Vis Sci 2000 41:1981–1989

Stone WL, Farnsworth CC, Dratz EA. A reinvestigation of the fatty acid content of bovine, rat and frog retinal rod outer segments. Exp Eye Res 28:387–97, 1979

Suzukawa K, Miura K, Mitsushita J, Resau J, Hirose K, Crystal R, Kamata T. Nerve growth factor-induced neuronal differentiation requires generation of Rac1-regulated reactive oxygen species. J.Biol.Chem. 2000; 275:13175-13178

Szoka F Jr, Papahadjopoulos D. Procedure for preparation of liposomes with large internal aqueous space and high capture by reverse-phase evaporation. Proc. Natl. Acad. Sci. U. S. A. 1978, 75, (9), 4194-4198

Tanito M, Masutani H, Kim Y-C, Nishikawa M, Ohira A, et al. Sulforaphane induces thioredoxin through the antioxidant-responsive element and attenuates retinal light damage in mice. Invest Ophthalmol Vis Sci 2005; 46:979–87

Tateyama M, Takeda A, Onodera Y, Matsuzaki M, Hasegawa T, Nunomura A, et al. Oxidative stress and predominant Abeta 42 (43) deposition in myopathies with rimmed vacuoles. Acta Neuropathol. 2003;105(6):581–5

Tavani A, Negri E, La Vecchia C. Food and nutrient intake and risk of cataract. Ann Epidemiol. 1996;6:41-6. doi: 10.1016/1047-2797(95)00099-2

Theodoropoulou S, Samoli E, Theodossiadis P, Papathanassiou M, Lagiou A, Lagiou P, Tzonou A. Diet and cataract: a case–control study. Int Ophthalmol. 2014

Toppo S, Flohe L, Ursini F, Vanin S, Maiorino M. Catalytic mechanisms and specificities of glutathione peroxidases: variations of a basic scheme, Biochim Biophys Acta 1790(11) (2009) 1486-500

Traber M G, Stevens J F. Vitamins C and E: beneficial effects from a mechanistic perspective. Free Radic Biol Med 2011 51, 1000–1013

Traber M G. Vitamin E inadequacy in humans: causes and consequences. 2014 Adv Nutr 5, 503–514

Tso MO. Pathogenic factors of aging macular degeneration. Ophthalmology 1985;92:628-35

Uchida K. 4-Hydroxy-2-nonenal: a product and modulator of oxidative stress. Prog. Lipid Res. 42:318–343; 2003

Uchida K, Stadtman E R. Modification of histidine residues in proteins by reaction with 4-hydroxynonenal. Proc. Natl. Acad. Sci. USA 89:4544–4548; 1992

Urtti, A, Salminen, L. Minimizing systemic absorption of topically administered ophthalmic drugs. Surv Ophthalmol., 1993, 37:435–56

Valavanidis A, Vlachogianni T, Fiotakis K, Loridas S. Pulmonary oxidative stress, inflammation and cancer: respirable particulate matter, fibrous dusts and ozone as major causes of lung carcinogenesis through reactive oxygen species mechanisms. Int J Environ Res Public Health. 10 (9): 3886–907; 2013

Valko M, Izakovic M, Mazur M, Rhodes CJ, Telser J. Role of oxygen radicals in DNA damage and cancer incidence. Mol Cell Biochem 266: 37–56, 2004

Van Leeuwen R, Boekhoorn S, Vingerling JR, Witteman JC, Klaver CC, Hofmann A, de Jong PT. Dietary intake of antioxidants and risk of age-related macular degeneration. JAMA. 2005;294:3101-7

Vazquez-Vivar J, Kalyanaramam B. Generation of superoxide from nitric oxide synthase. FEBS 2000, 481:304-307

Venugopal E, Bhat S K, Vallooran J J, Mezzenga R, Phase Behavior of Lipid–Based Lyotropic Liquid Crystals in Presence of Colloidal Nanoparticles. Langmuir, 2011. 27(16): p. 9792-9800

Vignais P V. The superoxide-generating NADPH oxidase: structural aspects a and activation mechanism. Cell Mol Life Sci 2002, 59:1428-1459

Viso E, Rodriguez-Ares MT, Gude F. Prevalence of and associated factors for dry eye in a Spanish adult population (the Salnes Eye Study). 2009 Ophthalmic Epidemiol 16:15–21

Walling C. The nature of the primary oxidants in oxidations mediated by metal ions. In: King TE, Mason HS, Morrison M, eds. Proceedings ofthe 3rd International Symposium on Oxidases anD Related Redox Systems. Oxford: Pergamon Press, 1982:85-97

Wang S, Su R, Nie S, Sun M, Zhang J, Wu D, Moustaid-Moussa N. Application of nanotechnology in improving bioavailability and bioactivity of diet-derived phytochemicals. Journal of Nutritional Biochemistry, 2014; 25, 363–376

Watanabe K, Tanaka M, Yuki S, Hirai M, Yamamoto Y. How is edaravone effective against acute ischemic stroke and amyotrophic lateral sclerosis? J Clin Biochem Nutr 2018; 62:20-38

Watanabe T, Yuki S, Egawa M, Nishi H. Protective effects of MCI-186 on cerebral ischemia: possible involvement of free radical scavenging and antioxidant actions. Journal of Pharmacology and Experimental Therapeutics March 1994, 268 (3):1597-1604

Weiner S, Kollman P A, Case D A, Singh U C, Ghio C, Alagona G, Weiner S P Jr, Weiner P. A new force field for molecular mechanical simulation of nucleic acids and proteins. J Am Chem Soc, 1984, 106, 765-784

Wiegand RD, Giusto NM, Rapp LM, Anderson RE. Evidence for rod outer segment lipid peroxidation following constant illumination of the rat retina. Invest Ophthalmol Vis Sci 24:1433–5, 1983

Williams RA, Brody BL, Thomas RG, et al. The psychosocial impact of macular degeneration. Arch Ophthalmol 116:514–20, 1998

Witting LA. Lipid peroxidation in vivo. J Am Oil Chem Soc 42:908–13, 1965

World Health Organization. World Health Statistics 2009. Geneva: WHO 2009

Wu D Y, Guo Z Y, Ren Z H, Guo W M, Meydani S N Green tea EGCG suppresses T cell proliferation through impairment of IL-2/IL-2 receptor signaling. Free Radic Bio Med 2009;47: 636–43

Wu J, Seregard S, Spangberg B, et al: Blue light induced apoptosis in rat retina. Eye 13:577–83, 1999

Yamamoto Y, Kuwahara T, Watanabe K, and Watanabe K. Antioxidant activity of 3-methyl-1-phenyl-2-pyrazolin-5-one. Redox Report: Communications in Free Radical Research, vol. 2, no. 5, pp. 333–338, 1996

Yamamoto K, Niki E. Interaction of alpha-tocopherol with iron: antioxidant and prooxidant effects of alpha-tocopherol in the oxidation of lipids in aqueous dispersions in the presence of iron. Biochim Biophys Acta 958: 19–23, 1988

Yamashita N, Murata M, Inoue S, Burkitt MJ, Milne L, Kawanishi S. Alpha-tocopherol induces oxidative damage to DNA in the presence of copper(II) ions. Chem Res Toxicol 11: 855–862, 1998

Yasui M, Kanemaru Y, Kamoshita N, Suzuki T, Arakawa T, Honma M. Tracing the fates of site-specifically introduced DNA adducts in the human genome. DNA Repair (Amst.). 2014; 15: 11–20

Young R W. Solar radiation and age-related macular degeneration. Surv Ophthalmol 32:252–69, 1988

Yuan J H, Li Y Q, Yang X Y. Inhibition of epigallocatechin-gallate on orthotopic colon cancer by upregulating the Nrf2-UGT1A signal pathway in nude mice. Pharmacology 2007;80: 269–78

Zhang B, Safa R, Rusciano D, Osborne N N. Epigallocatechin gallate, an active ingredient from green tea, attenuates damaging influences to the retina caused by ischemia/reperfusion. Brain Res. 2007, 1159, 40–53

Zhang G, Miura Y, Yagasaki K. Suppression of adhesion and invasion of hepatoma cells in culture by tea compounds through antioxidative activity. Cancer Lett 2000;159: 169–73.

Zhang J, Wang SL. Topical use of coenzyme Q (10)-loaded liposomes coated with trimethyl chitosan: tolerance, precorneal retention and anti-cataract effect. Int J Pharm. 2009, 372(1–2):66–75

Zhu N, Huang T C, Yu Y, La Voie E J, Yang CS, Ho C T. Identification of oxidation products of (−)-epigallocatechin gallate and (−)-epigallocatechin with H_2O_2. J Agric Food Chem 2000;48:979–81

Zhou P, Yu J F, Zhao C G, Sui F X, Teng X, Wu YB. Therapeutic potential of EGCG on acute renal damage in a rat model of obstructive nephropathy. Mol Med Rep 2013; 7:1096-102

Zigman S, Schultz J, Yulo T, Griess G. The binding of photo-oxidized tryptophan to a lens gamma-crystallin. Experimental Eye Research Volume 17, Issue 3, 11 November 1973, Pages 209-217

Zinellu A, Sotgia S, Scanu B, Forteschi M, Giordo R, Cossu A, et al. Human serum albumin increases the stability of green tea catechins in aqueous physiological conditions. PLoS One 2015;10:e0134690